# THE DIAGNOSTIC MONITORING OF THE ACOUSTIC EMISSION FROM A LABORATORY BALL MILL

**by**

**Douglas Arnoldus Theron**

Thesis submitted for the partial fulfilment of the requirements for the degree of Master in Engineering (Extractive Metallurgy) in the Department of Chemical Engineering at the University of Stellenbosch

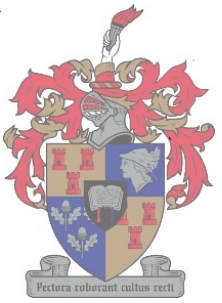


**Supervisors:**

**Prof C Aldrich**

**Prof DM Weber**

**DECEMBER 1999**

Stellenbosch

# Declaration

I hereby certify that this thesis is my own, original work, except where specifically acknowledged in the text. Neither the present thesis, nor any part thereof, has previously been submitted at any other university for degree purposes.

D.A.Theron

12 August 1999

# Synopsis

The harsh interior environment of mills makes on-line monitoring of these grinding systems difficult. Not only are conventional contact sensors expensive, but the nature of the grinding process makes their application impractical. Unfortunately few accurate quantitative measures are in place in industry to describe or assist in the operation and diagnosis of ball mills. In the South African context operators learn to control the mill based on a priori knowledge of the system gathered from years of process experience. It is common knowledge in industry that these operators associate the sound emission from the system with certain process conditions, and adjust the mill set points to obtain optimal grinding conditions. Unfortunately the high turnover of manpower in the mining industry has led to a drain of knowledge from many operations, leading to a loss of valuable control information.

In this work the acoustic emission from a ball mill was studied making use of a laboratory ball mill, acoustic microphones and a personal computer, equipped with a sound card. The mill signal was recorded for a series of batch experiments. These consisted of single parameter experiments where single parameters such as percentage filling, mill speed, percentage water and percentage charge mass were varied, while keeping all other parameters constant. A second series of experiments were conducted with two platinum ore types, namely UG2 and Merensky, to study the influence of changing particle size on the acoustic emission from the mill.

The acoustic signal was transformed into the frequency domain from the time domain by using Welch's averaged periodogram method. Hereby the power spectral density function for each acoustic sample was obtained and used as the basis for further data analysis. The structure of the data was investigated with a Sammon map obtained from the power spectral density data. This method confirmed that specific conditions in the mill each had a unique fingerprint which enabled differentiation of the acoustic information.

Feature vectors were obtained by principal component analysis of the power spectrum density function extracted from the original mill signal. These feature vectors were used for the modelling of different data sets. Linear regression was applied to the single parameter experiments yielding modelling results with $r^2$ values above 0.95. With the platinum ore data both linear regression and feed forward neural networks were used for modelling. However, the linear regression model was unable to predict the ore particle size from the acoustic data. The non-linear neural network models achieved accurate particle size predictions for both ore types on both known and unknown validation data sets. $r^2$ values greater than 0.93 for the test data and 0.97 for the training data were obtained .

# Oorsig

Monitering van balmeule in die Suid-Afrikaanse industrie word deur operateurs behartig. Dit is algemeen bekend dat ervare operateurs die klank wat tydens maling vrygestel word met sekere prosestoestande en produkgroottes kan assosieer. Die hoë tempo waarteen operateurs tans poste verwissel, het egter gelei tot die verlies van spesifieke kennis wat met bedryf van meule verband hou. Pogings om konvensionele sensors vir monitering te gebruik het hoofsaaklik gefaal as gevolg van die aggresiewe omgewing van maling en vergruising wat normale meetmetodes belemmer.

In hierdie werkstuk word die akoestiese sein wat tydens maling vrygestel word deur middel van 'n persoonlike rekenaar, toegerus met klankkaart en akoestiese mikrofone, en 'n laboratorium balmeul ondersoek. Akoestiese emissies tydens maling is vir 'n aantal kort enkellading-eksperimente ondersoek. Tydens hierdie lopies is enkel-parameter lopies uitgevoer waar die effek van persentasie meulvulling, meulspoed, pulpdigtheid en meulbelading op die akoestiese sein ondersoek is. 'n Tweede stel eksperimente is uitgevoer om die effek van verandererende partikelgrootte op die akoestiese sein te ondersoek. Hiervoor is twee verskillende platinumerts-tipes wat in die nywerheid bekend is vir hul verskil in klank tydens maling, nl. UG2 en Merensky, gebruik.

Die akoestiese sein is vanuit die tyddomein getransformeer na die frekwensie-domein deur van Welch se gemiddelde periodogram-metode gebruik te maak. Die spektrale digtheidsfunksie van elke akoestiese monster is bepaal en gebruik as die basis vir verdere analise. Die struktuur van die datastel is deur 'n topologiese Sammon netwerk voorgestel. Hierdie voorstelling het duidelik bevestig dat spesifieke toestande in die meul 'n unieke vingerafdruk, met onderskeibare klasse na gelang van die bedryfs- en prosestoestande van die meul, laat wat slegs gebaseer kan word op die akoestiese inligting wat uit die proses vrygestel word.

Kenmerksvektore is deur hoofkomponentanalise vanuit die spektrale digtheidsfunksie van die oorspronklike akoestiese sein bepaal. Die kenmerksvektore is vir verdere modelering gebruik. Lineêre regressie is op die enkelladingsdata toegepas met akkurate voorstellingsresultate vir die enkelparameter lopies. Beide lineêre regressie en 'n neurale netwerk is op die platinumertse toegepas om die partikelgrootte vanaf die akoestiese sein te modeleer. Die partikelgrootte vir beide Merensky en UG2 ertse is akkuraat deur die neurale netwerk vir beide die bekende, sowel as die toetsdatastelle voorspel, terwyl die lineêre regressiemetode nie akkurate voorspellings kon maak nie. Die slotsom is dus dat die akoestiese inligting wat van 'n balmeul vrygestel word, gebruik kan word vir onder andere diagnostiese analise, modelering en uiteindelik ook meer akkurate beheer van die balmeulstelsel waar tradisionele metodes oneffektief was.

# Acknowledgements

I would like to thank the following people who made this thesis possible:

1. Professors Aldrich and Weber for their guidance and encouragement during the project.
2. The Digital Signal Processing group, especially Jaco Breitenbach for the help on the electronic side and Carl Bellingham for writing the Millrecorder program which recorded the signals.
3. The Intelligent Process Systems Group for the know-how on the methods and algorithms.
4. My parents and grandparents for the faith to believe and the motivation to continue.
5. Marilie, for enduring in love and hoping and dreaming with me.

*To the Lord who sits on the throne, whose joy is His creation ……*

# TABLE OF CONTENTS

# LIST OF FIGURES

# LIST OF TABLES

# LIST OF SYMBOLS

| | | |
|---|---|---|
| $a_i$ | : | Coefficient of variance $S_{ij}$ |
| $a_i$ | : | Estimated coefficient in AR model |
| AR | : | Autoregressive |
| CAS | : | Charge (ball) addition experiment |
| $C_s$ | : | Critical mill speed |
| D | : | Mill diameter in m |
| d | : | Ball diameter in m |
| d+4000 | : | Fraction larger than 4000 µm |
| D1 | : | Particle size of Merensky ore in SAM experiment |
| d106 | : | 106 µm screen size |
| d1400 | : | 1400 µm screen size |
| d150 | : | 150 µm screen size |
| D2 | : | Particle size of UG2 ore in SAM experiment |
| d212 | : | 212 µm screen size |
| d2800 | : | 2800 µm screen size |
| d300 | : | 300 µm screen size |
| d425 | : | 425 µm screen size |
| d600 | : | 600 µm screen size |
| d75 | : | 75 µm screen size |
| d-75 | : | Fraction smaller than 75 µm |
| $e_l$ | : | Error between actual value, $x_l$, and estimated coefficient in AR model |
| $E_n$ | : | N'th Eigen values |
| f | : | Frequency component in Hz |
| f(0) | : | Fundamental frequency |
| F(w) | : | Fourier transform of signal f(t) |
| F(x) | : | Transfer function for feed forward neural network |
| F50 | : | 50% fraction of ore passing screen size, µm |
| F80 | : | 80% fraction of ore passing screen size, µm |
| FFT | : | Fast fourier transform |
| FILL | : | % ore content experiments |
| $g_i$ | : | Coefficient of error, $e_l$, in AR model |
| GP | : | Genetic programming |
| i | : | Time index |
| LR | : | Linear regression |
| M | : | AR model order |
| m | : | Feed Mass, kg |
| M-1 | : | Length of section for FFT calculation with Bartlett windowing function |
| MBx | : | X'th experimental recording for Merensky ore experiments |
| MSS | : | Mill speed experiments |
| n | : | Bin number in Bartlett windowing function |
| n | : | Number of samples |
| Nb | : | Number of small balls |
| NN | : | Neural Network |

| | | |
|---|---|---|
| p | : | Number of variables in principal component analysis |
| P(f) | : | Power spectrum periodogram |
| PCA | : | Principal component analysis |
| PCn | : | N'th principal component |
| PSD | : | Power spectral density |
| Px | : | X'th power spectral sample point with $x_{max}$=257 |
| SAM | : | Merensky and UG2 ore combination experiment |
| $S_{ij}$ | : | Variance of j'th variable |
| SLUR | : | Water addition experiment |
| $T_p$ | : | Period of the signal |
| UBx | : | X'th experimental recording for UG2 ore experiments |
| W | : | Mill speed, rpm |
| W(t) | : | Windowing function |
| x | : | Inverter frequency |
| x | : | Sample point |
| X | : | Ore type |
| **X,Y** | : | Feature vector in principal component analysis |
| X1 | : | Mass of Merensky ore in SAM experiment |
| X2 | : | Mass of UG2 ore in SAM experiment |
| $x_i$ | : | Measured state variable of discrete time series |
| $x_i$,$y_i$ | : | Vector component |
| $x_{ij}$,$y_{ij}$ | : | Matrix component |
| Y | : | Modelled variable |
| y | : | Mill speed |
| $z^{-1}$ | : | Backward shift operator |

# 1

# ACOUSTIC SIGNALS FROM MILLS

## 1.1 INTRODUCTION

Tumbling mills are large, noisy, communition machines typically consisting of a cylindrical drum rotated about the longitudinal axis. Grinding of the ore is achieved by random collisions with the media which are usually steel balls, rods or the ore itself. These collisions transfer energy to the ore particle, which results in deformation and breakage. Since tumbling mills are notoriously inefficient, most energy is dissipated in the form of heat and noise.

Most mills are controlled by the power draw which is correlated with operating conditions, such as charge mass and mill speed. Unfortunately the power draw is not a direct indication of the local mill conditions and as a result, the sound emitted from the mill during communition has been used by humans to associate certain operating conditions with the specific noise which is transmitted from the mill. Centrifuging, for example, reduces the number of collisions that occur inside the mill and leads to lower noise levels. A laboratory mill with excessive water added will lead to a slurry of low viscosity, and decrease the number of effective collisions, thereby also leading to lower noise levels. Further, overdosing of water on industrial mills washes the fines from the mill which leads to a reduction in dampening of the sound. The converse is true for mills with too much grinding media, where collisions between the grinding bodies and the mill shell dominate, thereby leading to excessively noisy operation. In operating plants there are concrete evidence that the sound from a mill contains information which is important for control and a better understanding of the grinding process.

Owing to the high turnover of manpower, specifically in the South African process industries, experienced operators have recently become relatively scarce, in turn

having an adverse affect on manually controlled milling systems. In principle, the interpretation of the acoustic signals emitted from a mill during operation can therefore be used as a basis for more systematic control and optimization of operations. Successful implementation of such a system should also alleviate the dearth of experienced operators and could aid in the training off less experienced plant staff.

## 1.2 SOUND AND HEARING

An acoustic signal is a pressure pulse which is transferred through a medium such as air (gaseous), water (liquid) and steel (solid) which can be sensed by the tympanic membrane of the human ear. The intensity of the sound can be correlated with the amplitude of the sound wave and the pitch or tone with the corresponding signal frequency. Hence, a louder sound will have a larger amplitude and a sound with a higher pitch a higher frequency. Noise is defined as an aperiodic non-repeating vibration, while periodic repeating vibrations are perceived as musical sounds. These musical sounds are made up of a primary sound wave which determines the musical pitch and a number of harmonics which determine the sound quality originating from any specific musical instrument. This gives rise to the difference in sound between a note of the same pitch played on two different instruments, e.g. harp and flute.

The amplitude of a sound signal can be expressed by the maximum pressure change which is experienced at the eardrum. The bel scale is a relative scale that has been derived from the ratio of the intensity of a sound to a reference sound in order to enable quantification of sound signals. The bel is therefore defined as

$$\text{bel} = \log \frac{\text{sound intensity}}{\text{reference sound intensity}}. \qquad (1.1)$$

The signal intensity is proportionate to the square of the sound pressure so that the bel is defined as

$$\text{bel} = 2 \log \frac{\text{sound pressure}}{\text{reference sound pressure}} \qquad (1.2)$$

The decibel (0.1 bel) is the most commonly used indication of sound intensity. The decibel scale uses the threshold of human hearing as reference (0 dB) and is the

most common scale for sound intensity measurement. The human ear is capable of handling intensities of up to 140 dB before permanent damage is incurred. Figure 1.1 shows the decibel scale with some common associations.


**Figure 1.1.** Common sounds with their typical decibel values.

The human ear is further capable of detecting frequencies between 20 and 20 000 Hz, with the greatest sensitivity in the 1000 to 4000 Hz region. Figure 1.2 depicts the audibility curve for the human hear. The solid line is for ideal conditions, the dashed for normal conditions and the dotted line for conditions above 140 dB where sound can be felt as well as heard. This curve indicates the actual limit of human hearing.

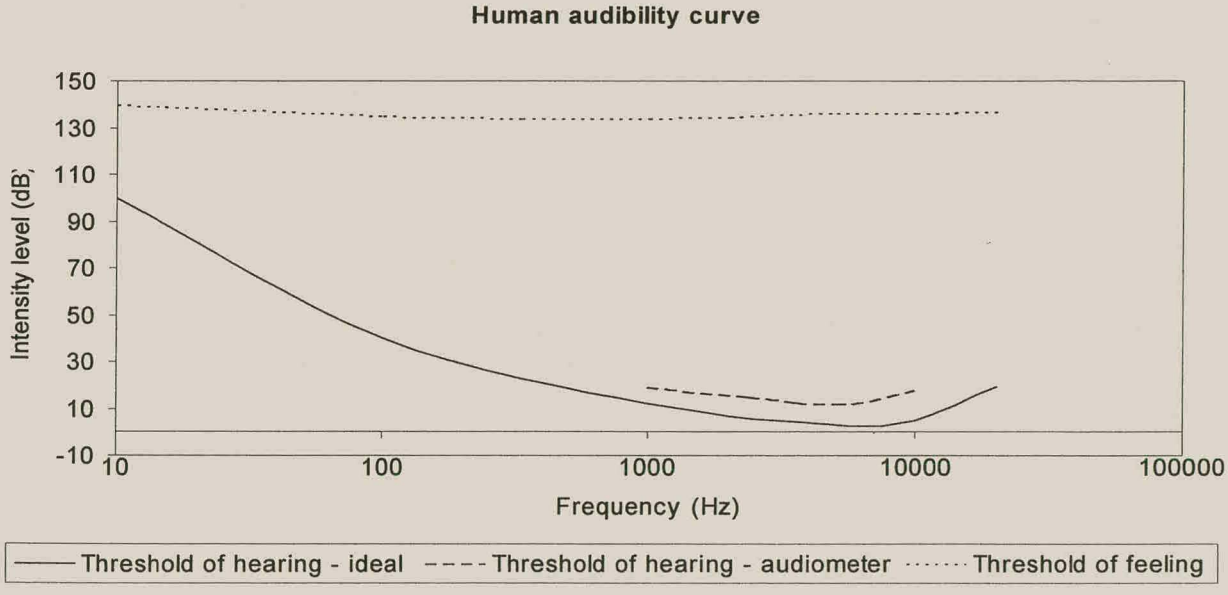


**Figure 1.2**. Human audibility curve

In a milling system the various sources of sound are almost numerous, with thousands of particles and grinding balls abrading and colliding at random in combination with the sound from the mechanical drive and gear. The sound which is emitted from a grinding mill therefore contains a large amount of information which can be harnessed for control and understanding of the milling process.

## 1.3 COMMUNITION MECHANISMS

Communition is generally viewed as the reduction of the particle size of an ore to a size where the minerals in the ore are freely separated from each other. Various stages of communition are encountered in the mining industry. The first stage is usually blasting in a mine, followed by primary crushing in crushers or autogenous mills and finally passing through to a stage of reduction in the grinding circuit. In grinding, breakage is achieved by one or all three of the following three mechanisms: crushing, impact and attrition.

According to Wills (1981), crushing breakage occurs due to compression of the rock particle. Two types of particles are formed when an irregular particle is fractured, namely coarse and fine. Coarse particles are formed by tensile failure and fine particles (fines) by compressive failure at the points of loading. Impact breakage gives particles of roughly the same size. These particles are formed mainly by tensile failure due to the large amount of energy imparted to the original particle. Attrition (or shear failure) produces fines owing to particle-particle interaction. This occurs when the feed rate is too high and results in contacting particles increasing the degree of compressive stress.

Grinding in a tumbling mill is an energy consuming process making use of only a small portion of energy to actually break the rock. Most energy is lost in the generation of heat while some is dissipated in the form of noise. Grinding is performed in cylindrical drums rotating around their own axes. The drums are filled with charges consisting of the ore itself and the grinding medium. The medium may be steel balls, rods or the ore itself, depending on the type of mill used. The mill charge is free to move inside the mill and leads to communition of the particles. The grinding process is influenced by the size, quantity, type of motion and the spaces between the media in the mill. Consequently the following mechanisms have been

attributed to grinding: impact due to forces normal on the particle, chipping due to oblique forces, and abrasion due to forces acting parallel to the surfaces. Wet grinding is usually performed in industry owing to downstream process requirements, and also because it is more energy efficient than dry grinding.

## 1.4 CHARGE MOTION

The tumbling speed of the charge plays a very important part in the motion of the mill charge and hence also the sound which is emitted. Wills (1981) attributes the driving force of the mill to be transmitted to the charge via the liners. At low speeds or in mills with smooth liners, the charge slips or rolls down to the toe of the mill, giving rise to abrasive communition. This is called cascading and gives rise to fine products, and typically this would lead to softer sounds with more clattering of balls.

At higher tumbling speeds the media are projected from the liner, in a parabolic path ending at the toe of the charge. This causes breakage by impact, with coarser sizes and longer liner life, aptly called cataracting. The noise emitted is typically a series of loud impacts or clashes as the flying balls collide with each other and the mill shell.

Centrifuging occurs at the critical mill speed, $C_s$. Here the contents of the mill are carried around the shell in a fixed position and no breakage occurs. The sound level is reduced as the number of impacts and general clattering caused by cascading are decreased due to the centrifuging motion.

## 1.5 VARIABLES INVOLVED IN THE MILLING PROCESS

The variables involved in the modelling and control of milling processes are depicted in figure 1.3. The variables which directly influence the process of grinding are shown on the left of the diagram. These are typical variables that have a direct impact on the performance of the mill. The dependent variables on the right hand side of the diagram are indications of the performance of the mill. Traditional mill control has focussed on the monitoring of the dependant variables such as product particle size, mill sound and slurry density. These variables are optimized by adjusting the independent variables until the required product quality is obtained. In this thesis the

acoustic mill signal is used to model the various dependent and independent parameters.

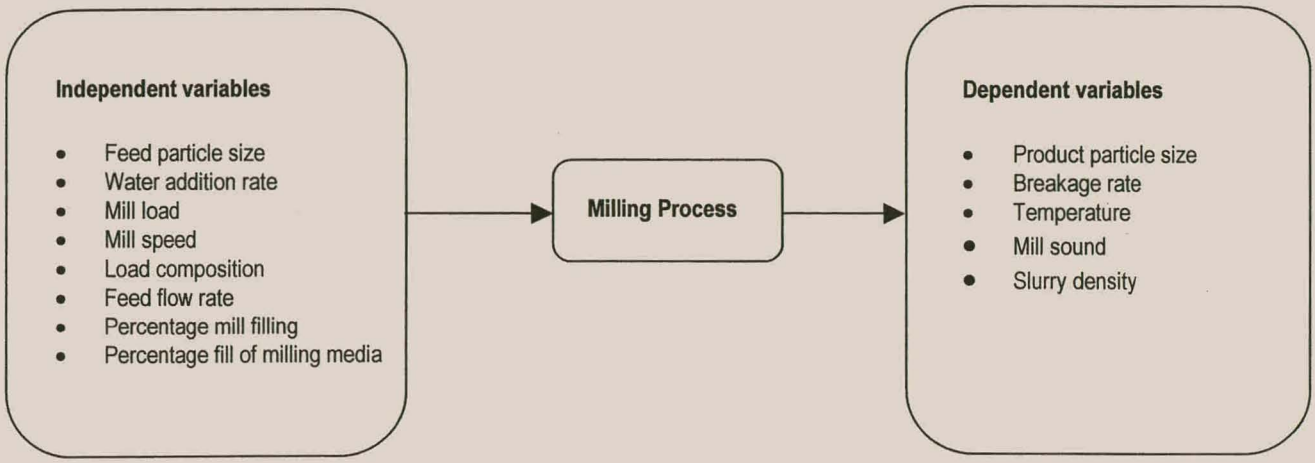


**Figure 1.3.** Variables involved in the milling process

## 1.6 MILL CONTROL

The primary goal for any model is to improve the control of the mill. Metzner (1993) outlined the following operational and economic reasons underlying optimal mill control:

- Stable operation results in fewer process upsets.
- Undesirable events such as rod tangles can be avoided.
- A well operated system is managed more effectively.
- The operator is free to focus on operation rather than stabilisation.
- Increase in tonnage throughput.
- The product particle size can be controlled for effective recovery.
- Improved milling efficiency.

Any deviation from the optimum particle size ultimately results in a decreased recovery. It therefore would be beneficial to have mill control to increase the mill output at an optimum particle size. However, mill control has been hampered by a lack of reliable instrumentation. (Rowland, 1963, Metzner, 1993)

Hulbert et al. (1990) developed a multivariable and optimising controller which controlled the mill product size on line in order to optimise downstream processing

conditions and to reduce down stream fluctuations. This led to a stabilisation of the milling circuit by the reduction of product fluctuations resulting in more consistent and maintainable grinding conditions. The milling efficiency was optimised through increased throughput and improved grind at the required output. The available process inputs such as solids feed rate, water addition, flow rate to the hydrocyclone, the feed sump level and the mill were all used to control the system.

Stange et al. (1997) indicated that optimum control could be obtained with a case study on the control of the Leeudoorn SAG milling circuit. By stabilising the milling circuit a consistent operation with maximum throughput was obtained. The product size distribution was stabilised, with minimised operating cost. According to Stange et al. (1997) the following factors posed practical problems to mill control:

- The milling process is non-linear and adaptive to both feed and operating conditions, which causes assumptions to the actual milling conditions.
- The operating environment is noisy and robust which makes direct measurements difficult and makes the application of a non-contact sensor favourable.
- The process is adaptive in the sense that the behaviour of the circuit changes along with changes in ore properties, equipment wear, etc.

An effective mill control system should therefore be easy to use by both operating and technical personnel and be able to adapt to local conditions.

## 1.7 MOTIVATION

From the previous discussion it is clear that milling is a complex process that is difficult to control, owing to a lack of adequate measurements, as well as the harsh environment of the process. Various authors, specifically Watson and Morrison (1986) and Zeng and Forsberg (1993a, 1993c) have proposed the acoustic monitoring of both laboratory and industrial scale ball mills. The prime motivation for this project is to simulate the work done by others, to increase the understanding of acoustic monitoring and to set a platform for the application of future research.

## 1.8 OBJECTIVES OF THE THESIS

The aims of this thesis are to:

- Give a critical literature survey of previous work on acoustic signal analysis in comminution systems.
- Experimental investigation of factors affecting the acoustics of communition in a laboratory scale ball mill.
- Analyses and interpretation (feature extraction) from acoustic signals.
- Modelling of milling, based on acoustic features extracted from acoustic signals.

The ultimate aim is to assist in the effective control and modelling of milling circuits by means of a non-contact sensor, based on the acoustic emission from the mill.

## 1.9 CHAPTER OUTLINES

Chapter 1 has focused on the rationale behind the acoustic monitoring of mills. The fundamental mechanisms and operating parameters which influence the acoustic signals were presented and explained.

In chapter 2, a literature survey on the subject of acoustic control and monitoring in chemical engineering is presented, which highlights the methods applied to process the sound signal from the audible time domain form to values which can be used for modelling purposes.

The experimental investigation and methodology is presented in chapter 3. The reader is introduced to the different types of mills used on mineral processing circuits, together with a description of the factors that affect the operation of a mill. The experimental procedure and equipment are described in detail for future reference. Finally the experiments and the factors which were investigated during the experiment are illustrated.

Chapter 4 gives a literature survey of the different methods used to process the data, e.g. the Fourier transform, principal component analysis, Sammon mapping, average

energy, linear regression and neural network modelling. The procedures of data acquisition and processing are further described.

In chapter 5 the different results which were obtained are presented along with the relevant figures and tables. The results are discussed in chapter 6 and the relevant conclusions and recommendations made in chapter 7.

The experimental results, principal component analysis results, regression results, neural network results, detailed description of milling operation, Sammon mapping technique and linear regression are presented in appendices A to I.

# 2

# LITERATURE SURVEY

## 2.1 INTRODUCTION

Acoustic methods have found important use in a wide range of industries and research fields. In this literature survey the various methods used to measure and record vibration signals, as well as the numerous ways in which the data have been analyzed and exploited in the process industries, are presented. It is the objective of this chapter to give the reader an understanding of the different methods available, as well as to describe other research important to this thesis.

Sound and vibration is one of the distinguishing factors governing the state of any matter. Intermolecular vibration is the source of heating while the bark of a dog sounds warning to the intruding burglar. As such, sound and vibration is an integral part of any process. In the past 40 years different approaches have been attempted to model the sound emitted from different processes with the operating and response variables. The description given is by no means complete and does not include the numerous applications of ultrasound. However, it covers some of the most important chemical engineering and mineral processing papers published so far in the field of acoustical process diagnosis.

### 2.1.1 Wood Drying

The acoustic emission from wood drying has been described by Booker (1994) and Ansell (1982). Booker (1994) describes the correlation of the acoustic emission of drying timber with the surface strain generated in the wood surface. During the drying of timber microfractures occur in the surface of the material due to the differential shrinkage between the rapidly drying surface and the moisture saturated internal regions. The resultant stresses generate a noise or vibration, known as acoustic

emission. The emission was measured by means of a transducer mounted on the surface of a drying timber board. Petroleum jelly was used as a transmission coupling to limit signal attenuation.

The sensor used had a resonant frequency of 60 kHz with an output of 40 dB. This signal was amplified further to 60 dB where a preset DC offset voltage was maintained. A digital counter was used to calculate the amount of times the threshold was crossed. The threshold was selected sufficiently high to exclude extraneous noise. A 15 second increment was used for data acquisition. This method is known as the "ring down counts" method. An undisclosed model was used to calculate the moisture content of the wood from the acoustic emission and it was also found that the ultimate instantaneous strain in the timber surface was correlated to the acoustic emission.

In previous work by Ansell (1982) on the acoustic emission from soft woods and other breakable materials during a variety of experiments, the use of acoustic emission in wood science is described. Noteworthy historical applications, which are mentioned by Ansell, are the creaking of mine timber which indicates imminent failure, as well as work on sound emissions on mine props using a microphone. Ansell made use of a lead-zirconate-titanate accelerometer used in conjunction with a pre-amplifier. The signal was filtered by a band-pass filter allowing the components between 100 and 300 kHz to pass through. The data consisted of sporadic bursts of variable frequency and amplitude, with decaying amplitudes in the final stages of each test. Ansell postulated that the stages of energy release from soft woods in tension were related directly to the specific ring structure of the wood as later described by Booker (1994). The acoustic emission recorded at failure was found to have a significant correlation with the wood toughness measured with an impact test.

### 2.1.2 Cooking Extrusion

Elsey et al. (1998) did research on the acoustic emission of steam escaping from a cooked product, after leaving an extruder in the cooking industry. The process is difficult to control, given the high standard of quality required in the cooking industry. This is especially true with regard to physical properties such as bulk density, texture and degree of cooking, all of which are difficult to measure on-line. The models

applied in the research made use of both the time domain, as well as the frequency domain information to model the product bulk density and the texture. Principal component analysis was used to reduce the dimensionality of the frequency domain data. This in turn was modeled using both genetic algorithm and neural network models.

Cooking extrusion is a continuous process for the drying of foodstuffs. As the product exits the extruder, moisture flashes and causes pockets of steam to form in the product. The moisture in turn bursts when close to the product surface and emits an audible noise. A microphone was connected to the sound card on a PC and the signal recorded onto hard disk. Additional noise from the drivegear and motor contributed significantly to the background noise sensed by the microphone. The operating parameters varied were the feed rate, moisture contents and feeder screw speeds. The measured variables were the bulk density, moisture content and textural properties. The sound signal was recorded at a sampling frequency of 22 kHz for 10 seconds per sample.

As the acoustic data set from the experiments was relatively small, it was expanded by breaking down the original data files into smaller files containing $2^{14}$ data points each. It was found that a greater number of points did not improve model accuracy. Observation of the extruder showed that different products had their own characteristic frequency and "popping" sounds during extrusion.

The time domain information (e.g. popping rate) was found by optimization of the number of peaks occurring per second and correlating with the bulk density of the sample. The average power of the signal was calculated by taking the root mean square value.

Frequency domain analysis was done by taking the Fast Fourier transform of the signal. The frequency range was divided into 512 bins and the average energy in each bin was taken to reduce the number of points in the data range. The principal components of the data were extracted to give a more concise description of the variation in the data and to further reduce the data set to a set of uncorrelated variables. The first 10 principal components were used for modelling and accounted for half of the total variance in the data.

Two modelling techniques were applied to the data, *viz.* genetic programming and artificial neural networks. The input parameters, 'popping rate', RMS power and the 10 principal components were used to model the bulk density and fracture force.

The genetic programming (GP) procedure performed symbolic regression to find the structure and complexity of the model while simultaneously estimating the parameters. The GP model for bulk density gave a fit with correlation coefficients of 0.93 and 0.91 on the training and verification data respectively. The model for fracture force gave coefficients of 0.94 and 0.92 for training and testing.

An artificial neural network consisting of 8 inputs and 8 hidden neurons was chosen, making a total of 81 internal weights to be determined. Correlation's of 0.98 for the training and 0.96 for the test set respectively, were obtained. The work of Elsey et al. (1998) showed that useful information was contained in the acoustic data emanating from an extruder which could be effectively used for modelling and control purposes.

### 2.1.3 Detection of Leaks in Heat Exchangers

Hsiung and Himmelblau (1992) described the use of hydrophones to detect leaks in double tube heat exchangers. An auto regression model was used to predict the power spectral density of the data, along with different classification models. The position and size of the leaks were varied and three classification strategies were employed to classify the acoustic data.

Hsiung and Himmelblau (1992) describe the following three reasons why acoustic signals were studied to detect faults in equipment. Acoustic waveforms are easy to collect from inaccessible places in equipment, they contain enhanced information above that obtained from typical process instruments and they possess the superposition property of linear systems. The superposition property allows different sources of acoustic noise to occur in each other's presence without altering the respective medium or other sources. This enables each signal to be detected individually. Too many sources of noise, however, will lead to distortion of the waveforms when passed through different media or reflected by other equipment. These extraneous noises corrupt the information in the signal. Analysis can only be done if the changes in the state of the system are detectable by their respective

change in waveform. Many applications in fault diagnosis with acoustic spectra have been researched, with internal leakage in steam, air and hydraulic valves being some of the applications cited.

In order to make use of the acoustic data the signal must be transformed into a set of feature vectors. These feature vectors reduce the amount of redundant information in the data set while at the same time isolating the significant information. Hsiung and Himmelblau (1992) chose an autoregressive (AR) model due to the ease of implementing such a model in real time. It could further represent waveforms with a reasonable number of coefficients. The AR model was of the form:

$$x_n + a_1 x_{n-1} + ..... + a_n x_{n-M} = a(z^{-1})x_n = e_n \qquad 2.1$$

where $x_i$ is the measured state variable in the discrete time series

$a_i$ is the coefficient to be estimated

$e_i$ is the error between the actual value $x_i$ and the estimated value of the time series

$i$ is the time index

$z^{-1}$ is the backward time shift operator and

$M$ is the order of the model.

By assuming that the time series is stable, the function $\alpha^{-1}(z^{-1})$ has an infinite number of terms involving $z^{-1}$. As such, a wide sense stationary process is a stable time series and the model can be converted to :

$$x_n = a^1(z^1)e_n = \sum g_i e_i \qquad 2.2$$

where $g_i$ are the coefficients of $e_i$.

Hereby the data space is reduced to a small set of features, namely the set $\{a_i\}$. To determine the order of the set Hsiung and Himmelblau (1992) assumed that the process was fitted by Gaussian statistics and found that the calculated order varied between 6 and 12. Too low an order resulted in a smoothed estimated power spectrum with little information. Too high an order resulted in too much undesirable detail. A Burg algorithm was used to divide the data into blocks, with each block

processed independently of the other. This method allows recursive calculations on later stages without affecting the earlier computations.

Three classifiers were examined, namely a quadratic discriminant model, nearest neighbour decision rule and artificial neural networks.

The classifiers can be summarized as follows:

- The quadratic decision rule made use of a pooled or within group covariance matrix, where the matrix is the basis of the measure of generalized squared distance. It was assumed that the covariance matrix of each class was different rather than being the same and it was found that the correct classification rate was higher with the within group than with the other option, namely the a priori probability of each class.
- The nearest neighbour procedure was dependent on the a priori probabilities, which were set equal, and the distance between two points calculated either by the Euclidean or Mahalanobis metric. Five nearest neigbours were chosen for classification purposes.
- A feed forward neural network with one hidden layer and Gausian transfer functions was used. The number of nodes was determined empirically by optimizing the error rate of the test set. This prevented overfitting and increased the generalization capacity of the network.

The experimental setup consisted of a counterflow double tube heat exchanger, fitted with two hydrophones. The heat exchanger was isolated from ambient noise by wrapping it in plastic foam and by placing sponge between the exchanger and the support to absorb structural noise. Factors affecting the sound were the flow rates, leak hole sizes and leak hole positions. Nine flow rate combinations were used, resulting in 63 experiments.

The data were divided into four sets. The first set was used for training and the other two sets were used for testing of the classifiers. Each experiment consisted of 32 data records with 2048 points each. 288 segments were obtained for each operating condition and were placed into the sets.

Analysis of the results showed that no natural period similar to the period of revolution of a rotating machine could be distinguished. As such the time record was divided artificially. The time record with 2048 points was divided into 9 segments with 256 data points and with an overlap of 32 points.

The Burg algorithm was used to calculate the coefficient set for the AR model of order 12 for each segment. A power spectrum was calculated for each set and showed that the 9 segments had a similar spectrum. By this analysis Hsiung and Himmelblau (1992) found that the time records should be divided into smaller segments and each studied individually. It was also found that extraneous noise could not be eliminated from the spectrum by averaging the data.

The following classifying results were obtained by Hsiung and Himmelblau (1992):

- For the detection of no leaks vs. leaks it was found that the neural network had the smallest average error rates, the quadratic classifier performed better than the nearest neighbour for the no-leak case while the converse was true for the leak case.
- Classification of leak size gave similar results for all three classifiers, but it was found overall that small leaks were more difficult to detect than large ones.
- For the detection of leak location the quadratic rule gave best results.

### 2.1.4 Pump Control by Means of Acoustic Emission

Kruft and Friedsch (1986) controlled the pump speed by means of the acoustic emission caused when a pump operates in the cavitating region. The controller described by Kruft made use of the acoustic pressure pulses that are formed with the collapse of the cavitation bubbles inside the pump casing. The acoustic measurement was taken externally and as such, no internal measuring points were required.

The controller logged signals with energy above the average level and adjusted the pump speed via the frequency inverter. For higher sound levels the pump speed was decreased and vice versa. The pump was calibrated to maintain the operating

conditions with the lowest possible suction or delivery height. Cavitation was thus reduced and substantial savings in energy could be realized.

The signals from the pump were first logged by a transducer that amplified the signal sent to the microprocessor. The input signal to the microprocessor was again amplified and filtered to allow only the relevant signals for processing. The input impulses were counted in the microprocessor circuit and compared to the calibrated value limits. The control actions were then taken according to the magnitude of the difference between the set-points and the input values. With the controller Kruft obtained better product quality and lower energy costs, noise levels and equipment wear.

## 2.2 COMMINUTION SYSTEMS

### 2.2.1 Mill Controller

In the Measurement and Control Magazine (1963) an anonymous author gave a good perspective on the use of acoustic sound in mill control. An acoustic controller was proposed to replace the existing mass load controller used on most mills at the time. The working of the controller was based on the volume of voids in the charge which were filled by fine ore. Fine ore caused a noise with lower energy levels than larger ore particles. A commercial system by International Combustion Products Ltd. made use of a microphone placed next to a mill shell opposite to the toe of the charge. A bridge circuit compared the signal from the mill with a pre-set reference signal and adjusted the feed rate to the mill accordingly. The basis for this commercial model was that an overloaded mill caused a low (dampened) sound level and vice versa. A lengthy calculation was done to prove that sound was in principle far superior to mass measurements as a basis for mill control.

However these conclusions were questioned by Rowland (1963). By listening to mill sound and by observing the load on a classifier in the process, plant operators learned by observation and experience to maintain an acceptably constant product size. Mill sound was the first basis of automation of grinding mills. The first controllers merely caused an on-off action with the feeders. Later incremental controls were made possible. The largest drawback for these controllers was extraneous noise. This noise was almost impossible to eliminate in such an environment with the

equipment available at the time. Furthermore, the equipment was not sufficiently sensitive at optimal conditions, as variations in frequencies and amplitudes were slight, unless there was a large change in feed or circuit conditions. At such an early stage it was noted that acoustic control was easier in pebble mills than mills with steel grinding media. This can be attributed to less noise from different materials in pebble mills where the ore being ground is comminuted with ore of the same type.

The influence of liners on the sound emission from tumbling mills is significant. In a discussion published by the Institute of Canadian Mineral Processors (1968) the merits of rubber and steel liners were debated. From measurements taken on industrial plants, mills with rubber liners emitted less noise than those equipped with steel liners. Readings for the rubber liners were in the order of 97 dB with steel appreciably louder at approximately 107 dB. Further results from industrial mills showed that the different types and thicknesses of the rubber linings generated acoustic signals of different amplitudes. In all, the results showed that rubber linings emitted acoustic signals of lower amplitude than stone liners, with stone liners emitting acoustic signals of lower amplitude than steel liners.

In papers by Zeng and Forssberg (1993a, 1993b) a single vibrometer was used to monitor vibration. The manipulated operating parameters were: feed rate to the crusher, close side setting and material charge volume. The accelerometer was placed at the central point of the crushing zone. The signal was filtered with one highpass (10 Hz) and one lowpass (1 kHz) filter before it was stored on digital audio tape. The recorded signal was sampled at 48 kHz with a 92 dB signal-to-noise ratio. A digital oscilloscope was used to resample the data at 5000 kHz, which gave a sample corresponding to 13 seconds in the time domain. These data could then be further processed by a personal computer. Subsequent analysis of the data was performed by segmenting the data into segments containing 2048 points each. The data were multiplied by a windowing function (Hanning window) to transform the data from the time domain into the frequency domain. The resulting periodograms were averaged to give asymptotically unbiased and consistent spectral estimates. The windows were overlapped by 60%. The area below each peak was calculated by dividing the spectral band into 50 sub-bands which gave the energy of the respective signals. Principal component analysis was applied to the spectra, as the peaks (independent variables) were linearly correlated, to reduce the number of

independent variables. Multiple linear regression was subsequently applied to relate the features of the acoustic signals to the operating variables of the crusher.

The method used to interpret the acoustic fingerprint divided the spectra into narrow frequency bands. By calculating the energy in each band the energy component of each frequency could be approximated and the influence thereof on the entire process determined. Principal component analysis reduced the number of source frequency bands into a number of latent variables that described the most variation in the signal. Before principal component analysis the data set was centred by subtracting the average energy of all the observations at the specific frequency bands from the frequency band of each individual frequency band. The first four latent variables collectively accounted for 91% of the variance in the data set, with the first accounting for 56.4%. Regression with three crushing parameters and the principal components yielded a model with a 99% significance level.

### 2.2.2 Milling Applications

#### *2.2.2.1 Mill Modelling with the Average Signal Energy*

Besides the initial work done during the 1960's on the average energy of the mill signal, Watson and Morrison (1986) applied the same method for the prediction of mill parameters, including slurry density and viscosity. According to Watson it is generally accepted that an optimum pulp density exists where optimum size reduction is realized. Below this optimum the probability of a particle being broken decreases due to the decreasing number of particles. On the other hand, higher pulp densities lead to higher pulp viscosity and increases particle agglomeration, which leads to less efficient breakage of particles.

Watson and Morrison (1986) showed that signal measurements could indicate size distribution, ore breakage rates and ore character. In effect the work relates the acoustics signals from the mill to the ability of the mill charge to cushion or prevent collisions between individual steel balls and the steel wall of the mill in the frequency ranges below 10 kHz. The ease of direct measurement without contact with the process stream, together with the ability to reflect the internal mill conditions, makes acoustic analysis potentially important in mill control.

The experimental set-up consisted of a 20 x 20 cm laboratory ball mill. The shell was manufactured from steel without any lining. 125 Steel balls with a diameter of 25 mm were used, with a total volume accounting for 33% of the total mill volume. The charge mass was 8.5 kg.

The mill speed was set to 65 rpm (i.e. 69% of the critical speed). The ore charge volume was calculated as 1 litre based on the voidage between the balls, with the average particle size smaller than 1600 µm. The charge was ground for 30 minutes and wet screened at 53 µm.

The mill acoustics were measured with a real time analyzer and an Apple II Microcomputer. A program was written in BASIC to monitor the acoustic signals in the frequency band between 25 Hz and 20 000 Hz and to integrate the sample over a 16 second sample period. The sampled data were further reduced to the frequency components between 2 and 8 kHz and the average power level of the signals were calculated for each minute of the grind.

Magnetite ores with pulp concentrations ranging form 60% - 84% solids by mass, as well as molybdenite ores with pulp concentrations ranging from 64% - 76% solids by mass, were investigated. This was followed by a study of the effect of grinding additives in the system.

Investigation of the results showed that the acoustic signal in the mill is mainly a function of ball-ball collisions and that the presence of particles in a certain size range modify or block these acoustic emissions. The results showed that as the number of particles of larger size decreased with increasing grinding time, the levels of the acoustic signals would rise accordingly. It was further illustrated that, as the pulp density increased, the change in the acoustic signals could be used to identify the rheological regime of the pulp. This in turn could be used to optimize the grinding process. Additives caused a reduction in pulp viscosity owing to increased particle dispersion in the pseudoplastic region. This further resulted in more effective grinding which could be attributed to the increased exposure of the ore particles to the grinding media.

#### *2.2.1.1 Mill Modelling with Acoustic Spectra and Principal Components*

In addition to their work on crushers, Zeng and Forssberg (1993a) studied the effects of operating parameters in laboratory-scale and industrial ball mills. The following discussion of their work is detailed in experimental, data analysis and modelling sections.

##### 2.2.1.1.1 Experimental:

Zeng and Forssberg (1993a) applied the technique to an industrial ball mill grinding iron ore. The feed material had a particle size smaller than 10 mm and consisted mostly of magnetite. The mill used in the study had an inside shell diameter of 3.92 m and length of 5.2 m. It was operated in an open circuit with a slurry density of 65% solids by weight. The mill was operated at 60% of the critical speed, with a charge volume of 35%. The charge was comprised of two sizes of steel balls (i.e. 60 and 40 mm) with each size accounting for 50% of the charge mass.

Two sensors were used to record the acoustic signals from the two sources, *viz.* the mill axis as well as the mill charge. The signal from the mill axis was measured by means of a shear structure piezoelectric accelerometer with a built-in pre-amplifier and AC output. The accelerometer was fitted with three lowpass (1, 5 and 15 kHz) and three highpass (3,10 and 1000 Hz) filters which were combined to eliminate disturbances of the DC and high frequency resonances to the original vibration signal. The sensor was mounted onto the bearing of the pinion axis after it was found that the sensor location affected the total signal energy (loudness), but that the effect on the variation of the signal spectra was minimal.

The acoustic sensor dedicated to the mill charge was a hypercardioid, condensing acoustic microphone. It had a reliable frequency range between 50 Hz - 20 000 Hz with a sensitivity of 6 mV/Pa (-44.4 dBV) at 1000 Hz. The output was an AC analogue signal. As the acoustic signal around the vertical cross section of the mill shell varied, the microphone was placed next to the mill shell at the center of the abrasion zone.

The source signals were amplified and recorded onto digital audio tape (DAT) in the left and right channels respectively. The DAT recorder was operated at a sampling frequency of 48 kHz and 16 bits linear quantisation. The signals were digitized with a digital oscilloscope before it was processed with an IBM compatible personal computer. Preliminary studies showed that the frequencies of interest were below 3 kHz. The source signal was passed through a set of 4-cascade lowpass filters before data acquisition. The oscilloscope was set at a sampling frequency of 10 kHz, giving the highest effective frequency of 4 kHz according to the Nyquist criterion. Each signal sample was limited to 6.5 seconds of actual grinding time, owing to the memory limitation of the oscilloscope.

Sampling of mill data was done 45 minutes after a process change to ensure steady state conditions. Acoustic and vibration signals were recorded continuously for 10 minutes, while material sampling over the mill was conducted in the following order: mill feed, pulp temperature, mill discharge (consisting of the pulp density and product size). Power draw and feed rate were automatically recorded on the mill control system. The particle size distributions were analyzed through sieving and the 80% as well as the 50% cumulative passing undersize determined. Five samples from the original 10 minute recording were used for signal analysis.

The parameters recorded during the experiment were:

- Feed rate [t/h]
- Pulp density [%]
- Power draw [kW]
- Pulp Temperature [°C]
- Feed size [80% and 50% passing]
- Product size [80% and 50% passing]
- Acoustic spectra from the mill axis
- Acoustic spectra from the mill charge

#### 2.2.1.1.2 Data Analysis

Data were analyzed by sectioning the acoustic waveform into either overlapping or non-overlapping sections. 2048 points of the FFT spectrum were used per section.

This section was then multiplied by the so-called windowing function to compute the periodograms. A Hanning window was used by Zeng and Forssberg with a 60% overlap per section to compensate for voids in the waveform caused by the windowing function. The authors found that the energies of the spectral peaks were linearly correlated and they could thus use principal component analysis to reduce the independent variables into a few latent variables. Multiple linear regression was applied to the data to establish the relationship between key grinding parameters and the variation of spectra. Partial correlation analysis indicated that the key grinding parameters were power draw, feed rate, pulp density and mill product size.

The area underneath the peak of the power spectrum represented the energy of the signal at the specific frequency. Analysis of the power spectra showed that the total energies under all peaks of the spectra were similar for both the axial vibrometer, as well as the microphone next to the mill shell. The microphone picked up the signal emitted from the mill shell on the abrasion zone. The accelerometer sensed the signal coming through the three bearings, with each bearing in turn dispersing the direct signal. Zeng and Forssberg (1993a) concluded that the signal from the microphone contained more signal information than the mechanical signal. The acoustic signal from the grinding system contained mostly the mechanical and grinding media noise, and, as such, variations relating to the operating state were hidden in the main spectrum of the system. To estimate the variation for a base state, average system spectra were calculated from all the sample spectra and used as a basis of comparison for other system states.

Significant variation in the spectra was found at 50 Hz and 450 Hz for all eight grinding conditions tested by Zeng and Forssberg (1993a). The acoustic signal derived from the mill charge contained more information than the accelerometer signal, with the frequency band 1200 Hz - 1400 Hz denoting the movement of the mill charge in the abrasion zone. A sensitive microphone is able to pick up this change in acoustic pressure while the bearings and pinion axis disperse the signal to the accelerometer. Hence, signals from the microphone contain more information.

Principal component analysis reduces the number of variables in a data set by finding linear combinations of these variables that explain most of the variation. A new set of variables is generated which are orthogonal and ordered according to the degree of variation. The original data were centred by subtracting the mean of all

samples for the observation from the value of the specific variable. Principal component analysis indicated 73 and 116 original frequency components relevant to the vibration and acoustic signals respectively. The frequency components of importance for the vibration signal principal components were 112 Hz, 117 Hz, 171 Hz and 283 Hz. The important frequency components for the acoustic signal principals were 73 Hz, 112 Hz, 117 Hz and 229 Hz.

#### 2.2.2.1.3 Model Developments

Zeng and Forssberg (1993a) found that four latent variables could describe most of the variations in the original spectra. By applying multiple regression analysis the grinding parameters were related with the scores of the principal components. It was found that power draw was mainly related to the first two principal components. The model was better at predicting power draw with high feed rates than low feed rates. This is due to the smaller probability of collision between the mill media when the mill is filled with more material. Feed rate, and hence the mill charge, was mainly related to the third principal component. However, the modelling error was larger than the natural variation in feed rate. Pulp density prediction was affected by the first and fourth components, with the result following the natural tendency in the mill. The absolute error of prediction was within 2%. Ground product size was affected by the third component, and could be predicted satisfactorily.

The acoustic signal from the microphone contributed more to the result than the vibration signal from the mill axis, with feed rate and product size giving satisfactory results. Power draw and pulp density were predicted as combination of the two signals.

## 2.3 SUMMARY

The literature survey has shown the various techniques that have so far been used to obtain modelling data from the acoustic emission of the process. The work of Zeng and Forssberg (1993a; 1993c) has been surveyed in detail and will form the chief reference to the project.

# 3

# EXPERIMENTAL INVESTIGATION

## 3.1 INTRODUCTION

All experiments are a source of information. However, the method by which this information is gathered, is the most important aspect of any experiment. The general mill configuration, together with the important operating parameters, combine into a complex system that requires detailed knowledge for optimal control. The different experiments that were conducted to simulate the general parameters encountered in industrial applications, along with the equipment, are described in this chapter. The aim of the chapter is to introduce readers unfamiliar with the overall behaviour of tumbling mills with reference material both to what is available in the field and to the manner in which the experiments for this project were conducted.

## 3.2 EQUIPMENT

### 3.2.1 Laboratory Mill

A laboratory mill was modified for the project as shown in figure 3.1. It was rubber lined and fitted with a flanged lid to facilitate loading and to provide watertight closure in the event of wet grinding. The mill had a diameter of 200 mm and a length of 280 mm.

The mill was fitted with a 1.1 kW motor to provide the necessary torque for the application. Motor speed could be controlled by means of a variable speed drive, as well as a set of pulleys that permitted mill speeds of up to 98 rpm.

The mill was calibrated with a tachometer and the following relationship was found between the mill rotational speed and the inverter frequency, i.e.

$$y = 1.6382x + 0.3364 \qquad (3.1)$$

with y the mill speed and x the inverter frequency. A perfect fit was obtained for all the measured data points.

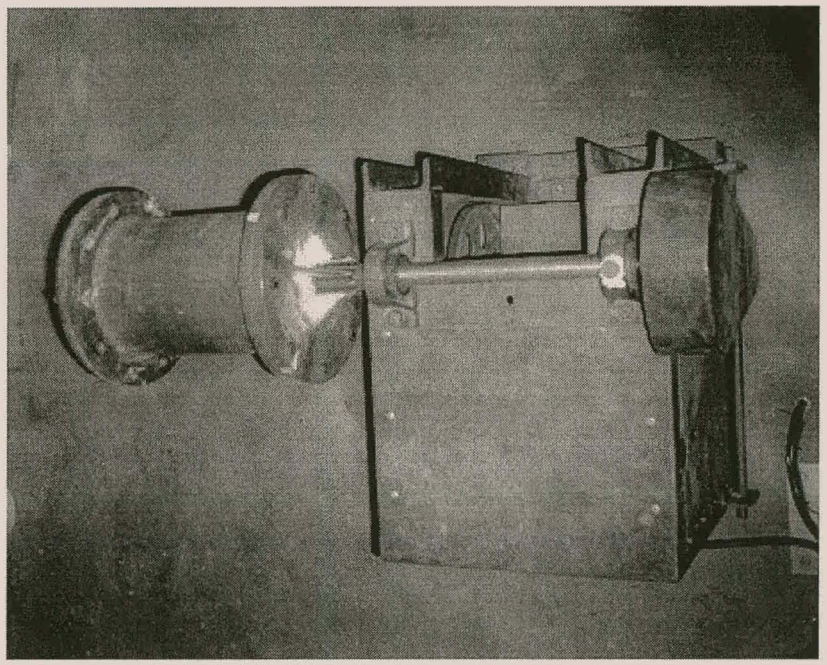

**Figure 3.1**. Photo of actual experimental set-up.

With the mill diameter 200 mm, the critical speeds ($C_s$) for the specific ball sizes were calculated from:

$$C_s = \frac{42.3}{\sqrt{D-d}} \quad \text{rpm} \qquad (3.2)$$

with D the mill diameter and d the ball diameter in metres. (See Table 3.1)

**Table 3.1**. Critical speeds for various grinding media sizes.

| **Ball size** | **Theoretical Critical Speed [rpm]** |
|---|---|
| 43 mm | 107 |
| 37 mm | 105 |
| 25 mm | 101 |
| Critical speed used in calculations | 100 |

### 3.2.2 Acoustic Equipment

Two directional microphones (Table 3.2) with cardioid pick-up patterns were used to record the sound emission from the mill. The specific microphone positions are described in chapter 4 together with the rationale behind the equipment placement.

**Table 3.2**. Microphone details.

| **Microphone details:** | |
|---|---|
| Manufacturer | Shure |
| Model | Prologue 16L-LC |
| Type | Condenser (Electret Bias) |
| Frequency Response | 50 to 15000 Hz |
| Polar Pattern | Cardioid (unidirectional) |
| Output level | -69.5 dB (0.33 mV) |
| Signal-to-Noise ratio | 48 dB (at 94 dB SPL) |

The signals from the microphones were amplified before further processing. A pre-amplifier was designed and constructed by CES (Centre for Electronic Services, Department of Electronic Engineering, University of Stellenbosch) for this purpose. The gain on the two input channels could be adjusted independently, with the amplified output signal sent to a PC for further processing.

An Intel Pentium II, 200 MHz with 32 megabyte RAM and a 2 gigabyte hard disk was used for signal and data capturing purposes. The amplified stereo signal from the pre-amplifier was routed to a sound card in the PC for processing. The features of the sound card are summarized in table 3.3. The signal was converted to digital form by the soundcard and stored on the PC's hard disk.

**Table 3.3.** Features of the sound card used to process acoustic signals.

| AWE 64 gold creative sound card details: |
|---|
| Stereo digitized voice channel |
| Full duplex |
| 16-bit and 8-bit digitizing in stereo and mono modes |
| Programmable sampling rates, 5 kHz to 44.1 kHz in linear steps. |
| Built in stereo amplifier |
| 6 W per channel with 4 Ω stereo output |
| Internal or external audio output amplifier |

## 3.3 EXPERIMENTAL PROCEDURE

A shematic diagram of the experimental setup is depicted in figure 3.2.

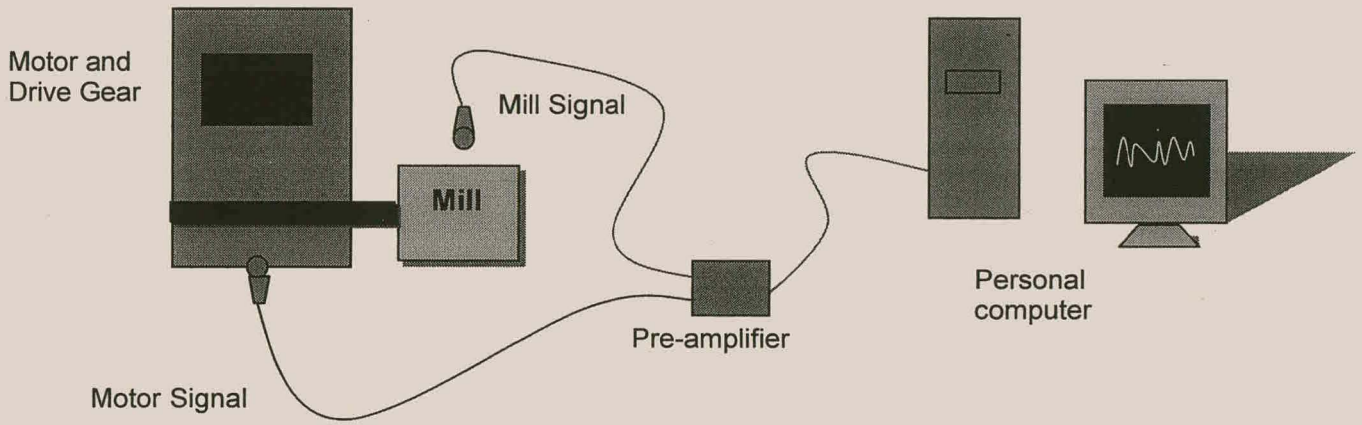


**Figure 3.2.** Schematic diagram of the experimental set-up.

### 3.3.1 Loading and Unloading the Mill

The mill was fitted with a flanged lid with a rubber seal for all tests. The entire milling unit was further fitted with a hinge to facilitate ease of loading. After cleaning the mill with compressed air (to remove trace amounts of dust remaining from previous experiments), the unit was tilted to the vertical loading position and the grinding media added to the mill. The pre-sieved sample was added afterwards. The flanged lid was bolted tight and the unit tilted to the horizontal milling position. The mill speed

and direction were set on the motor drive by selecting the corresponding frequency to the required mill speed, and selecting it on the LCD display.

The microphones were placed in their respective predetermined positions, one next to the toe of the charge and the other in the motor housing. The microphones and pre-amplifier were switched on at their respective power switches, and the pre-amplifier checked for the correct amount of gain on each channel. All leads and jacks were checked prior to recording.

The recording program was activated, and the filename as well as any experimental information deemed necessary were entered into a log file.

The mill was started with a ramp time of 15 seconds. This meant that the speed of the mill was ramped up exponentially to full speed over a period of 15 seconds. This provided mixing of the mill contents as well as sufficient time to start the recording program.

Data were recorded automatically. With the completion of a run, the mill and recording program were stopped and the contents removed from the mill. The contents were removed with the unit in a horizontal position. Containers were placed beneath the mill opening and the flanged lid removed. The mill charge was transferred to the containers, with fines brushed out with a soft brush. The grinding media were removed and the batch screened. In the event of a wet run, the slurry was pressure filtered and dried before being screened.

### 3.3.2 Screening

The 1 kg sample was split into ten 100g fractions with a rotary splitter. Two samples were taken as representative of the batch and screened.

The large fractions, e.g. 600 µm, 1400 µm, 2800 µm and 4000 µm, were sieved by hand to reduce fines build-up on the wire mesh, while the smaller fractions, e.g. <75, 75 µm, 106 µm, 150 µm, 212 µm, 300 µm and 425 µm, were sieved using a mechanical shaker. Initially problems were encountered with fines in the fractions smaller than 212 µm owing to blockage of the screen apertures. This problem was

alleviated by the addition of small (10 mm) ceramic balls between the various screens. The ceramic balls acted as micro-shakers and significantly improved the efficiency of screening. After 5 to 10 minutes on the shaker, each fraction was weighed and the mass recorded.

Wet screening was attempted, but after various failed batches it was decided to continue with the dry screening regime. It was found that the values of the different sieved samples were comparable when the same screening method was applied to all the samples. This made the general trends that occur during grinding visible and as such did not jeopardise the aim of the research described in this thesis.

## 3.4 EXPERIMENTS

Experiments were designed to study the effect of known process conditions on the sound emission from the mill. The main process parameters, e.g. particle size, amount of milling media, mill speed, mill load, slurry density and ore type were simulated and varied in order to cover the widest possible range of conditions in a laboratory mill. Please refer to Appendix A for all the experimental details.

### 3.4.1 Batch Experiments with Silica

A series of experiments were conducted with silica to study the effect of different process conditions on the sound emission. A uniform particle size was selected with all of the particles between 250 µm and 500 µm. In this way the particle size could be kept comparatively constant and the effect of different operating conditions could be studied.

#### *3.4.1.1 Media*

By varying the number of balls in the mill, the influence of the steel grinding media was studied in the laboratory. The number of large (13) and medium (13) balls were kept constant, while the number of small balls was varied. It was decided to vary the number of small balls rather than the number of large balls, as the degree of possible

experimental error would be smaller when varying a large quantity of small balls in contrast to varying a small number of large balls.

#### *3.4.1.2 Mill Speed:*

The rotational speed of a mill determines the rate and manner in which the grinding media and the ore collide and abrade inside the mill. As mentioned previously, high speeds tend to lead to cascading of the charge, where particles are broken by impact. Lower speeds lead to cataracting and abrasion where the grinding media roll down the face of the charge, grinding the particles by abrasion and leading to finer product. The mill speed was increased from 16 rpm to 98 rpm during the experiment in order to obtain the acoustic information over the entire range of mill speed operation.

#### *3.4.1.3 Ore Content*

Batch experiments were conducted with different quantities of ore to simulate the effect of changing feed rate in a laboratory mill. The charge and speed were kept constant, while the ore quantity was varied between 500 g and 5000 g for the various experiments.

#### *3.4.1.4 Water Addition*

Water addition plays an important role in wet grinding, as the most efficient grinding takes place when the pulp density and slurry viscosity are optimally controlled. Experiments were conducted with different slurry densities. 1 kg of ore was used with water volumes that varied between 0.3 and 5 litres, e.g. between a dry, sticky slurry and a low density slurry.

#### *3.4.1.5 Dry Conditions*

On many different concentrator circuits, different ore bodies are treated in the same circuit. With many platinum group metal concentrators, both UG2 and Merensky ore

bodies are often treated in the same concentrator. Unfortunately these two ore types exhibit different flotation properties, leading to inefficient performance if the operators are not alerted in time. These two ores were selected owing to the common knowledge on South African platinum group metal concentrators that operators can distinguish between the two ores by listening to the sound of the mill.

Please refer to Appendix A for the mineralogical details of these two ores.

With the aforementioned in mind, specific experiments were designed to simulate the effect of both changing ore type and particle size on the mill sound. Four batches of ore were made up, one batch containing coarse (+4000 µm) and the other fine (-4000+2800) particles for each ore type. From these batches, samples were made up containing 70% of Merensky ore and 30% of UG2 ore, and vice versa for each particle size. This gave six combinations for batch recordings. A final experiment was conducted with equal quantities of ore with similar particle sizes.

Table 3.4 shows the experimental design for the combination experiments.

The samples made up for combination experiments one to four were tested in slurry with a 60% solids concentration. Again this was done to compare the efficiency of sound monitoring on wet and dry grinds.

**Table 3.4**. Experimental design for ore combination experiments.

| Experiment | Merensky ore size | UG2 ore size | Merensky ore quantity | UG2 ore quantity |
|---|---|---|---|---|
| 1 | +4000 | +4000 | 70% | 30% |
| 2 | +4000 | +4000 | 30% | 70% |
| 3 | -4000+2800 | -4000+2800 | 70% | 30% |
| 4 | -4000+2800 | -4000+2800 | 30% | 70% |
| 5 | +4000 µm | -4000+2800 | 70% | 30% |
| 6 | -4000+2800 | +4000 | 30% | 70% |

### 3.4.2 Merensky Ore :

*3.4.2.1 Dry Run*

Pre-crushed Merensky ore was milled in order to study the effect of changing particle size on the sound emission. The experiment was conducted in 10 steps. Each step represented a time milled from 5 to 50 minutes, with each step starting at the initial condition. This led to a data structure where each consecutive experiment contained sound information comparable to the preceding experiment, along with the additional information contained in the extended experimental period as indicated in figure 3.3.

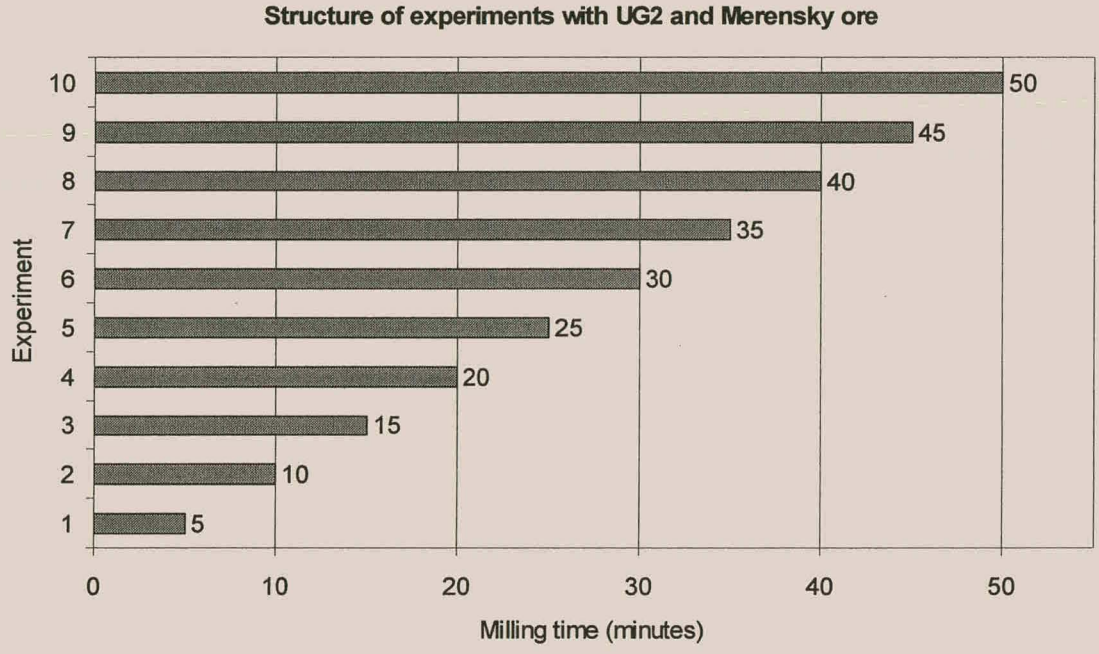


**Figure 3.3**. Particle size experiments: experimental structure.

This method was followed after it was found that the milling curve for a single batch, which was stopped at five minute intervals, screened and then milled again, differed from a continuous grind. This can be attributed to the accumulation of particles in the dead zone of the mill, which are removed when the mill contents are removed. As such, the ore was continuously ground for the required time without stoppages as shown in figure 3.3. The product of each run was screened and the milling curve and cumulative percentage undersize determined for the Merensky sample.

#### *3.4.2.2 Merensky Ore : Wet Run A*

In order to study the effect of slurry on the mill sound emission, five samples that had already been milled from the Merensky dry grinding experiment were made up to a slurry of 60% solids content. A batch recording was made for the first 10 seconds of operation and the mill was then stopped. With the particle size distribution known, the differences in sound emission could be compared for dry and wet conditions.

#### *3.4.2.3 Merensky Ore : Wet Run B*

A second exploratory run was conducted with Merensky ore in wet media. However, in this experiment a slurry with a 60% solids content was made up and milled for 25 minutes. The milling process was recorded continuously.

### 3.4.3 UG2 Ore

The same procedure was used for fine crushed UG2 ore as was used for crushed Merensky ore, described above. Trials were conducted with the ore at different milling times and hence different particle sizes. The particle size distribution was measured by screening after the grind. Analysis of the recorded signals showed that five recordings were corrupted during the experiment owing to hardware malfunctions. This was not a serious problem, as data for the specific duration could be sampled from longer runs and the particle sizes correlated with the time milled. No wet milling was conducted on UG2 ore, as the wet milling done on the Merensky ore was purely for exploratory purposes.

## 3.5 SUMMARY

The equipment used in this study, consisting of the mill and drive, as well as the cardioid microphones and PC with sound card have been detailed and described together with the various considerations taken in using them. The different experiments conducted on silica, Merensky ore and UG2 ore have been presented with their experimental designs in order to give an indication of the milling systems that have been investigated in this thesis.

# 4

# ACQUISITION AND PROCESSING OF ACOUSTIC SPECTRA

## 4.1 INTRODUCTION

Data processing plays a crucial role in the way the information obtained from the process is described. Incorrect and insufficient sampling and processing techniques can lead to erroneous results, which can render the experiment useless. In this chapter the theory and the methods which were followed in the acquisition and processing of the data are discussed.

## 4.2 GENERAL THEORETICAL CONSIDERATIONS

### 4.2.1 Signal Processing

In order to make use of the information contained in the signal the correct methods for extracting the data have to be applied. The fast Fourier transform (FFT) is a mathematical tool which involves the decomposition of the signal in terms of its frequency components (Proakis and Manolakis, 1996).

The original signal is broken into components in the same way a prism breaks light into distinct bands of colour. By analyzing the components of the FFT, a unique signal signature can be obtained. Alternatively, by adding the different components the original signal can be reconstructed.

Without going into the mathematics involved in generating the necessary equations, the function for the Fourier series coefficients can be written as

$$F(w) = \frac{1}{T_p}\int_{T_p} f(t)e^{-j2\pi F_0 t}dt \qquad (4.1)$$

with $T_p$ the period and F(0) the fundamental frequency.

Parseval's relation gives the relation between a time signal f(t) and its Fourier transform F(w) as

$$\int_{-\infty}^{\infty}|f(t)^2|dt = \frac{1}{2\pi}\int_{-\infty}^{\infty}|F(w)|^2 dw \qquad (4.2)$$

By using this relation the distribution of the energy in the signal can be obtained as a function of the frequency components. This in turn gives rise to the signal's power density spectrum.

Stremler (1990) summarized the power spectral density of a signal as the energy per unit of frequency which displays the relative energy contributions of the various frequency components. The area under the power spectral density function gives the energy within a given band of frequencies.

Various methods have been devised to estimate the power spectrum from the given signal. Parametric methods make use of extrapolation to calculate autocorrelation and need a priori information on how the data were generated. Non-parametric methods are relatively simple and do not make use of any assumptions regarding the generation of the data set. Non-parametric methods are also easier to compute using fast Fourier transforms. Welch's method (1967) for averaging periodograms was used in this research. The method allows the data sections to overlap and windows the data segments before computing the periodogram.

This gives the periodogram as

$$P(f) = \frac{2}{T_p}\left|\int_0^{Tp} w(t)f(t)e^{-j2\pi Ft}dt\right| \qquad (4.3)$$

with w(t) the windowing function that is used to isolate the data segments from the data set. The final periodogram is averaged, unbiased and consistent.

The windowing function used in this investigation was the triangular Bartlett function (Proakis and Manolakis, 1996)

$$w(n) = 1 - \frac{2\left|n - \frac{M-1}{2}\right|}{M-1} \quad \text{for } 0 \leq n \leq M\text{-}1 \qquad (4.4)$$

where n is the bin number and M-1 the length of one section for the calculation of the FFT. Principal component analysis (Appendix H) can subsequently be used to reduce the number of highly correlated input variables (components of the frequency spectra). The few latent variables can be used as the inputs to models relating the acoustic signaler to the comminution parameters of interest.

### 4.2.2 Statistical Modelling

The acoustic data obtained from the mill were modelled by making use of linear regression and an artificial neural network (Appendix I). The linear regression models are discussed in Appendix G.

## 4.3 DATA ACQUISITION

The necessary theoretical relationships have been explained in the previous section. The proceeding sections will describe the methods involved with the acquisition of the data, together with the methods employed in the data analysis of the acoustic spectra.

### 4.3.1 Equipment

The sound emitted during the milling process was recorded by using two acoustic microphones, a pre-amplifier and a soundcard in a personal computer. The signals were recorded and stored on hard disk.

Other authors (Zeng and Forssberg, 1993a; 1993c) have made use of both acoustic microphones and accelerometers for the acquisition of the mill acoustic signal. After

investigation of Zeng and Forssberg's results (1993a) it was decided to discard the accelerometer from the investigation. According to Zeng and Forssberg, the accelerometer recorded the same signal as the microphone used, but with the added noise from the drive gear included in the spectra. The mill signal therefore gives a better indication of the actual conditions inside the mill. An additional microphone was included in the study to enable the use of an adaptive filter on the data.

#### *4.3.1.1 Microphone Positions*

The microphone positions play a critical role in the determination of the correct signal from the mill. For this reason a study was undertaken by the Digital Signal Processing group (DSP) of the Department of Electrical and Electronic Engineering at the University of Stellenbosch (1997) to determine the optimal microphone positions. Two microphones were used in the study, mainly owing to the limitation of two input channels (2 x mono = 1 stereo) posed by the sound card. It was decided to use one microphone to record the signal emitted from the mill during grinding and to use the other for the recording of ambient noise. The background noise could therefore be eliminated by applying an adaptive filtering method to the composite signal.

The mill microphone was placed next to the shell of the mill, with the sensor face approximately 10 mm – 15 mm away, placed perpendicular to the shell. The mill rotation was set in such a direction that the mill was turning toward the microphone, with the mill contents sliding and abrading against the shell of the mill, towards the toe of the charge. This is the region in the mill where the most noise is generated by the tumbling media. Figure 4.3 gives a schematic representation of the sensor position.

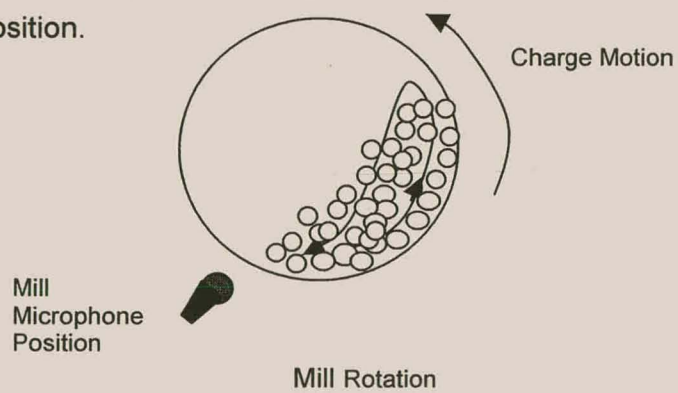


**Figure 4.3.** Schematic diagram of the position of the mill microphone.

The tests by the DSP group made provision for the following microphone positions as indicated in figure 4.4:

(In all cases the mill sensor was left in the same position.)

1. Pointed at the motor, at the furthest point from the mill.
2. Pointed at the motor with the protective cover shielding the microphone from the mill.
3. At the same position as the mill microphone, but facing in the opposite position.
4. On the other side of the laboratory, facing away from the mill.

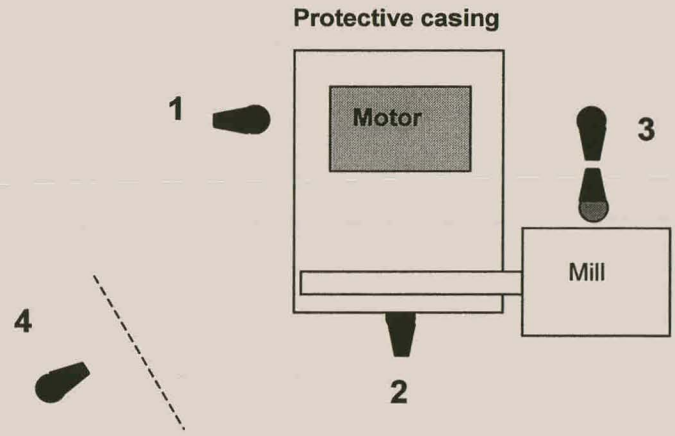


**Figure 4.4.** Different sensor positions that were investigated.

After analysis of the filtered data, it was found that position 2, with the sensor inside the mill casing, yielded the best results with filtering techniques.

#### *4.3.1.2 Signal Recording*

Microphone position 2 was used for all the experiments. The signal from each microphone was amplified from 0.33 mV by a pre-amplifier built specifically for the purpose. Each channel had its own gain control for individual gain adjustments. The amplified signal was recorded onto the hard disk of a personal computer via a sound card. By making use of Nyquist's sampling theorem, which states that the sampling rate should be at least 2 times higher than the desired highest frequency, a sampling rate of 11025 Hz was chosen, giving a highest recorded frequency of 4410 Hz. Analysis of the signal showed that the lower frequencies contained most of the

information from the grinding process. Samples were thus recorded at 11025 Hz with 16 bit linear quantization (samples stored in 16 bit data packages).

### 4.3.2 Recording programs

Two programs were used to record the raw signals on to hard disk, e.g. *Mill Recorder* and *Coolpro* as described in more detail below. In order to make comparison of different acoustical samples possible, the acoustical data was sectioned into files with an identical number of sample points with *Coolpro.*
All sound files were saved in the standard Windows PCM ".wav" format.

#### *4.3.2.1 Mill Recorder*

The Mill Recorder was specifically written for the project in Delphi code by DSP group member, Carl Bellingham. The program had the following features:

- Continuous batch-wise recording.
- Adjustable sampling rate (datapoints per second), recording interval (duration between recordings) and recording time (length of recording).
- Log file.

The program made it possible to record continuous runs with exact sample sizes at pre-determined intervals. This method of sampling made comparison between samples of different runs, measured at the same grinding time, possible. All the continuous Merensky and UG2 ore runs were recorded using this program.

A typical run was recorded by first entering the desired file name and adding any additional information to the log file in the text box provided. This information was combined with the log of files recorded during the trial and stored in an ASCII text ('.txt') format for reference purposes. The desired sampling rate (typically 11025 Hz), recording interval (50 seconds) and recording time (10 seconds) were selected before starting the recording. The mill was started manually with a ramp delay of 15 seconds. This gave the operator enough time to start the mill, move over to the

personal computer and start the recording once the mill had reached operating speed.

The program performed well for the given parameters. However, the following comments can be made with regard to the program:

- Recordings with large sampling rates (44 kHz) and long durations (30 seconds) were not possible. This can be attributed to limited computer memory and not necessarily a fault in the program.
- The data log file was useful for reference purposes.
- The program is a useful tool, which avoids the hassles of manually recording acoustic samples every few seconds.

*4.3.2.2 CoolPro*

Coolpro is a commercial program with various sound editing features such as recording, multichannel mixing and batch processing to name but a few. The program was used for recording of batch trials where only one sound sample per run was recorded.

To record a signal, a sampling rate was chosen and the recording started when it was deemed necessary. After the sample was recorded for the desired duration, the recording was stopped and the file saved under a file name. Typical sample lengths were in the order of 10 to 15 seconds. The real-time display of the recorded signals was useful for the early detection of experimental errors, such as microphones or the pre-amplifier left off during a run.

The program was further used to edit the sound files from stereo to mono, and to change the sampling rate when required. This proved very useful for the separation of the mill signal from the motor signal for processing purposes. Files were transformed in a batch process from stereo to mono, as well as down sampling from 16 to 8 bit linear quantisation. All batch recordings for the silica and combined Merensky and UG2 ore experiments were recorded with this program.

## 4.4 PRE-PROCESSING

The recorded signals were pre-processed to omit as much of the irrelevant data from the database before applying detail processing and classifying methods to the data. The following methods were used:

### 4.4.1 Signal Isolation

The mill signal was isolated from the motor signal by digitally removing the motor signal components from the combined stereo signal. This was done by making use of a transformation in CoolPro. The recorded signal was downsampled from 16 to 8 bits to allow processing in Matlab 4.0.

### 4.4.2 Computing the Power Spectral Density

The second stage of processing was done in MATLAB 4.0, by Mathworks. The monotonic mill signal was read into memory in MATLAB. The power spectrum density function of each signal (approximately 100 000 data points) in the data set was computed in MATLAB, using a Bartlett windowing function. The Bartlett function is triangular, and was chosen as a simple windowing function without large side lobes such as found with a rectangular function. Large side lobes lead to undesirable ringing effects in the filter frequency response. It is therefore desirable to reduce the ringing effect and hence the smoothing of the data in the transformed frequency domain.

The power spectral density (PSD) of the signal was computed using Welch's averaged periodogram method. The signal was divided into 512 overlapping sections, each of which was detrended in MATLAB, then windowed by using the Bartlett window. The signal was zero-padded to a length of 512 points. The power spectrum was formed by squaring the length of the overlapping sections and averaging their discrete Fourier transforms. The sections were overlapped with 128 points per neighbouring section. The result was a power spectrum vector with 257 samples. These samples explain the intensity or volume of each respective

frequency in the mill signal. The power spectral densities were saved in ASCII format from where they could be exported to a spreadsheet (EXCEL).

### 4.4.3 Database Construction

Two databases were constructed in a spreadsheet, with one containing the 257 power spectral density (frequency) variables and the other containing the manipulated, measured response and operating variables.

The process variables involved, besides the frequency variables were:

- W (mill speed, rpm)
- Nb (# small balls)
- m (feed mass)
- X (ore type)
- d+4000**
- d2800
- d1400
- d600
- d425
- d300
- d212
- d150
- d106
- d75
- d-75
- F80 (80% passing size)
- F50 (50% passing size)

**The d-* sizes were calculated as percentage undersize. For this reason d+4000 was discarded as all ore particles were smaller than 4000 µm and d+4000 was a constant, e.g. 100%.

## 4.5 DATA PROCESSING

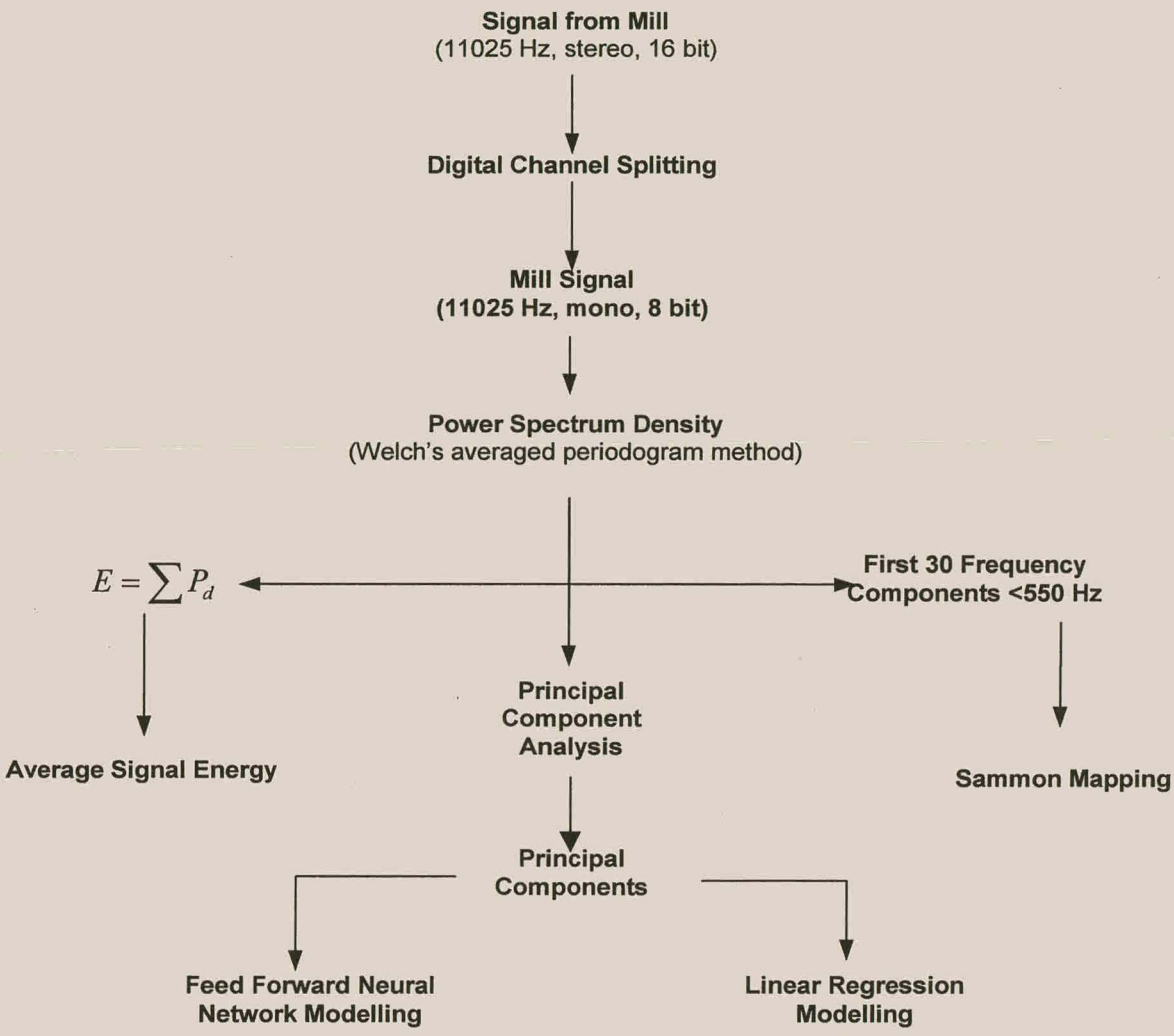


**Figure 4.5**. Data processing routes

The different routes followed for data processing are illustrated in figure 4.5. The power spectrum of the mill signal was used as the basis for further processing. Two main routes were followed, e.g. direct application of the power spectra in the average energy method and Sammon mapping, as well as the extraction of the principal components for modelling purposes.

### 4.5.1 Average Signal Energy

The average signal energy was calculated from the power spectra. Each power spectrum vector was integrated over the period of the signal. This gave a direct indication of the energy or volume of the signal for the duration of the recording. The sample duration was 10 seconds for the UG2 and Merensky recordings, while the batch recordings had durations between 10 and 15 seconds.

### 4.5.2 Sammon Map

A Sammon map is used to condense a set of data containing *n* variables into a data set containing data of lower dimension. The most common application is to reduce a set of data to 2 or 3 dimensions for visualization. From these data clusters with similar properties are grouped together. Sammon maps find particular use in system control as various operating regimes tend to cluster according to the generic property of the group. For example, if control is based on the colour of a liquid, a clear liquid would map to a different region on the Sammon map than an opaque liquid. If a system change results in a milky liquid between the two operating regions, it would be possible to track the changes on the Sammon map, and adjust the system setpoints to return to the original operating state provided that the relationship between the original variables and positions on the Sammon map are known. Similarly, the acoustics originating from the mill during grinding may be plotted on a Sammon map and used for control.

An algorithm developed by G.P.J. Schmitz (Intelligent Process Systems Group, Department of Chemical Engineering, University of Stellenbosch) was used to give a Sammon representation of the acoustic data. The algorithm made use of the same principles as those proposed by Mao and Jain (1995) by using a neural network to obtain the smallest error in the representation of the data. (See appendix F for more on Sammon maps).

The number of free parameters or nodes in the Sammon network were calculated from *N x d* where N is the number of samples and d the number of variables or dimensions of the original data set.

183 normalised power spectrum samples were presented to the Sammon map. The number of free parameters were calculated as 47 031 with 257 frequency components per sample. Such a large network would definitely not converge in a matter of seconds! The number of frequency components were reduced to 30 by analysis of the various power spectra. Visual inspection revealed that the components below 550 Hz contained most of the variance in the data between the individual sample vectors. For this reason the components below 550 Hz were used as input to the Sammon map. The number of free parameters for this input matrix were 5 490 (183 x 30) and was processed on a Pentium Pro II personal computer for 10 000 iterations without significant hardware limitations.

### 4.5.3 Principal Component Analysis

The power spectrum data were normalised and the number of dimensions reduced by principal component analysis. Five principal components were extracted by using the STATISTICA software package from Statsoft, California. The respective factor loadings, eigenvalues and factor scores were obtained for the different data sets, e.g. Merensky ore, UG2 ore and the batch experiments, and saved in a spreadsheet for further processing. Five factors were selected as this was the smallest number of principal components which could describe 80% of the variance in the data for all the data sets. The principal components extracted were further used for modelling by linear regression and neural networks. Please refer to Appendix H for the deriviation of principal components. The principal component results are presented in Appendix B.

### 4.5.4 Modelling by Linear Regression

Linear regression was applied to the Merensky, UG2 and short batch experimental data sets. The F50 and F80 (50% and 80% passing cumulative undersize fractions) parameters were modelled for the two ore types by using the principal components of the frequency spectra. The individual process parameters which were studied in the batch experiments, e.g. mill speed, % ore content, % water content, ball charge number and combination parameters, were modelled by using linear regression in

EXCEL, by Microsoft. The model results are summarized in Appendix C and the theory in Appendix G.

### 4.5.5 Modelling by a Feed forward Neural Network

The feature vectors of the UG2 and Merensky data sets that were extracted by principal component analysis, were predicted by means of a feed forward neural network in MATLAB, by Mathworks. The network consisted of 5 input nodes, two hidden layers with 9 nodes each and an output layer with 12 nodes. 63 Merensky and 38 UG2 samples were respectively used to train the network by means of backpropagation. The five principal components were first normalised before training for 10 000 iterations.

To test the network, the same that were used for prediction by the network, were first used as inputs, and the outputs predicted by the feed forward network. A validation data set was constructed for both ore types from acoustic data obtained from independent recordings on the same mill, with ore samples from the same batch as those of the training set. The first 10 minutes of a continuous recording were used for the validation data set. The data were divided into samples of 10 seconds each, giving a total of 60 samples.

Please refer to Appendix I for some general introducing theory on neural networks. Results are given in Appendix D.

## 4.6 SUMMARY

This chapter has focussed on the methods followed to process the signal originating form the ball mill. The different methods, e.g. extraction of the power density spectrum of the mill signal, average signal energy, principal component analysis and feed forward neural network modelling have been presented. The theory behind these methods, as well the application thereof has been discussed and presented to give the reader a clear indication of the procedures followed to reach the results which are presented in chapter 5.

# 5

# RESULTS

## 5.1 INTRODUCTION

The results presented in this chapter demonstrate the deductions that can be made with regard to the condition of the mill and its charge by analysing the acoustic signature. The different breakage curves and cumulative undersize fractions are first given as an indication of the ore properties that influence the grind. This is followed by the results of the three main data processing routes studied in this research, e.g. linear regression and neural network modelling, Sammon mapping and average energy of the signal. In general it has been found that large particles have a pronounced effect on the mill acoustics, while small particles have a dampening effect on the amplitude of the mill signal. In the text, particle size refers to the particle size of the mill contents pertaining to each specific recording.

## 5.2 PARTICLE SIZE DISTRIBUTIONS

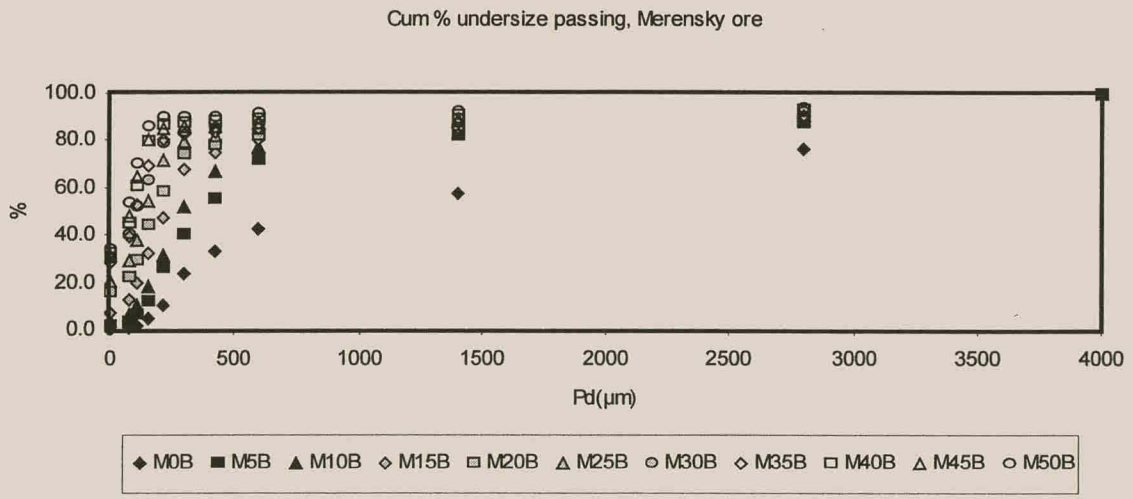


**Figure 5.1**. Particle size distributions for Merensky ore milled in a laboratory mill. Total milling time=50 minutes. (In the legend, M10B refers to milling of Merensky ore with steel balls for 10 minutes)

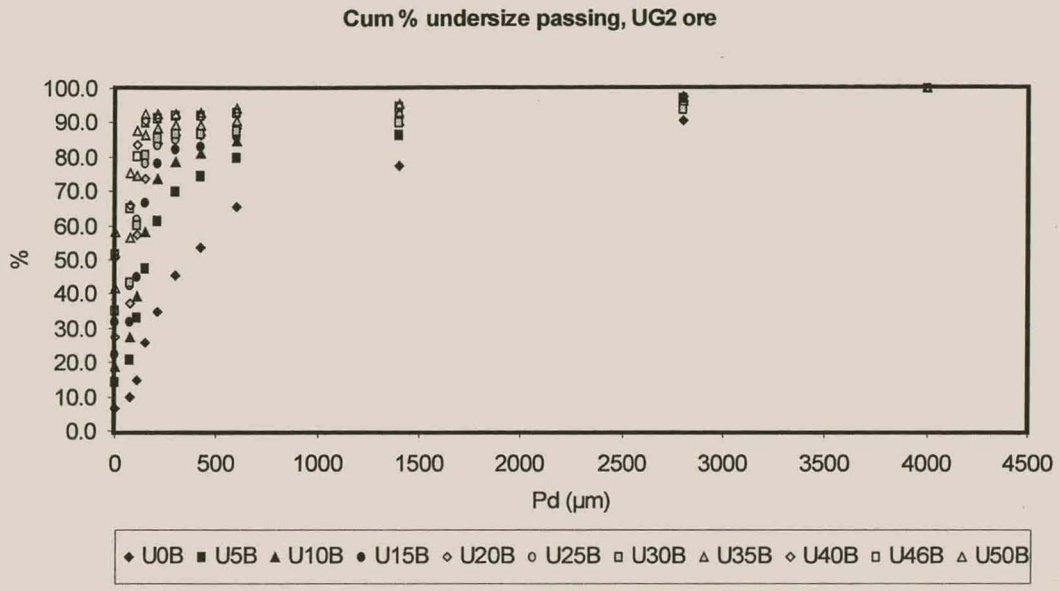


**Figure 5.2.** Particle size distributions for UG2 ore milled in a laboratory mill. Total milling time=50 minutes. (In the legend, U10B refers to milling of UG2 ore with steel balls for 10 minutes)

From the cumulative undersize curves of the Merensky and UG2 ore samples depicted in figures 5.1 and 5.2 the difference in initial sample makeup (U0B and M0B respectively) is observed. When the particle sizes passing 80% (F80) and 50% (F50) of the total sample mass, are plotted against time, an exponential breakage curve is obtained, as is shown in figure 5.3. From this curve the difference in breakage characteristics between the two ores are evident, with higher rates of breakage occurring with Merensky ore.

With a Rosin-Rammler distribution frequency, the various particle sizes in a sample would exhibit a linear relationship between the particle sizes and ln 100 (100-P) for an ideal ore, with P the cumulative % undersize. The slope of the line would therefore indicate the difference between various particle sizes and the total particles in the respective smaller sizes. A steep slope would indicate a sample with a large difference in size between the different particles. Conversely, a gradual slope would indicate a sample with little difference in mass percentage between the respective particle sizes. In figure 5.4, the particle size distributions and cumulative percentage undersizes for both Merensky and UG2 ores after 5 minutes, 25 minutes and 50 minutes grinding are plotted according to the Rosin-Rammler method respectively. From figure 5.4 it is clear that the ore samples

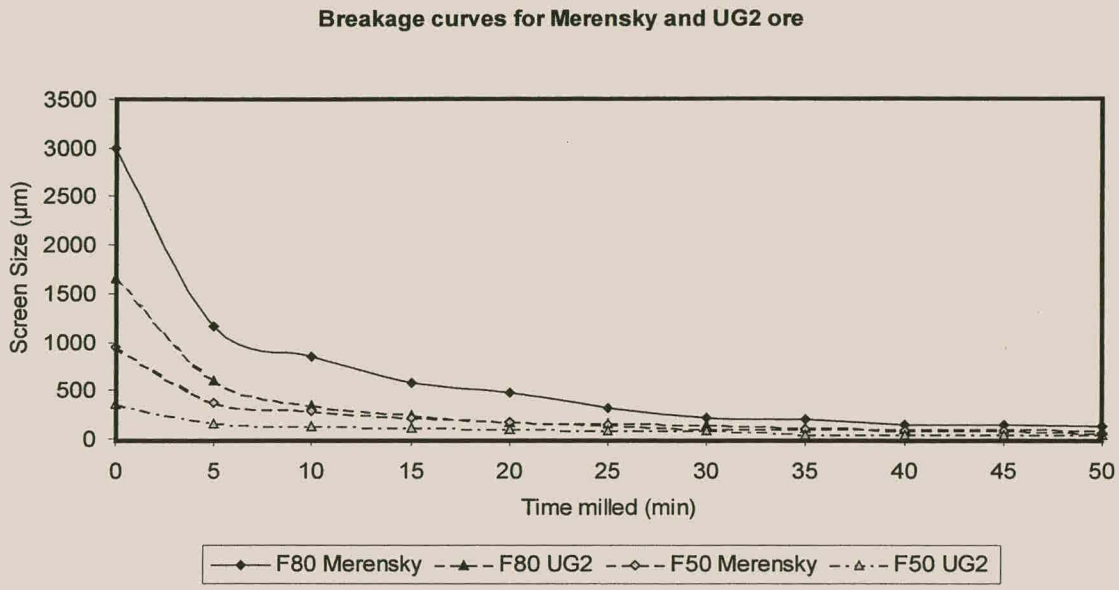


**Figure 5.3.** Breakage curves for 80% and 50% passing sizes for UG2 and Merensky ore.

do not exhibit perfect Rosin-Rammler distributions i.e. not an exact linear relationship, but consideration of the slopes of the various samples shows the great difference in slope between the samples milled at different milling durations. The samples with short milling times, i.e. 5 minutes, still showed a large variation in particle size distribution. The samples of both Merensky ore and UG2 ore show how the particle size distribution becomes more evenly spread after 50 minutes of

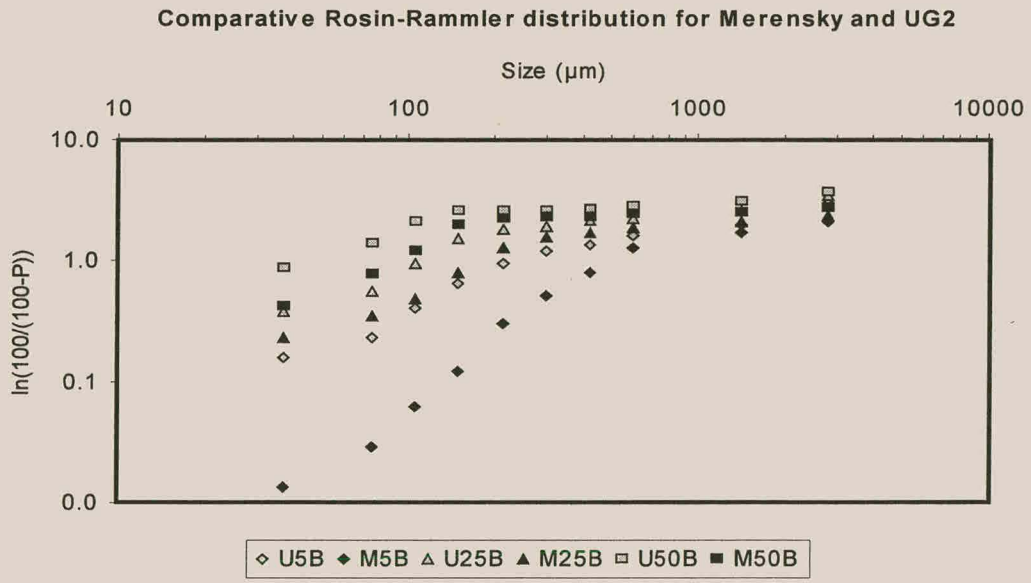


grinding.

**Figure 5.4**. Rosin-Rammler distributions for selected UG2 and Merensky samples

The Merensky and UG2 ores exhibit much the same slope in the Rosin-Rammler representation. Ideally the distribution would approximate a straight line with slope 1 for exponential breakage and particle size distributions. This confirms that with the time milled and initial particle size known, a reasonable approximation can be made of the mass of ore broken into any particular size fraction. The actual mass frequency of distribution for each size fraction is shown in figure 5.5. The same examples are used as in figure 5.4.

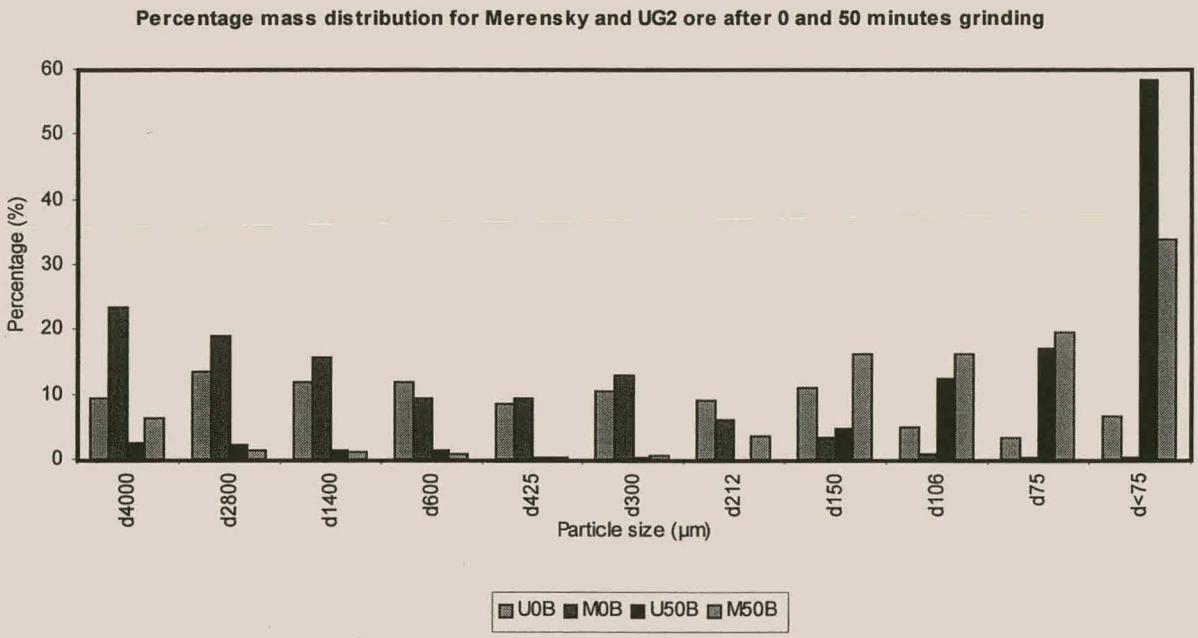


**Figure 5.5**. Frequency of distribution in each size fraction for 0, 25 and 50 minutes milled.

Analysis of figure 5.5 shows that the feed distribution for Merensky ore consisted mainly of particles larger than 212 µm, with the dominant fraction being larger than 4000 µm. UG2 ore was much finer in overall size distribution, with most fractions containing between 5% and 15% of the total sample mass.

Analysis of the sieve data shows that Merensky and UG2 ores do not have similar breakage characteristics. Both ores exhibited exponential breakage curves and when plotted according to Rosin Rammler's method for particle size distributions, the same tendency was observed for both ore types. The initial size fraction differed significantly, which gave rise to different acoustic spectra at start up.

## 5.3 DATA REPRESENTATION

Slight changes in sound are difficult to detect by the human ear. The following section will focus on two techniques which allow exploration of the data obtained from the experiments, i.e. the average signal and Sammon mapping methods.

### 5.3.1 Average Energy Measurements

The noise volume or amplitude of the signal is the principal parameter used by experienced operators to control the mill. In this work the average amplitude of the signal was determined from the power spectrum values. By integrating the power spectrum values, the average energy of the of the sample period could be obtained (Proakis and Monolakis, 1996). The average energy is expressed in decibels with regard to the system signals, i.e. 1 dB = 10 log (integral of the PSD).

#### *5.3.1.1 Short Batch Experiments*

The average level of noise emitted during the different batch experiments with silica ore, i.e. mill filling, mill speed, water content, ball charge and combination experiments, are depicted in figure 5.6.

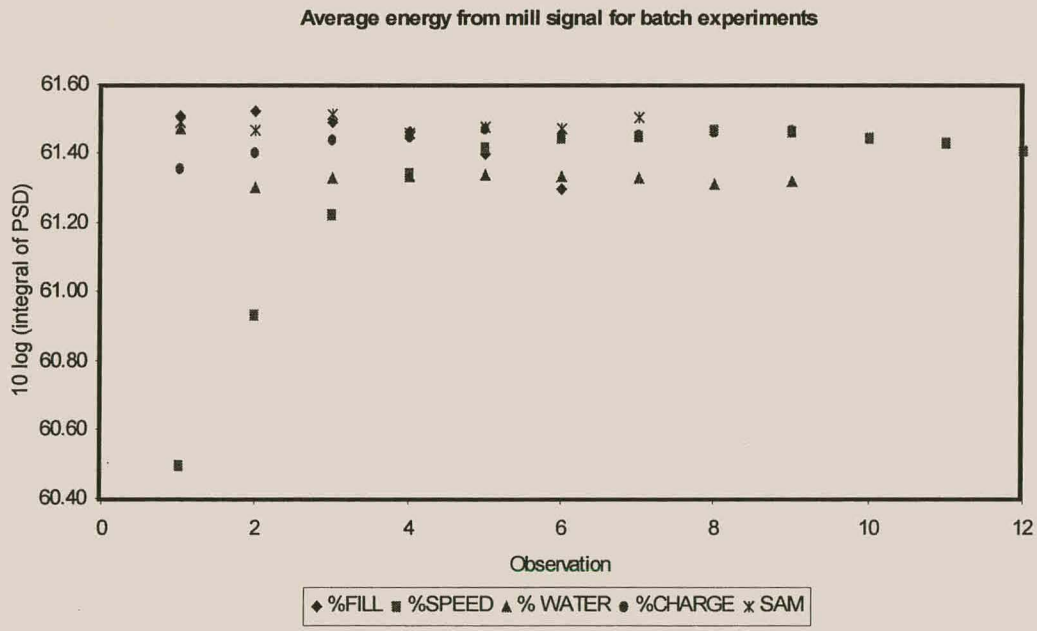


**Figure 5.6.** Average energy level of batch experiments

The mill speed experiment (solid squares) had the most pronounced effect on the noise level. From the graph it can be seen that the initial low speeds gave noise levels of 60.5 dB. The noise level followed the increase in mill speed until a maximum of approximately 61.5 dB was reached, further increase in mill speed led to reduced sound levels. This can be attributed to centrifuging of the charge at higher rotational speeds.

Change in the ore mass for the % Fill experiment (solid diamonds) led to an increase to 61.5 dB for the second experiment, where after all additional experiments led to a dampening of the level as the voids between the grinding media was filled by ore particles.

An increase in the number of small grinding balls (solid circles) led to an initial rise in sound level, after the fourth experiment however, the maximum sound level was reached at 61.45 dB. No increase in the sound level was observed for further ball additions.

Combination experiments (asterix) revealed that the average noise level did not deviate much. Noteworthy however, is that maximum levels of 61.5 dB were obtained for the experiments with large particles (+4000μm), while 61.45 dB was measured for the experiments involving small particles (-4000+2800μm).

Addition of water (solid triangles) revealed that the first experiment with a small percentage of water gave high noise levels of 61.47 dB. The first increase in water content gave a level of 61.30 dB, but with further addition of water the noise values remained constant around 61.33 dB. This indicates that too much water in a mill hampers the grinding process in a laboratory batch mill, which leads to a reduction in the amount of effective collisions whereby ore particles are broken as water content increases.

The increase in quantity of the respective variables gave a clear indication of the effect of a single parameter on the intensity or amplitude of the signal. In these experiments the basic mill operating regions were simulated, i.e. underfilled and overloaded mill, slow and fast rotating mill and mill steel content. General operating deviations would not be determined accurately by the average signal amplitude. The main advantage however, lies with major deviations from the normal operating state.

A good example is the mill load (% Fill, solid diamonds, figure 5.6) which reduces the amplitude substantially during overloaded mill operation. This was also the basis of design for the mill controller described in the Measurement and Control magazine (1963).

From the silica experiments discussed above, it was found that dampening played the most important role in the acoustic emission from the mill. This was well explained by the ore filling (FILL) and water addition (SLUR) experiments where the available free area for ball-ball collisions decreases as the contents of the mill increases, either by addition of water or ore.

The most pronounced effect on the acoustic signals from an external operating condition is from the steel charge. After a maximum number of balls (60), the number of ball-ball collisions dominate the characteristics of the signal. The mill speed is the only parameter which is directly related to the motion of the charge. As more momentum is transferred to the charge, more ball-ball interactions are made possible by an increase in the mill speed. With increasing mill speed, the rate and intensity of collisions increase, until the mill load starts to centrifuge. At this point the intensity of the collisions starts to decrease, with a corresponding decrease in the total acoustic energy emitted from the mill.

With the Merensky and UG2 combination experiments the average particle size was kept uniform for each fraction of ore. As no real change in the distributions or variations in particle sizes was encountered, no real change in acoustic emission was expected. This was confirmed by the average energy, where no meaningful variation in the energy level was found for the different combinations.

#### *5.3.1.2 UG2 and Merensky Experiments*

The calculated noise level for both the UG2 and Merensky experiments conducted for 50 minutes of grinding are depicted in figure 5.7. From the graph it is evident that the UG2 ore maintained a slightly higher noise level than the Merensky ore. The slight fluctuation in the noise level can be attributed to the 10 second sample window used at each experimental sample point. The random processes occurring in the mill would therefore, either be included or excluded from the sample window. Of note is that both grinds terminated at similar noise levels, which might indicate that grinding

led to similar product sizes over the 50 minute grinding interval as indicated by the particle size distributions in figure 5.3.

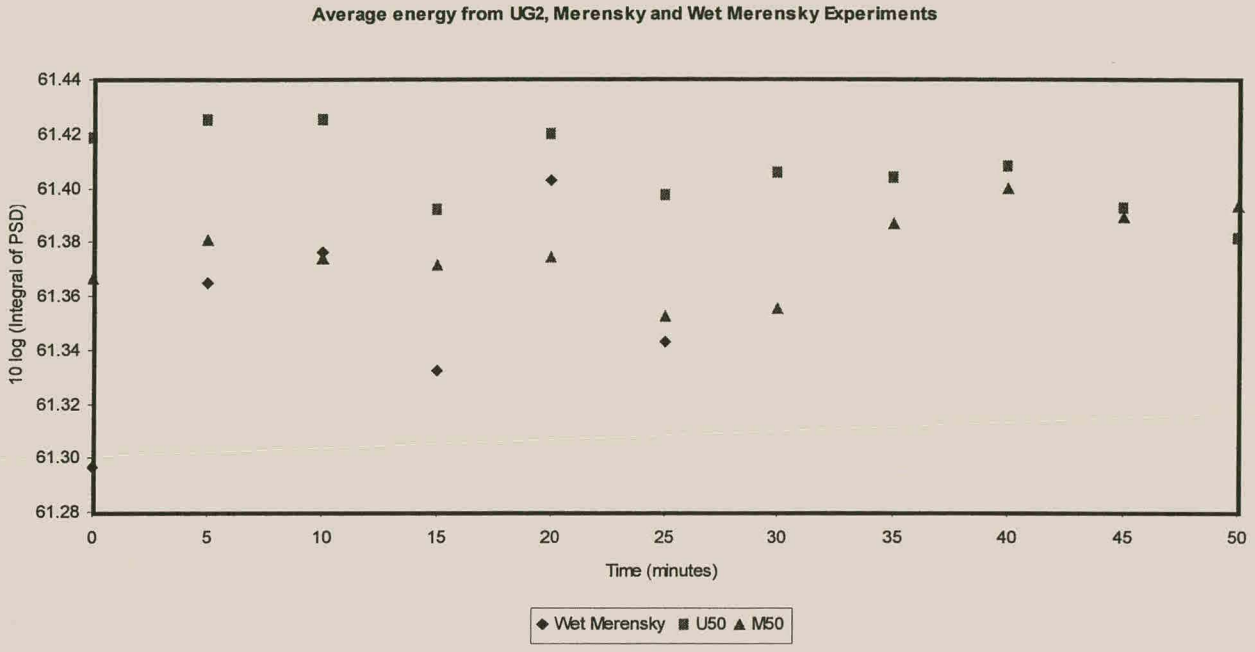


**Figure 5.7**. Average noise level for UG2 and Merensky experiments.

The third curve in figure 5.7 is a recording of a slurry with 60% solids Merensky milled for 25 minutes. The general trend of the wet run corresponds to the results of Watson and Morrison (1986), which indicated increasing noise volume with increasing milling time in batch mills. Again the fluctuations in the data can be attributed to the 10 second sample window which occasionally included or excluded large random deviations occurring in the process during grinding.

The continuous UG2 and Merensky runs revealed that the average signal power emitted from the grind was proportional to the product size. Particle size was the only manipulated variable in these experiments. Particle size distributions for UG2 ore with more mass fractions in the larger size ranges emitted less power than those in the small size ranges. The Merensky ore on the other hand emitted less energy with larger particles than for small sizes. It was found that samples with similar particle size distributions emitted sound of similar amplitude for both Merensky and UG2 ores after approximately 50 minutes grinding. From the UG2 and Merensky results the effect of particle size dominates the effect of ore type with regard to the average

energy emitted from the mill. The mineralogical effect of each ore would however have to be investigated before particle size could be regarded as the governing parameter in this experiment.

According to the mechanism of grinding, communition occurs according to the intensity and type of the ball-particle interactions. A great amount of energy is wasted when ball-ball collisions do not lead to the reduction of particles. Ball-ball collisions result in louder acoustic emissions, as larger bodies resonate with higher intensity than smaller bodies (particles). Thus the more fines in a mill, the less distinct the acoustic spectra as a result of particle resonance and damping.

The likelihood of direct ball-ball collisions decreases as more fines are produced, but the intensity of these ball-ball collisions increases for systems with more fines. As small particles are crushed between two grinding balls, the transfer of excess energy would still cause the balls to resonate. Larger particles however, would absorb more energy and leave less free energy for the steel balls to resonate.

The results from the various experiments indicate that the average mill power is only useful for the determination of significant changes in the operating state of tumbling mills. As a control parameter the sound level could give a very rough indication of the operating state, but should not be used as the only source of information for mill operation.

### 5.3.2 Sammon Mapping

A Sammon map was used to reduce the number of variables to 2 feature vectors, and hence give values unique to each vector. The original power spectrum frequency components were used as input to the Sammon network. An example of original power spectra is shown in figure 5.8. The number of frequency components were reduced to 30 from the original 257 components after it was determined that the first 30 frequency components below 550 Hz contained most of the signal information.

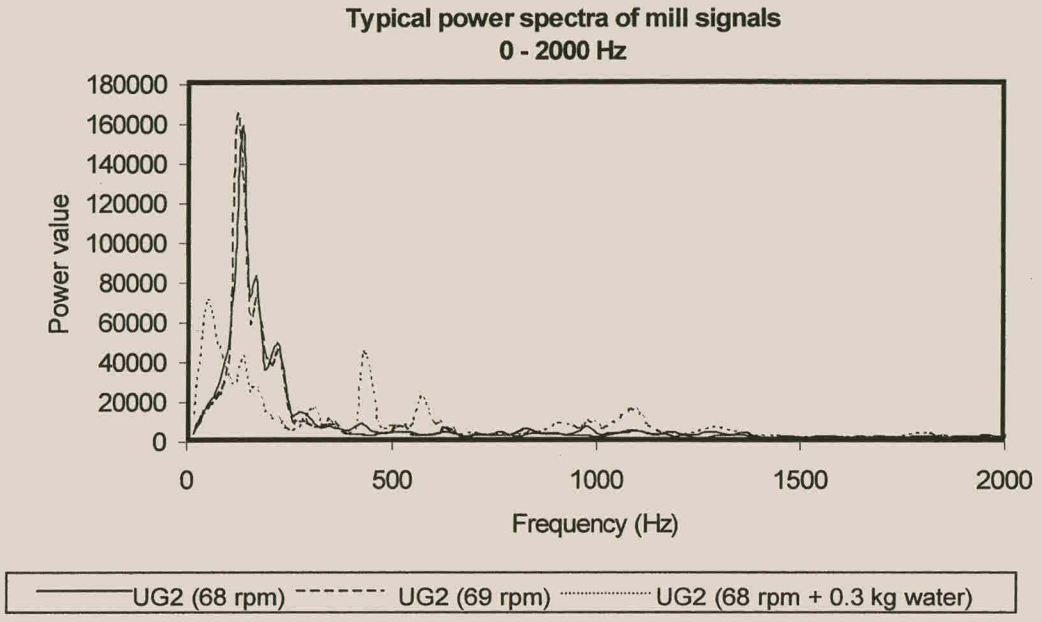


**Figure 5.8.** Power Spectrum density functions in 0-2000 Hz range for UG2 ore after 10 minutes of grinding. Ug2 (68) indicates baseline experiment at 68 rpm, UG2 (69) indicates run at 69 rpm and UG2 (0.3 kg water, 68 rpm) indicates the effect of addition of 300 g of water to the UG2 ore at 68 rpm.

The Sammon map in figure 5.9 shows well defined clustering for all the experiments conducted. The map indicates that the different experiments with similar conditions, e.g. dry or wet, separate into definite clusters. For the experiments containing water in the milling system, e.g. WETSAM (wet combination), slur (water addition), Misc wet (exploratory) and wet M-ore (wet Merensky run) it was found that each experiment formed its own sub-cluster. Similarly the SAM (UG2 and Merensky combination) and the Fill (% ore content) experiments are clustered in the same regions. A common property may be uniform particle size.

An interesting cluster is the group consisting of UG2, Merensky, CAS (Charge addition) and MSS (mill speed). Although some definite grouping is found, some overlap is encountered. The clustering of MSS and CAS can be attributed to the number of ball-ball collisions encountered in the mill. With increasing mill speed the chance of ball-ball interaction is higher than at low speeds. This is due to an increase in the amount of collisions with increasing mill agitation. Charge addition increases the amount of balls in the mill and hence the number of ball-ball collisions.

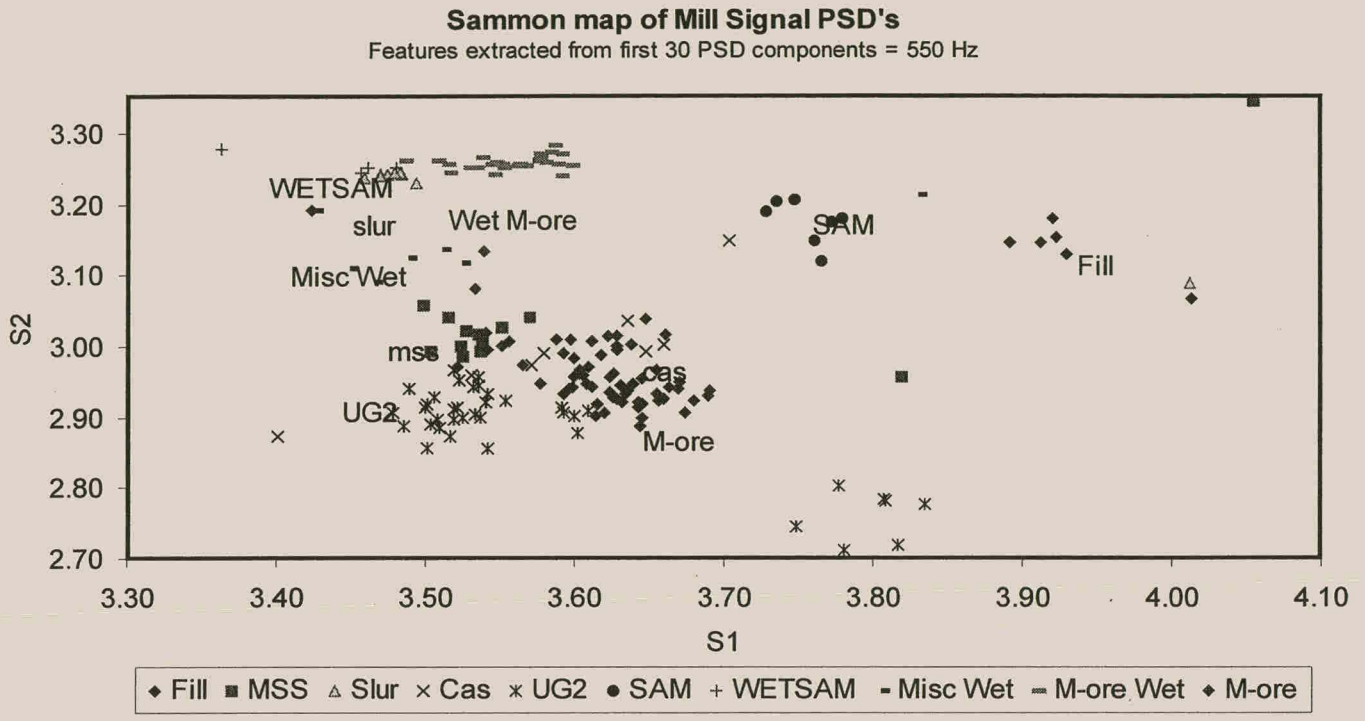


**Figure 5.9** Sammon map showing the first 550 Hz frequency components of each experiment.

With Merensky and UG2 in the region of the mill speed and charge addition experiments, it can be suggested that the main component of the signal emitted during these experiments are due to the interactions between the grinding balls themselves. The large particles in the charge inevitably lead to random scatter of the collisions, as these would also influence the noise from the mill.

Figure 5.10 represents the Sammon map of the UG2 and the Merensky samples. The data were classified according to grind time, with large relating to 0 to 20 minutes grind, intermediate to 20 to 35 minutes grind and small to 35 to 50 minutes of grinding. No significant separation was obtained for particle size, except possibly for the large Merensky fraction. From figure 5.10 the two separate regions of the two ore types, e.g. Merensky and UG2, can clearly be distinguished.

Analysis of the original data indicated that all the points scattered in the right bottom corner belonged to the U30B experiment. This possibly indicates a low microphone battery level for this particular case, although the possibility of differing mineralogical

properties in the UG2 samples may not be ruled out. Future work should therefore analyse each ore sample to investigate the effect of mineralogical composition.

The Sammon stress was calculated as 0.028 with the final error of the network approximately 0.2% after 10 000 iterations. The error of reducing the interpoint distances of the original data in 30 dimensions to the two dimensions of the Sammon map, can therefore be taken as approximately 3%, which shows that the method was effective in representing the data sets.

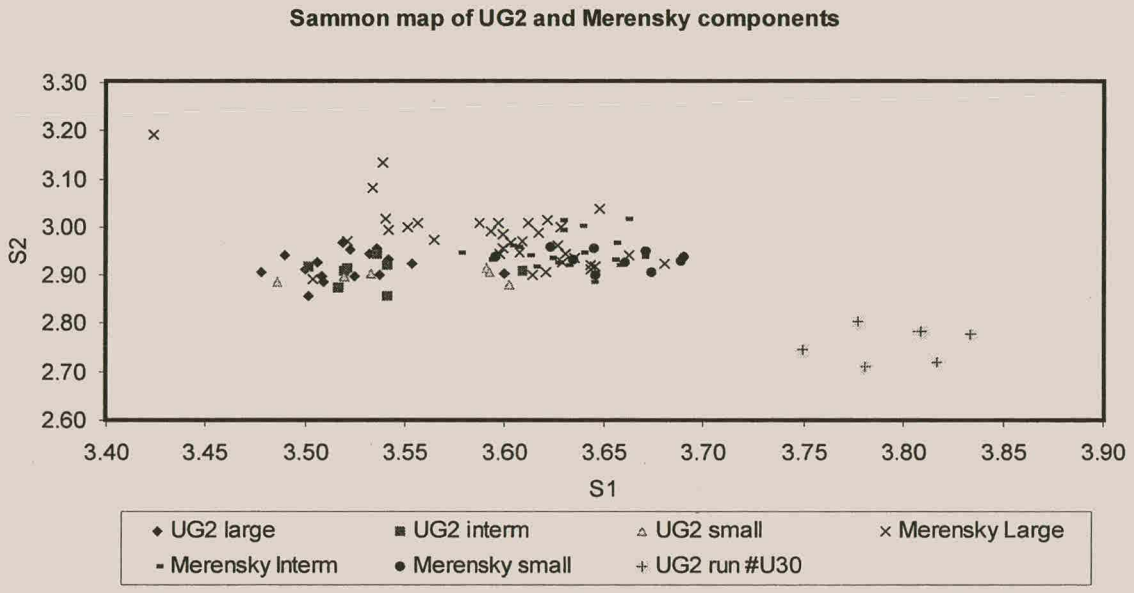


**Figure 5.10**. Sammon map of UG2 and Merensky components.

The selection of the first 30 components of the calculated power spectrum vectors gave good results despite taking only approximately 11% of the total recorded spectra into account. Analysis of the various spectra from the different experiments revealed that only the experiments involving water had important frequency components above 550 Hz, which was the cut off frequency for the samples. Dry grinding formed the basis of the study, therefore the loss of data in the higher frequency ranges could be accommodated. On higher level systems it would not be required to reduce the data set, if adequate computing power is available.

The Sammon map gave a good indication of the operating region for each process condition. Three definite regions could be distinguished from the map depicted in figure 5.9. The fill and combination experiments were situated in the top right hand quarter of the map. Each of the individual conditions formed their own sub-clusters, with the common parameter for both experiments being a fairly constant particle size, although the mass of ore was varied during the fill experiment.

The corresponding top left region is associated with all experiments containing water or a slurry. Again the different sub-clusters are easily distinguished.

In the centre region of the map the experiments are characterized by loud acoustic emissions which are mostly caused by ball-ball interactions, such as high mill speed and steel charge volumes. The experiments involving UG2 and Merensky ore were found in this same region with clear separation between the two ore groups. The presence of the ore data in the vicinity of the speed and steel charge data indicates that these experiments could all be distinguished by ball-ball interactions. It is therefore suggested that a range of particle sizes in a series would give rise to more random and hence more ball-ball interactions than for a uniform particle size distribution. It can further be concluded that the UG2 and Merensky ores were clustered differently on the Sammon map. It remains to be proved however, that the different ores would be distinguishable with identical particle size distributions. Attempts to cluster different size classes of UG2 and Merensky ore proved unsuccessful.

## 5.4 MODELLING

The previous section has shown how it was possible to distinguish between the data obtained from different experiments. However, the main field of application of the mill signal lies in the construction of a model which is capable of predicting a process variable from the mill signal (sound). Two techniques, e.g. linear regression and modelling by means of a feedforward neural network were investigated and compared. The regression and neural network results are summarised in Appendix C and Appendix D respectively.

### 5.4.1 Linear Regression on Silica Batch Experiments

Specific process conditions were simulated in the mill by means of batch experiments conducted over short intervals of up to 15 seconds duration each. With these experiments a specific parameter was varied in order to determine its effect on the acoustics of the mill. The data were processed as described in chapter 4, with the power spectrum data forming the basis for the principal component analysis. The dependent measured parameters were modelled by means of linear regression with the principal components as the explanatory variables.

The parity plots of figures 5.11, 5.12 and 5.13 give a clear indication of the accuracy of the linear regression models used to model the amount of grinding balls, mill speed, water content and ore filling respectively. These plots are constructed with the values of the predicted data set plotted against the values of the observed data set. For an accurate model the predicted data set would approximate a straight line on the graph, as was observed with the prediction for the ore-fill experiment (figure 5.13). All experiments were predicted with a small degree of error, as can be observed from the three different graphs.

Mill speed and the addition of balls to the milling charge were modelled with a slight degree of variation, with the best results obtained for the increasing ore content experiment, which was closely followed by the water addition trials.

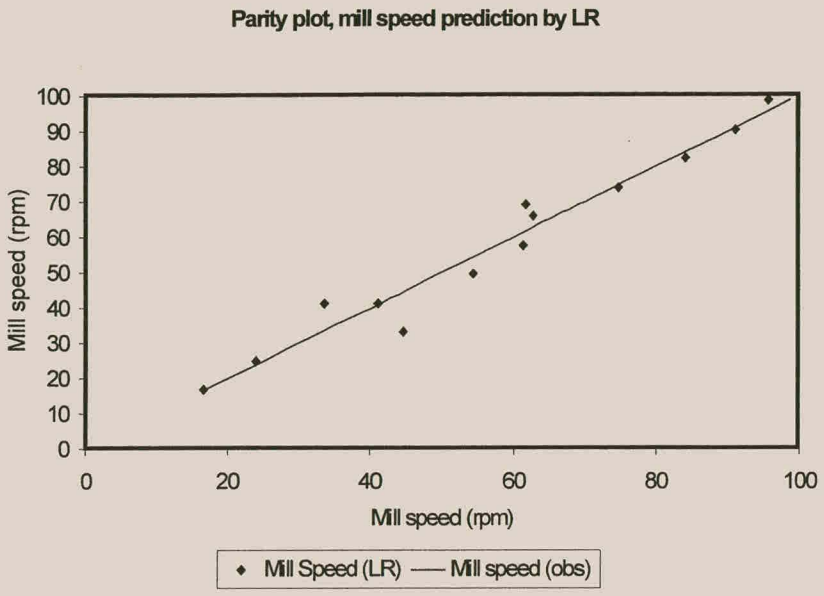


**Fig 5.11**: Parity plot for number of grinding balls, described by $y = 82.22-30.82x_1+42.59x_2+21.82x_3$ , where $x_n$ denotes the n'th principal component of the spectral data set.

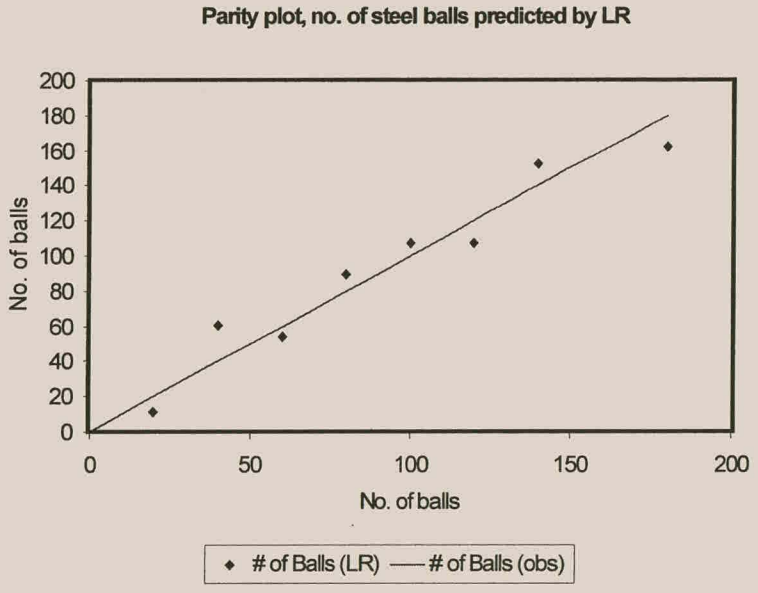


**Fig 5.12.** Parity plot for mill speed described by $y = 57.30-15.48x_1+5.69x_2+15.36x_3-10.12x_4$, where $x_n$ denotes the n'th principal component of the spectral data set.

Linear regression was applied to the data from the silica experiments in order to investigate the potential of modelling for different operating conditions. Each experiment was analyzed individually for the specific process parameter observed. The results obtained are therefore specific to the experiment of concern and do not

show much promise for generalization. Investigation of the frequency components which influenced the principal components revealed that the highest contribution was made by the frequencies in the bands between 2200 Hz to 3100 Hz, 103 Hz to 360 Hz as well as between 1000 Hz and 1300 Hz.

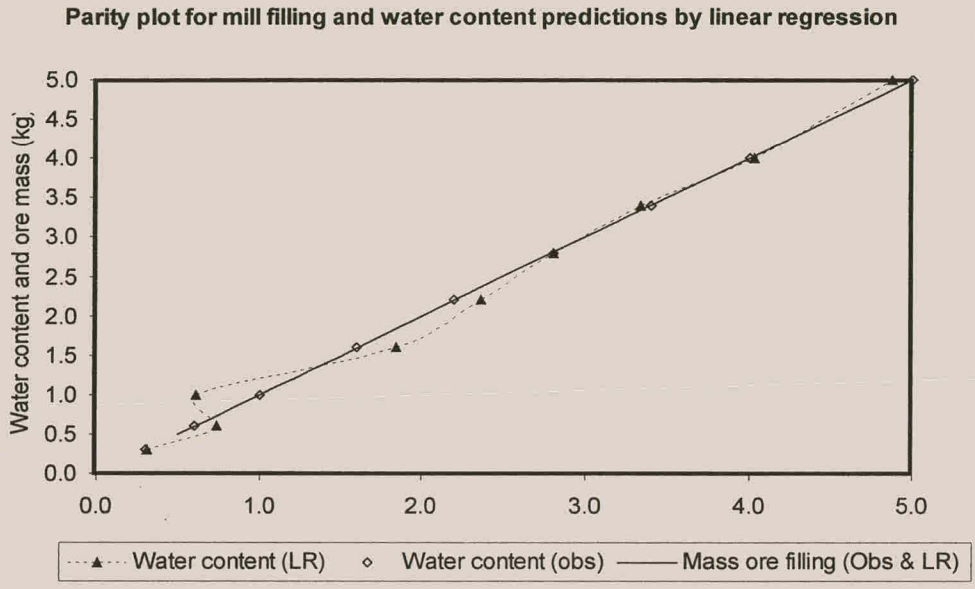


**Fig 5.13** Parity plot for mass ore filling, $y=2.583-1.605x_1+0.647x_2+0.150x_3$ with water content $y = 2.322+0.898x_1+1.301x_2$, where $x_n$ denotes the n'th principal component of the spectral data set.

### 5.4.2 Linear Regression on UG2 and Merensky Combination Experiments

Many mineral processing plants treat ore bodies from different locations which differ in mineralogy, such as UG2 and Merensky in the platinum group metal bearing ore types. These changes are related to a distinct change in operating noise, which can be detected by an experienced operator. The following results are presented for the ideal condition where Merensky and UG2 ores of uniform particle size are mixed. Figure 5.14 relates the different fractions of the two ores that are mixed, while figure 5.15 gives an indication of the particle sizes and prediction of the respective ores. Observations 1, 3 and 6 yielded an almost perfect fit, while observations 2, 4 and 5 gave inaccurate predictions. Closer investigation of these cases shows that the observations which were modelled well contained ore fractions with large particle sizes (>4000 µm). This is in contrast with those experiments which contained small particle sizes (>2800 µm) and which gave relatively poor approximations when modelled.

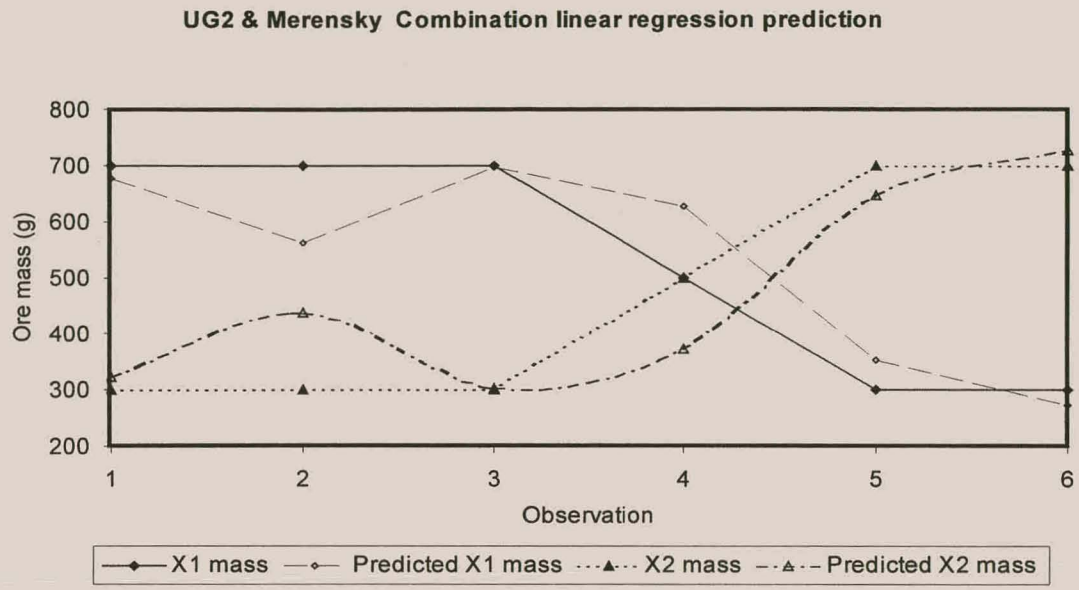


**Figure 5.14.** UG2 and Merensky combination experiments showing the different ore masses predicted by linear regression, with model of the form $y = 500+36.29x_1+109.75x_2+86.61x_3$, where $x_n$ denotes the n'th principal component of the spectral data set.

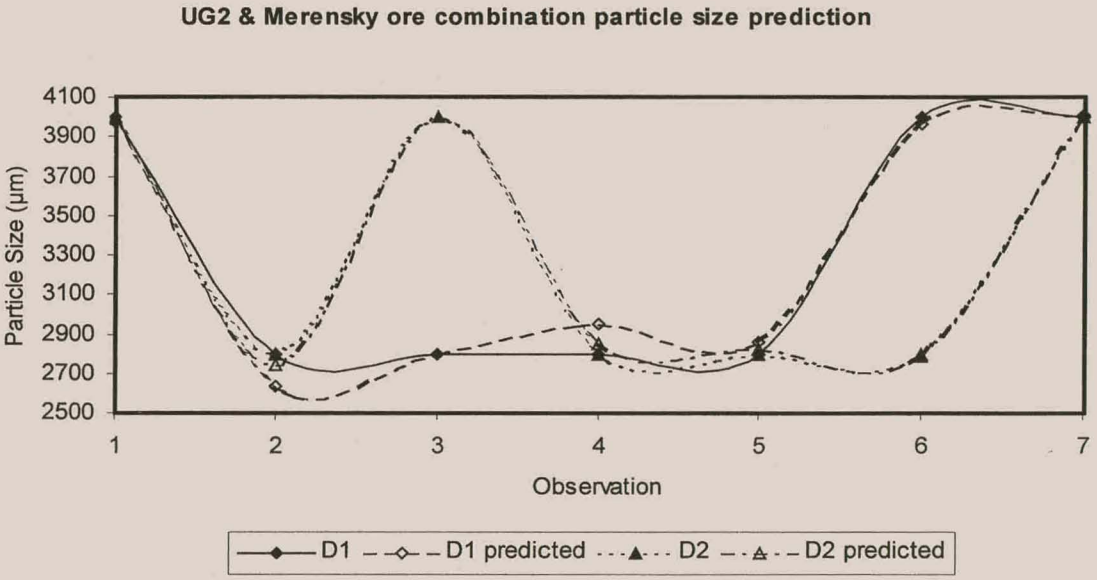


**Figure 5.15**. Different particle sizes for the combination experiments with linear regression results obtained from the model: $y = 3314.29-561.59x_1-14.72x_2-71.62x_3$, where $x_n$ denotes the n'th principal component of the spectral data set.

Comparison of the two relevant figures shows that no direct relation can be attributed to any specific ore type when modelled by linear regression. This indicates that the most influential parameter in this specific experiment was particle size and not necessarily ore type. Large particle sizes would therefore lead to more distinct acoustic signals when particle–ball interactions are encountered than for smaller sizes. It was found that the frequency bands 3000 Hz to 4200 Hz and 1000 to 1300 Hz contained the most significant acoustic information for linear regression.

### 5.4.3 Accuracy of the Linear Regression Model for the Batch Experiments

The significance and $r^2$ values for the predicted values from the batch experiments were calculated to obtain an indication of the accuracy of the model. The $r^2$ is calculated by taking the square of the Pearson product moment correlation coefficient (r). This can be interpreted as the proportion of the variance in the data that is accounted for by the model.

**Table 5.1.** $r^2$ and significance (p) values for the different batch experiments.

| Experiment | $r^2$ | p-value |
|---|---|---|
| % Fill | 1.000 | <0.001 |
| % Slurry | 0.987 | <0.001 |
| Mill Speed | 0.960 | <0.001 |
| # of Balls | 0.951 | <0.001 |
| Combination, Merensky Fraction | 0.836 | 0.004 |
| Combination, UG2 Fraction | 0.836 | 0.004 |
| Combination, Merensky Size | 0.977 | <0.001 |
| Combination, UG2 Size | 0.997 | <0.001 |

Table 5.1 gives the calculated $r^2$ values along with the p-value. The p-value is an indication of the significance of the predicted data set. Values for p larger than 0.05 are often regarded as insignificant as the probability of the model being insignificant is more than 5%. The p-values in table 5.1 indicate that the predictions obtained from the principal components are significant. The model with the best results was obtained for the ore fill experiment, whereas the worst results were obtained for the prediction of mass fraction.

Linear regression has been applied to the batch experiments. Good results have been obtained throughout with the worst prediction for the mass fractions in the combination experiment having a $r^2$ value of 0.84.

### 5.4.4 Merensky and UG2 Experiments

The experiments for the two respective ores, e.g. Merensky and UG2, were conducted over a total duration of 50 minutes each. The acoustic signals were recorded and sampled at 11 kHz and the power spectra of the signals were extracted. Analysis of the principal component results indicated that at least 80% of the variance of the original spectral data could be explained by five principal components. These principal components were used to model the cumulative undersize distribution as well as the 80% (F80) and 50% (F50) passing sizes for each ore type by multiple linear regression and feedforward neural networks. The neural network was first trained by backpropagation for each ore type with the observed process parameters as outputs. With the weights trained, the original training set was given to the network as inputs and the process parameters predicted to give the "predicted" data set. The two networks (UG2 and Merensky) were further tested giving the network a related, but unknown data set as input. The validation set results were accordingly analyzed and compared to both the predicted and observed values as an indication of the generalization capability of the model.

#### *5.4.4.1 Merensky Ore*

##### 5.4.4.1.1 Multiple Linear Regression vs. Feedforward Neural Network

The figures below show the response of the two models on the Merensky data set for prediction of the F80 and F50 parameters. The observed data points are shown in figures 5.16 and 5.17 as solid diamonds, with the regression model a solid line and the neural model as a dashed line.

For both cases it is obvious that the neural network gave much better results than the regression model. The regression model struggled to follow the data for the F80 parameter, although slightly better results were obtained for the F50 parameter. The neural network model performed better on the smaller size ranges with the larger

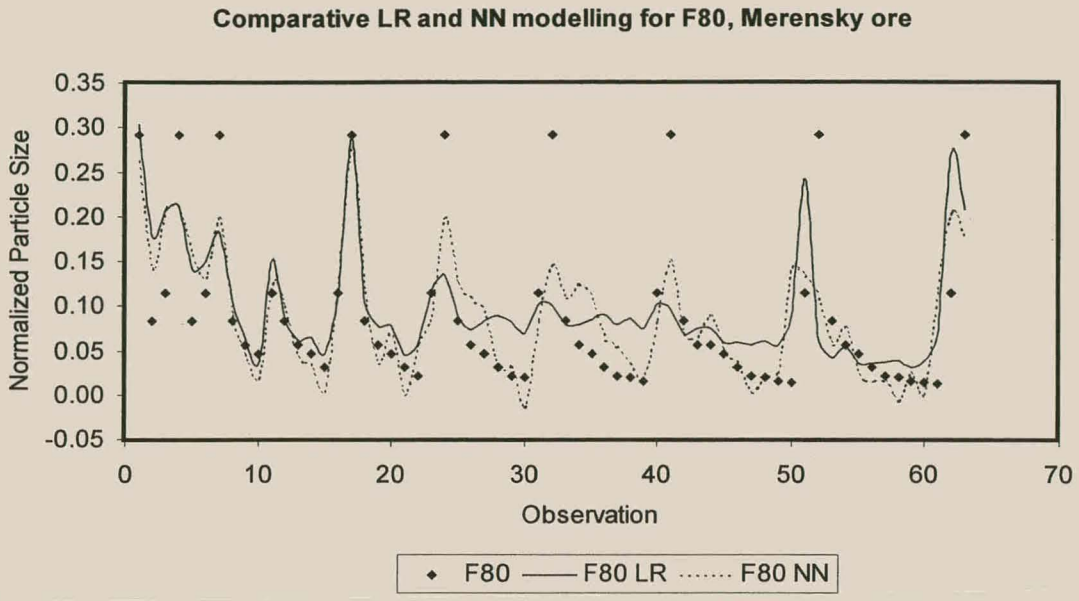


initial values giving rise to errors in the prediction. On average the F50 parameter was predicted better for both the neural network and the regression models.

**Figure 5.16.** Comparative modelling results for Merensky on the F80 parameter.

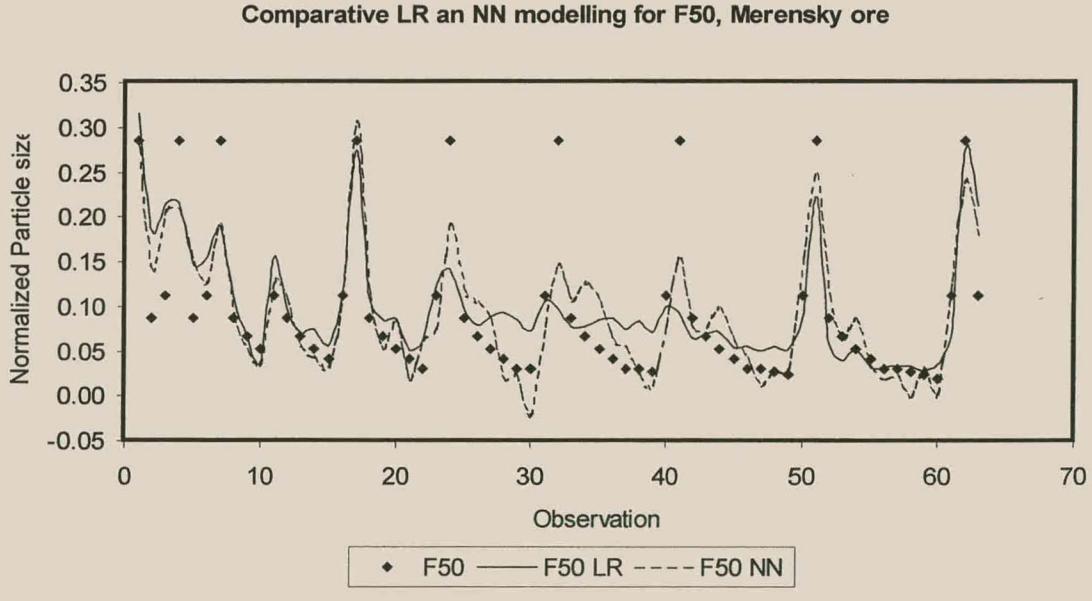


**Figure 5.17**. Comparative modelling results for Merensky on the F50 parameter.

5.4.4.1.2 Merensky Validation

The validation data set was given to the feedforward network in order to test the generalization potential of the model.

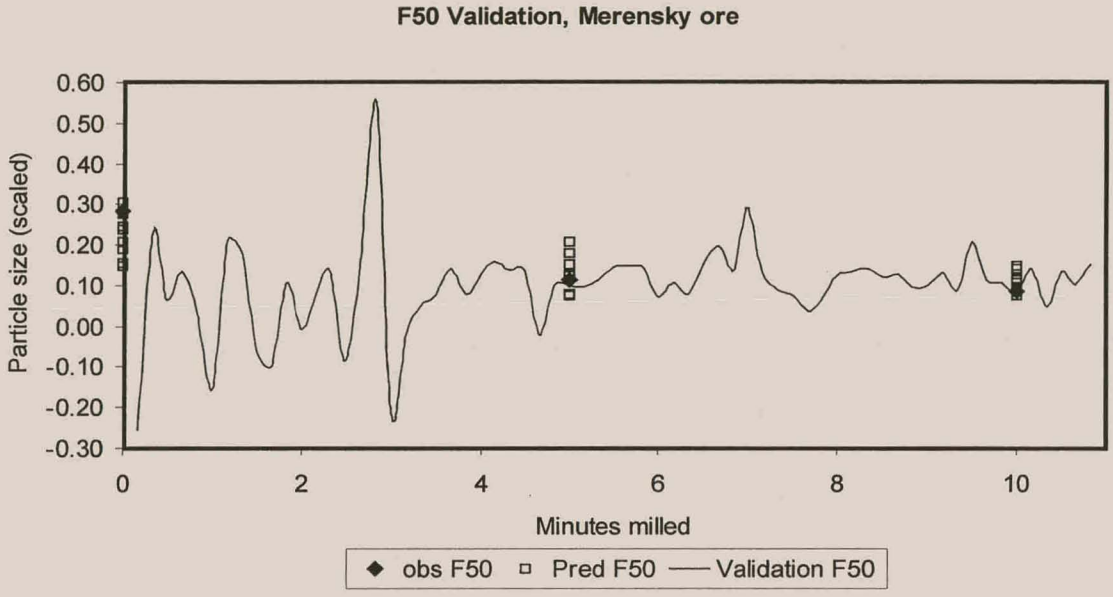


**Figure 5.18.** F50 Validation response for Merensky ore. *obs* indicates the observed particle sizes. *Pred* indicates the particle sizes predicted by the neural network from the known data set. *Validation* indicates the values predicted by the neural network from the test data set.

The validation data were obtained from a different system, but the same ore was used in the experiment as for the original system. The first 10 minutes of a continuous signal recording were given to the network to model. In figure 5.18 the actual observed F50 values are depicted by the solid diamonds at 0 minutes, 5 minutes and 10 minutes grinding respectively. The data points were then modelled by a neural network with the observed signal as input and the F50 parameter as output (solid squares). The validation data were further used as input to the trained network. Although at first glance the predicted F50 parameter (solid line) seems noisy, the respective points at 0, 5 and 10 minutes on which the data were trained, are close to the observed values. The values below 5 minutes are very haphazard and can be attributed to extrapolation errors occurring in the network, but between 5 and 10 minutes grinding the results are promising. Here the model closely followed the general trend of the observed data. In figure 5.19 the observed, predicted and validation data after 0 and 10 minutes of grinding are shown on a parity plot.

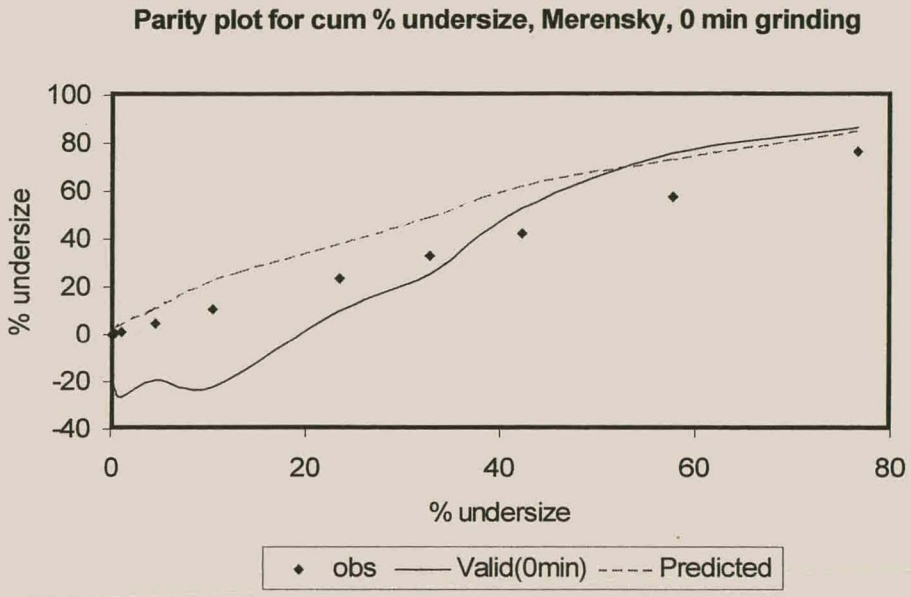


**Figure 5.19**. Parity plot for cumulative undersize prediction on Merensky ore at the start of the experiment (0 minutes) using a feedforward neural network.

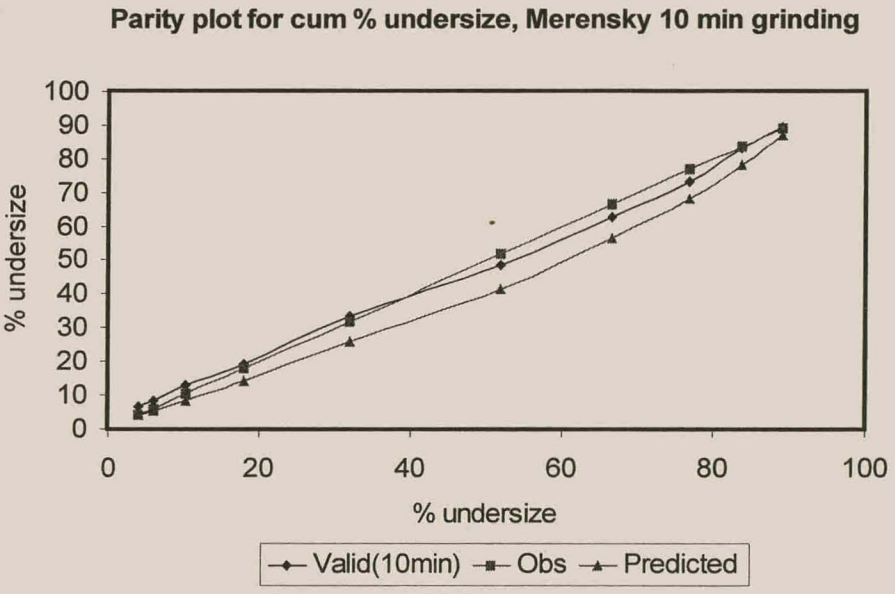


**Figure 5.20**. Parity plot for cumulative undersize prediction on Merensky ore after 10 minutes of grinding using a feedforward neural network.

From figure 5.19 the deviation of the model results using the unknown data is evident. Large errors were obtained for cumulative undersizes smaller than 40%.

Figure 5.20 clearly shows that the results based on the unknown, as well as the known input data, give good approximations of particle size for longer grinding times. This could be due to more steady state conditions of operation existing in the mill for grinds of longer duration.

The data represented in figure 5.21 indicates the accuracy of the model for the prediction of the cumulative undersize distributions after 10 minutes grinding. The validation and prediction curves closely followed the observed cumulative undersize curve. The validation set for the 0 minute curve proved to yield the worst results which could be attributed to the unsteady state of the mill directly after startup.

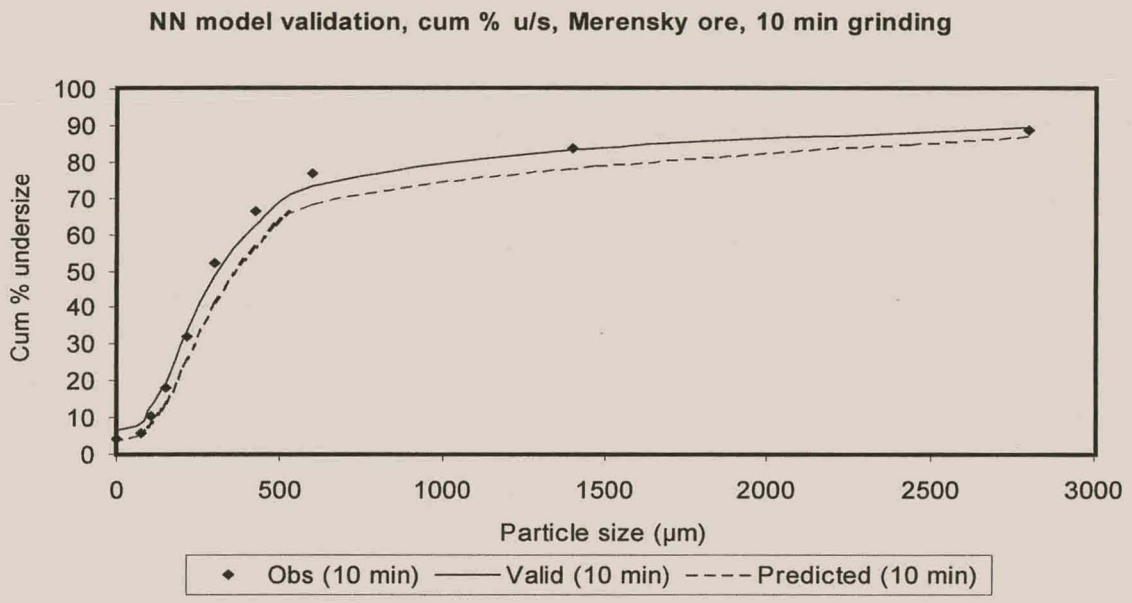


**Figure 5.21**. Cumulative undersize predictions for Merensky ore.

*5.4.4.2 UG2 Ore*

5.4.4.2.1 Multiple Linear Regression vs. Feedforward Neural Network

For the UG2 ore the regression and neural network results are similar for both F50 and F80, although a slightly better fit is obtained for the F50 data with the neural model. As with the Merensky data the regression model followed the general trend in the data, but did not reach the observed value. The neural network performed better and shows a closer fit to the various observed data points. As the initial values where not as large by comparison to the Merensky values, a much better approximation could be obtained.

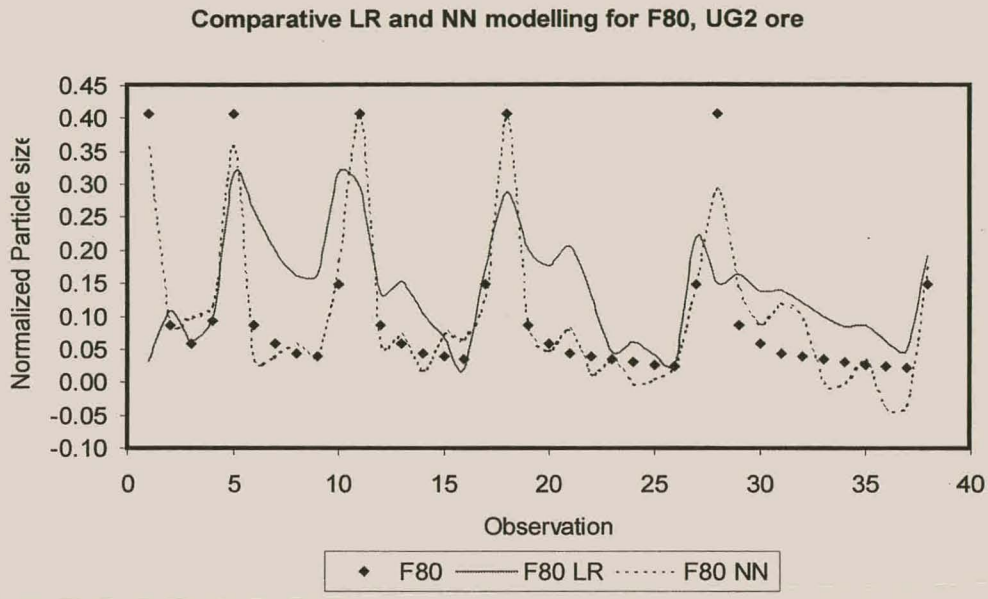


**Figure 5.22**. Comparative modelling results on UG2 ore for the F80 process parameter.

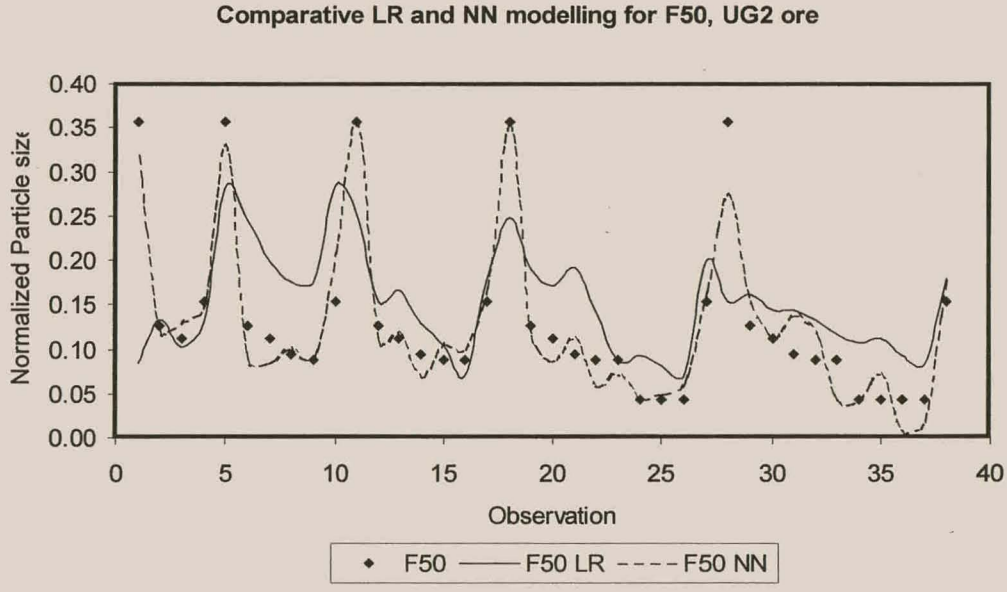


**Figure 5.23.** Comparative modelling results on UG2 ore for the F50 process parameter.

5.4.4.2.2 UG2 Validation

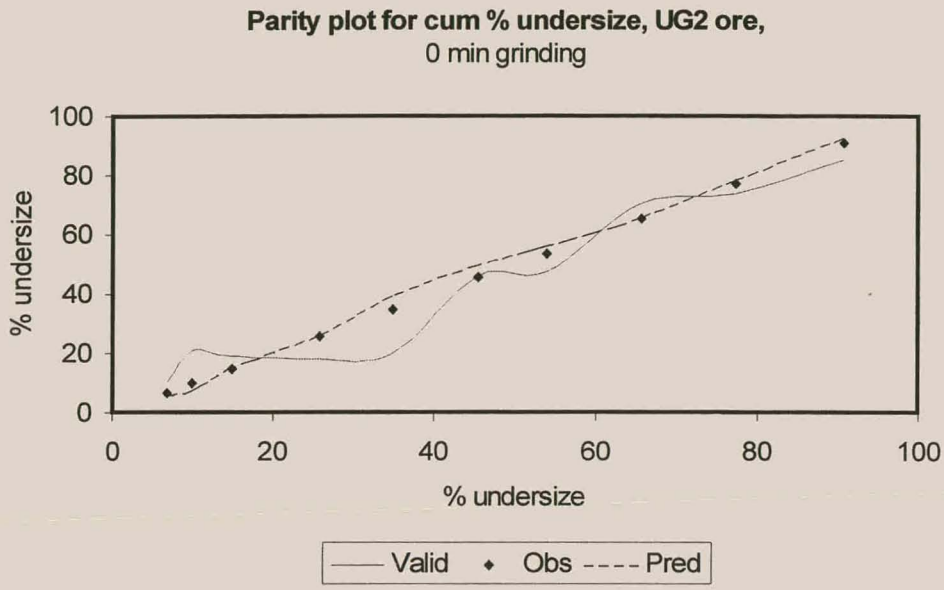


**Figure 5.24**. Parity plot for cumulative undersize prediction on UG2 ore after 0 minutes grinding with a feedforward neural network

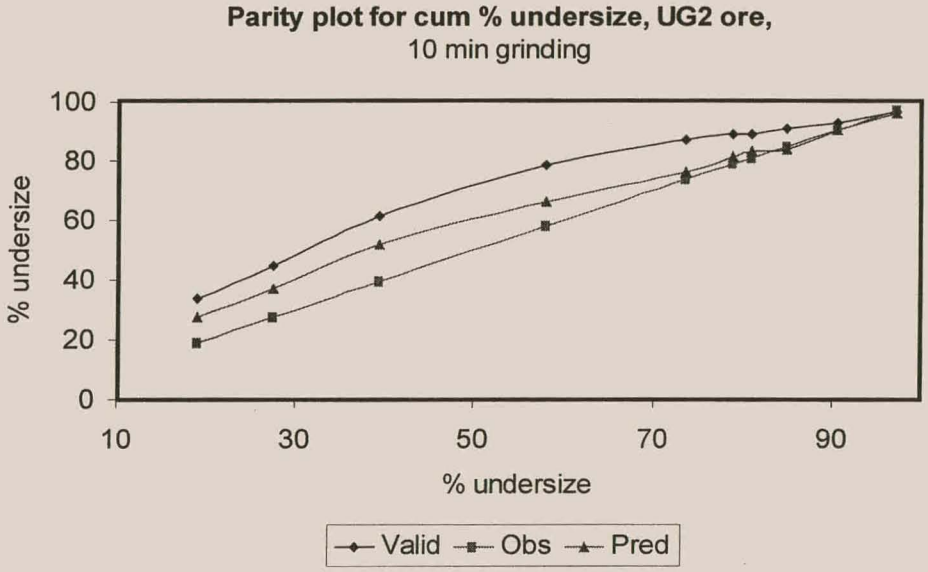


**Figure 5.25.** Parity plot for cumulative undersize prediction on UG2 ore after 10 minutes grinding with a feedforward neural network

Similarly to the Merensky validation data, a UG2 validation data set was constructed to validate the neural network model. Figure 5.24 and 5.25 show the parity plots after

0 and 10 minutes grinding for UG2 ore. From these figures it is plain to see that the neural network model with the validation data as input did not give good results for the 0 minute cumulative percentage undersize prediction. After 10 minutes a much better approximation was made as is seen in figure 5.25. The most accurate predictions were again found for sizes passing below 80%. These results illustrate that the model does have generalization potential.

Figure 5.26 indicates the predicted 50% passing values for the UG2 validation data set. Similar to the Merensky data the first 5 minutes of grinding were not predicted accurately due to initial unsteady state and extrapolation errors made by the network. However, after 5 minutes the general trend in the data followed the trend of the observed parameters.

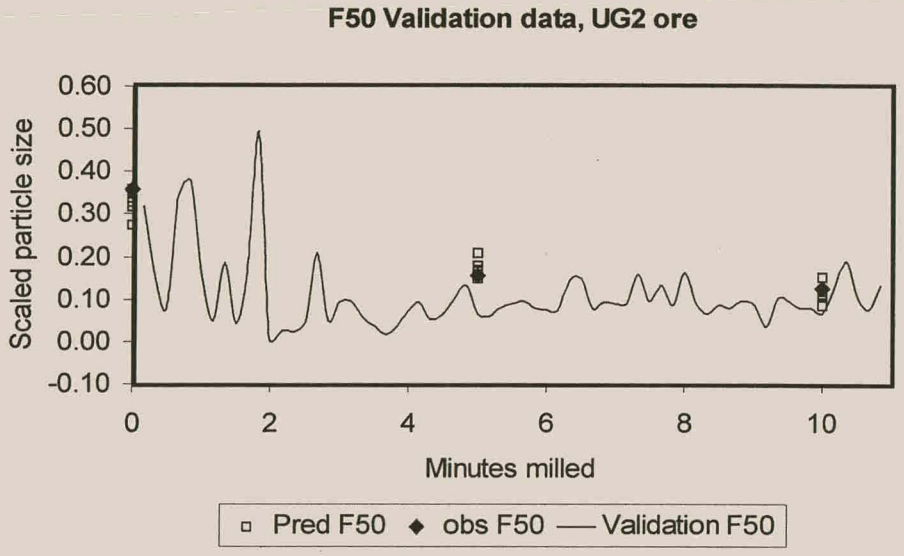


**Figure 5.26**. F50 prediction for validation data with UG2 ore. *obs* indicates the observed particle sizes. *Pred* indicates the particle sizes predicted by the neural network from the known data set. *Validation* indicates the values predicted by the neural network from the test data set.

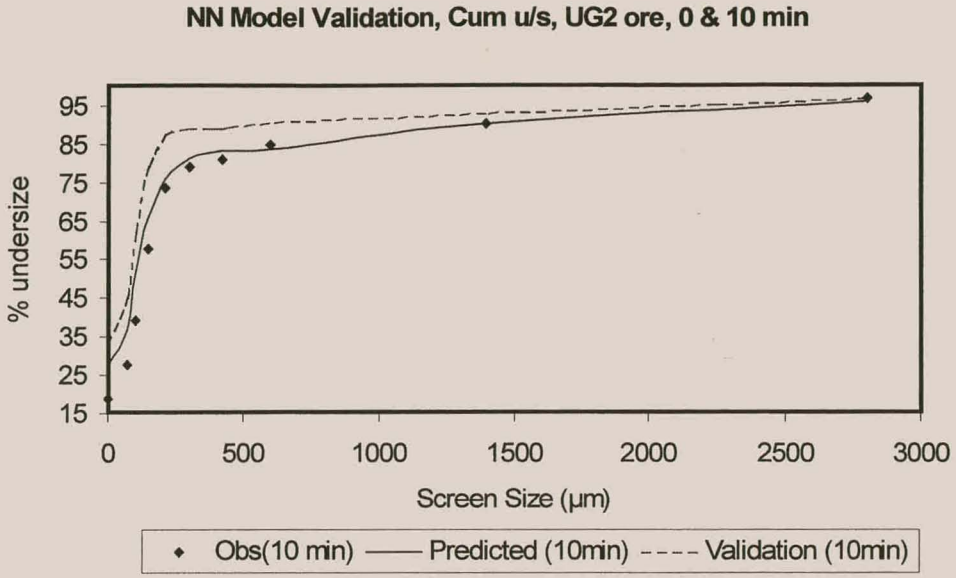


**Figure 5.27**. Modelled cumulative % undersize for UG2 data.

The plot in figure 5.27 shows a close fit for both the UG2 validation and prediction data to the observed parameters. The initial condition (0 minutes) again leads to unstable validation data, although this is not as severe as for the Merensky case. All in all the general degree of prediction for both the original and validation data is satisfactory.

### 5.4.5 UG2 and Merensky Comparison

#### *5.4.5.1 Multiple Linear Regression and Neural Network Modelling*

It was found that the feedforward neural network model was the most accurate for both Merensky and UG2 ores. The F50 and F80 parameters could be predicted by both the neural network and regression models, although the neural network gave the best results, with $r^2$ values in the region of 0.9 for the neural network model compared to the 0.3 for the linear regression model. The UG2 data proved to give more accurate predictions than the Merensky data for both models.

The accuracy of prediction is described by the $r^2$ values given in table 5.2 together with the significance values(p). The $r^2$ values were found to be much larger for the neural network than for the regression model, with both models giving significant predictions.

**Table 5.2**. $r^2$ values for F80 and F50 prediction

| | $r^2$ values | | p values (significance) | |
|---|---|---|---|---|
| **Parameter** | **Linear Regression** | **Feedforward Neural Network** | **Linear Regression** | **Feedforward Neural Network** |
| **Merensky : F80** | 0.46 | 0.59 | <0.0001 | <0.0001 |
| **Merensky : F50** | 0.62 | 0.73 | <0.0001 | <0.0001 |
| **UG2 : F80** | 0.26 | 0.90 | 0.0012 | <0.0001 |
| **UG2 : F50** | 0.29 | 0.90 | 0.0005 | <0.0001 |

*5.4.5.2 Neural Network Validation*

The neural network was tested for generalization on a specific ore type by taking a totally different test set for both Merensky and UG2 ore and applying this to the different trained networks. The $r^2$ values for the validation set are given in table 5.3.

**Table 5.3.** Validation $r^2$ results for neural network modelling

| **Time milled** | **0 min** | **5 min** | **10 min** |
|---|---|---|---|
| **Merensky ore** | | | |
| Validation set | 0.97 | 0.99 | 0.99 |
| Prediction set | 0.97 | 0.99 | 0.99 |
| **UG2 ore** | | | |
| Validation set | 0.93 | 0.92 | 0.96 |
| Prediction set | 0.99 | 0.99 | 0.99 |

All predictions were found to be significant with the calculated p-values practically zero. From the given data it is apparent that the network was able to give good results based on the available data for both the predicted and validation data. The generalization capability of the network and method for both UG2 and Merensky has therefore been proven for the laboratory ball mill condition.

### 5.4.6 Summary of Merensky and UG2 results

The only variable for these two series of experiments was the grinding time which is directly proportional to the particle size of a continuous batch grind. The particle size distribution for a milled ore was therefore determined from the sound emission. Important frequencies were found to lie between 2100 Hz to 2600 Hz and 360 Hz to 700 Hz.

At first linear regression was applied to the data. In contrast to the other experiments studied, the particle size distribution was the variable under consideration. The approximation of the exponential breakage curve was inaccurate with linear regression. The particle size distribution of each ore was obtained at 5 minute intervals for a total of 50 minutes, and used as the output for the model. The principal components obtained from the power spectra vectors were used as the input.

The respective 80% (F80) and 50% (F50) cumulative percentage passing undersizes were first modelled using linear regression. It was shown that the F80 and F50 parameters for both UG2 and Merensky ores could be modelled by linear regression. The prediction accuracy however, was not meaningful. $r^2$ values below 0.65 were obtained, with the UG2 ore giving the largest errors. For both ore types the F50 parameter gave the best prediction.

In order to improve the prediction accuracy of the linear regression model a feed forward neural network was applied to the data. The network weights were initially trained by setting the outputs equal to the observed cumulative undersize fractions and F80 and F50 parameters. The first 5 principal components were used as input to the network. With the neural network trained, the initial data set was used for the prediction of the observed values. For both the F80 and F50 parameters the neural network gave significantly better results than the linear regression model. The neural network handled the large initial values much better than the linear regression model, although the much larger particles of the initial Merensky state did give rise to a higher degree of misfit.

With the much higher accuracy obtained on the F80 and F50 parameters by the neural network model, the model was further tested on the cumulative undersize distribution fractions. The values predicted by the UG2 and Merensky models from the original training set gave a very accurate approximation of the observed values. For these parameters even higher $r^2$ values above 0.97 were obtained. The closeness of fit did however increase with increasing milling time. This again suggests that the milling noise is more uniform for smaller particles and hence increases the modelling capabilities of the system.

In order to test the model, a validation data set was constructed from a totally independent recording of the same ore type. The first 10 minutes of grinding were used as source data. Again 5 principal components were extracted from the power spectrum vectors of the raw validation data set and given to the network to model with the weights from the original training data set. The results indicate that the model was capable of accurately predicting the observed cumulative undersize distributions for both the Merensky and UG2 ores. The initial conditions prior to 5 minutes grinding were not modelled as accurately as after 5 minutes. This can be attributed to the initial unsteady state of mill, with many large particles causing scattered noise variations. The neural network further encountered problems with extrapolation of the data for the first 5 minutes, hereafter the results were more reliable as steady state conditions were reached inside the mill

## 5.5 SUMMARY

In this chapter the results of data analysis on the different experimental signal recordings have been presented. Particle size distribution analysis showed that the UG2 and Merensky ores exhibited similar trends during grinding over a given period of time. The average Merensky particle size, however was larger at the beginning of a sample than the corresponding UG2 particle size.

The average signal energy and Sammon mapping were showed to be effective exploratory tools for initial analysis of the mill signal data.

Modelling was applied to the principal components of the different spectral data. Linear regression was effective in the prediction of system parameters in the short batch experiments where only one parameter was varied. However, linear regression proved ineffective for the prediction of particle size in the Merensky and UG2

experiments. A feedforward neural network was applied to the same data and good approximations were obtained, even with unknown validation data.

# 6

# CONCLUSIONS AND RECOMMENDATIONS

The results presented in chapter 5 demonstrate that by examining the acoustic signals emitted during grinding, numerous deductions can be made with regard to the condition of the mill and the charge. In general it has been found that large particles have a pronounced effect on the acoustics in the mill, while small particles have a dampening effect on the amplitude of the signal. An optimum particle size therefore exists where the mill noise can be used to effectively model the mill process parameters.

## 6.1 CONCLUSIONS

It has been demonstrated that the acoustic emission from a laboratory ball mill can be used for analytical as well as modelling purposes. The research in this thesis has focussed on the analysis, interpretation and modelling of the acoustic emission from a laboratory ball mill. The information gathered from the mill has been successfully used to give approximations of the state of the mill during the experiments that were conducted. The objectives of the thesis have been met and well as follows:

- The average signal energy is a good initial estimate of the milling condition. The most significant results were obtained for the batch experiments where only one parameter was adjusted per experiment.
- The average energy of the signal gives an overall indication of the state of the milling system.
- Sammon maps can be used to give an indication of the specific region of the operation of the mill and can be used to track changes in operating state of the mill.
- Particle size distributions for UG2 and Merensky ore with higher mass fractions in the larger size ranges emitted signals with less power than those in the small size ranges.

- Samples with similar particle size distributions emitted sound of similar amplitude for both Merensky and UG2 ores after approximately 50 minutes of grinding.
- Large particles have a significant effect on the accuracy of the model?
- Linear regression applied to the silica and combination experiments gave meaningful results for single process parameter modelling.
- The neural network was capable of predicting the particle size for the UG2 as well as the Merensky samples tested.
- The neural networks used on the UG2 and Merensky ores were capable of accurately validating the data from the same ore body.
- The work presented in this thesis is capable of forming the basis of future research on this topic regarding the method followed and the general results. The author has attempted to bridge the gap existing between mineral processing and basic signal processing techniques for future research.

It was shown that the acoustic emission from a laboratory ball mill can be harnessed to provide meaningful information with regard to the operating state and product of the mill. It was found that five principal components could be extracted from the power spectrum density function. These components were used to train a feed forward neural network by backpropagation. The network was able to accurately model the particle size of a validation set of the same ore batch. Investigation of the average energy and clustering by means of Sammon mapping revealed interesting associations between various experiments. It was found that experiments of similar operating state, e.g. wet grinds, were clustered in the same regions, with the separate experiments forming individual clusters.

It has therefore been shown that the acoustic information obtained from a ball mill contains substantial information which can be used for system monitoring, modelling and control purposes.

## 6.2 RECOMMENDATIONS

Although the objectives of this thesis have been met, the following recommendations can be made with regard to future research:

- For further laboratory work it would be worthwhile to investigate the effect of mineralogical properties of the ore on the acoustical signal.

- Most of the experiments conducted in the research were done under dry milling conditions. As milling in the industry is mostly done with wet grinding, future research should focus on the mill acoustics during wet grinding.
- The signal analysis techniques have made use of established signal processing techniques, it may be worthwhile to investigate alternative means of signal processing.
- Linear principal component analysis was used for feature extraction. However non-linear methods such as non-linear principal component analysis may achieve more accurate results.
- To improve the accuracy and application of the Sammon map, an algorithm using all 257 frequency components should be used, although this will probably lead to increased computer processing time.
- It still remains of paramount importance to isolate ambient noise from the mill signal so that only the signal from the mill is processed. Advanced digital processing techniques need to be developed to make this possible.
- All tests were done in a simulated laboratory environment. The effects of individual parameters on the mill acoustic signal have been investigated and effectively modelled by using principal component analysis and applying various modelling techniques to the data. The next logical step in the research would be to investigate the mill signal from an industrial mill and apply and refine the knowledge presented in this thesis.
- While the results presented in this work are related to a laboratory batch mill only, it would still be possible to use the techniques developed and apply them to a continuous mill in an industrial plant. For initial work the mill should be monitored and a fairly simple tool developed to gather data and present this on a Sammon map. This, correlated with the mill operating parameters, would enable detection of system changes that would enhance operator efficiency.
- With the increase of system understanding and improvement of current signal processing and feature extraction algorithms an on-line system monitor and finally a system controller could be developed based on the acoustics emitted from the mill during grinding.

# 7

# References

Amestica,R., Gonzalez,G.D., Barria,J. and Magne, L. 1993. *A SAG mill circuit dynamic simulator based on a simplified mechanistic model.* XVIII International Mineral Processing Congress, Sydney, 117-130.

Amestica,R., Gonzalez,G.D., Menacho,J. and Barria,J. 1993. *On-line estimation of fine and coarse ore, water, grinding rate and discharge rates in semi-autogenous grinding mills.* XVIII International Mineral Processing Congress, Sydney, 109-115.

Anon. 1963. *Acoustic controller for improving grinding mill output.* Measurement and Control, Institute of measurement and Control, 2, 11, 444-446.

Ansell, M.P. 1982. *Acoustic emission from softwoods in tension.* Wood Science and Technology, 16, 35-58.

Booker, J.D. 1994. *Acoustic emission related to instantaneous strain in Tasmanian eucalypt timber during seasoning.* Wood Science and Technology, 28, 249-259.

Canadian Mineral Processors, 1968. *Noise and rubber mill liners.* Canadian Mining Journal, 89, 10, 88-91.

Desbiens,A., Pomerleau,A. and Najim,K. 1994. *Adaptive predictive control of a grinding circuit.* International Journal of Mineral Processing, 41,17-31.

Digital Signal Processing Group. 1997. *Optimum placement of microphones on a laboratory mill for adaptive filtering techniques.* Internal report. Department of Electrical and Electronical Engineering. Univerisity of Stellenbosch.

Elsey, J., Barton, G. W. and Jungk, S. 1998, *Acoustics based on-line quality estimation*, Computers and Chemical Engineering, 22, S925-928,

Felix, Alba and Murray, 1989. *Method and apparatus for determining particle size distribution and concentration in a suspension using ultrasonics*, IBM U.S. Patent

Server Database, Patent number: 5121629.
[http:/patent.womplex.ibm.com/details/5121629] Visited: 1998/06/24.

Fenton, K., Tallon, S. and Davies, C.E. 1996. *Characteristic oscillations in the discharge of granular materials from small vessels.* CHEMECA'96 ,5 ,87-92.

Gai, G. and Chen, B. 1993. *Similarity modelling and multi-objective optimization of ball mills.* VIII International Mineral Processing Congress, Sydney, 67-71.

Grujic, M. and Salatic, D. 1993. *Optimization of ball charge kinetics in ball mills.* XVIII International Mineral Processing Congress, Sydney, 181-185.

Hsiung, J.T. and Himmelblau, D.M. 1992. *Detection of leaks in a liquid-liquid heat exchanger using passive acoustic noise.* Internal report, Department of Chemical Engineering, University of Texas.

Jamsa-Jounella, S-L. 1994, *Design of the integrated control systems for mineral processing plants.* Internal Report, Helsinki University of Technology.

King, R.P. 1993. *Communition research - a success story that has not yet ended.* XVIII International Mineral Processing Congress, Sydney. 39-45.

King, R.P. and Bourgeois, F. 1993. *A new conceptual model for ball milling.* XVIII International Mineral Processing Congress, Sydney. 81-86.

King, R.P. and Schneider, C.L. 1993. *Mineral liberation in continuous milling circuits.* XVIII International Mineral Processing Congress, Sydney.

Klimpel, R.R. 1993. *Some industrial experiences in modifying fine grinding environments for improved downstream product performance.* International Journal of Mineral Processing,133-142.

Kruft, R. and Friedsch, J. 1986. *Cavitation as a means of control?* North European Diary Journal, 52, 8, 267-271.

Kolacz, J. 1997. *Measurement system of the mill charge in grinding ball mill circuits.* Minerals Engineering. 10, 12, 1329-1338

Lederman, F.L. 1993. *Why is the mineral processing field behind in the application of new technology?* XVIII International Mineral Processing Congress, Sydney. 7-13.

LiMin, Fu. 1994. *Neural networks in computer intelligence.* McGraw and Hill, New York.

Lo, Y.C., Kientzler, P. and King, R.P. 1993. *Fundamentals and system research in ultrasonic communition technology.* XVIII International Mineral Processing Congress, Sydney.

Mansfield, P.H. 1973. *Electrical transducers for industrial measurement.* Butterworths, London.

Moa, J. and Kain, A.K. 1995. *Artificial neural networks for feature extraction and multivariate data projection.* IEEE Transactions on neural networks. 6, 2, 296-317.

Metzner, G. 1993. *Multivariable and optimizing mill control - the South African experience.* XVIII International Mineral Processing Congress, Sydney. 293-299.

Miettunen, J., Lahteenmaki, S. and Jamsa-Jounella, S-L. 1993. *New methods for the control of autogenous grinding circuit.* XVIII International Mineral Processing Congress, Sydney. 301-317.

Moys, M.H. 1980. *The control of autogenous and semi-autogenous mills: the relationship between measurements of bearing pressure and parameters describing the mill load.* Journal of the S.A. Institute of Mining and Metallurgy, Nov, 401-408.

Mozley, R. 1993. *Resistance to the introduction and testing of new technology in mineral processing.* XVIII International Mineral Processing Congress, Sydney. 15-20.

Mullen. 1996. *Mineral communition circuits – their operation and optimisation.* JKMRC, Brisbane.

Najim,K., Del Villar,R. and Valnezuela, J., 1996. *Self optimization of an autogenous grinding circuit.* Minerals Engineering, 8, 12 , 1513-1522.

Natarajan, K.A. 1996. *Laboratory studies on ball wear in the grinding of a chalcopyrite ore.* International Journal of Mineral Processing, 46, 205-213.

Powell, M.S. 1991. *The effect of liner design on the motion of the outer grinding elements in a rotary mill.* International Journal of Mineral Processing, 31, 163-193.

Proakis,J.G. and Manolakis,D.M. 1996. *Digital signal processing.* Prentice Hall International Editions, New Jersey, Third Ed.

Pulkinnen, K., Ylinen, R. and Jamsa-Jounella, S-L. 1993. *Integrated expert control system for grinding and flotation.* XVIII International Mineral Processing Congress, Sydney. 325-334.

Rajamani, R.K., Agrawala, S. and Mishra, B.K., 1993. *Mill scale up: ball collision frequency and collision energy density in laboratory and plant-scale mills.* XVIII International Mineral Processing Congress, Sydney. 103-107.

Rajamani, R.K., Agrawala, S. and Mishra, B.K. 1994. *Simulation of charge motion in ball mills. Part 1: experimental verifications.* International Journal of Mineral Processing, 40, 171-186.

Rowland, C.A., 1963. *Automation of grinding circuits.* Pit and Quarry, 56, 1,176-179.

Sammon, J.W. 1963. *A non-linear mapping for data structure analysis.* IEEE Transactions on computers. C-18, 5, 401-409.

Stange,W., McInnes, C., Norris, N. and Van Niekerk, L. 1997. *Optimum control of the Leeudoorn semi-Autogenous milling circuit.* SAIMM Extraction Metallurgy Conference, Western Cape Branch.

Stremler, F.G. 1990. *Introduction to communications systems.* Addison-Wesley Publishing Company, Third Ed, Massachusetts.

Swingler, K.1996. *Applying neural networks – a practical guide.* Academic Press, Harcourt, Brace and co. Publishers, London.

Wallace,R.H. 1970. *Understanding and measuring vibration.* Wykeham Publications, London, 1970.

Watson, J.L. and Morrison, S.D. 1986. *Estimation of pulp viscosity and grinding mill performance by means of mill noise measurements.* Minerals and Metallurgical Processing, Nov, 216-227.

Welch, P.D. 1967. *The use of fast Fourier transform for the estimation of power spectra: A method based on time averaging over short modifed periodograms.* IEEE Trans. Audio and Electroacoustics. AU-15. 70-73.

Whiten, W.J., Jian, L. and Ju Hoa, L. 1993. *Grinding control at the Fan Kou mine.* XVIII International Mineral Processing Congress, Sydney.

Williams, M.C. and Meloy, T.P. 1993. *Assessment of the functionality of selection and breakage rate functions in grinding systems.* XVIII International Mineral Processing Congress, Sydney. 73-79.

Wills, B.A. 1988. *Mineral processing technology.* 4'th ed. Pergamon Press. Oxford. 200-212, 253-308.

Zeng, Y. and Forssberg, E. 1993a. *Monitoring grinding parameters by signal measurements from an industrial ball mill.* International Journal of Mineral Processing. 40, 1-16.

Zeng, Y. and Forssberg, E. 1993b. *Application of vibration signals to monitoring crushing parameters.* Powder Technology, 76, 247-252.

Zeng, Y., Zheng, M. and Forssberg, E. 1993. *Monitoring jaw crushing parameters via signal measurement.* International Journal of Mineral Processing, 39, 199-208.

Zeng, Y. and Forssberg, E. 1993c. *Application of digital signal processing and multivariate data analysis to vibration signals from ball-mill grinding.* Transactions, Institute of Mining and Metallurgy, C39-C43.

Zeng, Y. and Forssberg, E. 1991. *Effects of mill feed size on product fineness and energy consumption in coarse grinding.* Minerals Engineering, 4, 5/6, 599-609.

Zeng, Y. and Forssberg, E. 1992. *Effects of operating parameters on vibration signal under laboratory scale ball grinding conditions.* International Journal of Mineral Processing, 35, 273-290.

Zeng, Y. and Forssberg, E. 1996. *Vibration signal measurement from mono-particle breakage.* International Journal of Mineral Processing, 44-45, 59-69.

# APPENDIX A

# EXPERIMENTAL DETAILS

**Table A1**.Typical experimental parameters.

| Parameter | Value |
|---|---|
| **Critical speed** | 100 rpm |
| **Mill Speed** | 68 rpm (68% of critical) |
| **Charge%** | 35 |
| **Charge volume** | 3 L |
| **Mill volume** | 8 L |
| **Ball sizes & (number)** | 43 mm (13) |
| | 37 mm (13) |
| | 25 mm (110) |
| **Ore mass** | 1 kg |
| **Charge Mass** | 6.8 kg |
| **Screen sizes** | -75 µm |
| | 75 µm |
| | 106 µm |
| | 150 µm |
| | 212 µm |
| | 300 µm |
| | 425 µm |
| | 600 µm |
| | 1400 µm |
| | 2800 µm |
| | 4000 µm |
| **Signal recording frequency** | 11025 Hz |
| **Linear quantization** | Stereo, 16 bit |
| **Recording duration** | 10 seconds |
| **Recording interval** | 50 seconds |

**Table A2.** Charge addition experiment: number of small balls used for each run.

| Experiment no. | File name | # small balls |
|---|---|---|
| **CAS1** | CAS1.wav | 0 |
| **CAS2** | CAS2.wav | 20 |
| **CAS3** | CAS3.wav | 40 |
| **CAS4** | CAS4.wav | 60 |
| **CAS5** | CAS5.wav | 80 |
| **CAS6** | CAS6.wav | 100 |
| **CAS7** | CAS7.wav | 120 |
| **CAS8** | CAS8.wav | 140 |
| **CAS9** | CAS9.wav | 180 |

**Table A3.** Mill speed experiment: mill speed and corresponding variable speed drive frequency for each run.

| Experiment no. | File | Mill speed<br>Drive frequency (Hz) | r.p.m. |
|---|---|---|---|
| **MSS0** | MSS0.wav | 10 | 16.7 |
| **MSS1** | MSS1.wav | 15 | 24.9 |
| **MSS2** | MSS2.wav | 20 | 33.1 |
| **MSS3** | MSS3.wav | 25 | 41.3 |
| **MSS3b** | MSS3b.wav | 25 | 41.3 |
| **MSS4** | MSS4.wav | 30 | 49.5 |
| **MSS5** | MSS5.wav | 35 | 57.9 |
| **MSS6** | MSS6.wav | 40 | 65.8 |
| **MSS7** | MSS7.wav | 42 | 69.1 |
| **MSS8** | MSS8.wav | 45 | 74.0 |
| **MSS9** | MSS9.wav | 50 | 82.2 |
| **MSS10** | MSS10.wav | 55 | 90.4 |
| **MSS11** | MSS11.wav | 60 | 98.6 |

**Table A4.** Percentage ore fill experiment: ore content per run.

| Experiment no. : | File | Mass silica Kg |
|---|---|---|
| **FILL1** | Fill1.wav | ½ |
| **FILL2** | Fill2.wav | 1 |
| **FILL3** | Fill3.wav | 2 |
| **FILL4** | Fill4.wav | 3 |
| **FILL5** | Fill5.wav | 4 |
| **FILL6** | Fill6.wav | 5 |

**Table A5.** Water addition experiment: mass water used per run.

| Experiment no. | File | Slurry density % | Volume water L |
|---|---|---|---|
| **SLUR1** | Slur1.wav | 30 | 0.3 |
| **SLUR2** | Slur2.wav | 60 | 0.6 |
| **SLUR3** | Slur3.wav | 100 | 1 |
| **SLUR4** | Slur4.wav | 160 | 1.6 |
| **SLUR5** | Slur5.wav | 220 | 2.2 |
| **SLUR6** | Slur6.wav | 280 | 2.8 |
| **SLUR7** | Slur7.wav | 340 | 3.4 |
| **SLUR8** | Slur8.wav | 400 | 4 |
| **SLUR9** | Slur9.wav | 500 | 5 |

**Table A6.** UG2 and Merensky combination experiments: sample compositions for each run.

| Experiment no. | File | Ore mass | Particle size µm |
|---|---|---|---|
| **SAM1** | SAM1.wav | 700g Merensky | +4000 |
| | | 300g UG2 | +4000 |
| **SAM2** | SAM2.wav | 300g Merensky | +4000 |
| | | 700g UG2 | +4000 |
| **SAM3** | SAM3.wav | 700g Merensky | -4000+2800 |
| | | 300g UG2 | -4000+2800 |
| **SAM4** | SAM4.wav | 300g Merensky | -4000+2800 |
| | | 700g UG2 | -4000+2800 |
| **SAM5** | SAM5.wav | 700g Merensky | -4000+2800 |
| | | 300g UG2 | +4000 |
| **SAM6** | SAM6.wav | 300g Merensky | +4000 |
| | | 700g UG2 | -4000+2800 |
| **SAM7** | SAM7.wav | 500g Merensky | -4000+2800 |
| | | 500g UG2 | -4000+2800 |

**Table A7.** Experimental details.

| Process Condition | *Merensky –dry run* | *Merensky – wet run A* | *Merensky – wet run B* | *Charge Addition- silica* | *Mill Speed- silica* | *Ore Content- silica* |
|---|---|---|---|---|---|---|
| **Ore Mass** | 1000 g | 1000 g | 1000 g | 1000 g | 1000 g | 500 to 5000g |
| **No. of Small Balls** | 110 | 110 | 110 | 0 to 180 | 110 | 110 |
| **Ore Type** | Merensky | Merensky | Merensky | Silica sand | Silica sand | Silica sand |
| **Parameters Varied** | Grinding time<br>Particle size distribution | Particle size distribution | Particle size distribution<br>Milling time (25 minutes) | Number of small grinding balls | Mill speed | Amount of ore in mill |
| **Mill Speed** | 69 rpm | 69 rpm | 69 rpm | 69 rpm | 0-98 rpm | 69 rpm |
| **Mass Water** | 0 g | 600 g (60% slurry) | 600 g (60% slurry) | 0 g | 0 g | 0 g |
| **Sampling Frequency** | 11025 Hz @ 16 bit | 11025 Hz @ 16 bit | 11025 Hz @ 16 bit | 11025 Hz @ 16 bit | 11025 Hz @ 16 bit | 11025 Hz @ 16 bit |
| **Filenames:** | M5B1.wav,...,M5B6.wav;.....,M50B51.wav | M5W.wav,<br>M15WW.wav,<br>M25W.wav,<br>M35W.wav,M50W.wav | M-Wet1.wav,<br>.....,M-wet26.wav | CAS1.wav,.....,<br>CAS9.wav | MSS1.wav,.....,<br>MSS11.wav | Fill11.wav,.....,<br>Fill51.wav |
| **Note:** | Files recorded at 10 second intervals.<br>Each run was 5 minutes longer than the previous run. | Batch acoustic recordings.<br>Samples tested: M5B, M15B, M25B, M35B M50B. | Continuous run, 10 second recordings @ 60 second intervals. | Batch recordings. | Batch recordings. | Batch recordings. |
| **Number of Acoustic Samples** | 285 | 5 | 26 | 9 | 12 | 6 |

**Table A8.** Experimental details.

| *Process Condition* | *Ore Content silica* | *Water Addition – silica* | *Dry run – UG2 ore* | *Composition – Merensky & UG2* | *Composition- wet Merensky & UG2* | *Grinding balls only – No ore* |
|---|---|---|---|---|---|---|
| **Ore Mass** | 500 to 5000g | 1000 g | 1000 g | 1000 g | 1000 g | 0 g |
| **Number of Small Balls** | 110 | 110 | 110 | 110 | 110 | 110 |
| **Ore Type** | Silica sand | Silica sand | UG2 ore | Combination of UG2 and Merensky | Combination of UG2 and Merensky | Media only |
| **Parameters Varied** | Amount of ore in mill | Pulp density, mass water | Grinding time Particle size distribution | Ore combination Particle size | Ore combination Particle size | None |
| **Mill Speed** | 69 rpm | 69 rpm | 69 rpm | 69 rpm | 69 rpm | 69 rpm |
| **Mass Water** | 0 g | 0.3 to 3000 g | 0 g | 0 g | 600 g | 0 g |
| **Signal Sampling Frequency** | 11025 Hz @ 16 bit | 11025 Hz @ 16 bit | 11025 Hz @ 16 bit | 11025 Hz @ 16 bit | 11025 Hz @ 16 bit | 11025 Hz @ 16 bit |
| **Filenames:** | Fill11.wav,.....,Fill51.wav | Slurry11.wav,....., Slurry51.wav | U15B1..16.wav, U25B1..26.wav, U30B1..31.wav, U45B1..46.wav, U50B1..51.wav | SAM1.wav,....., SAM7.wav | WetSAM1.wav,....., WetSAM4.wav | ballonly1.wav,....., ballonly5.wav |
| **Number of Acoustic Samples** | 6 | 5 | 170 | 7 | 4 | 5 |

**Table A9.** Mineralogy of typical Merensky ore

| MINERAL | New 10S Head | | | | | |
|---|---|---|---|---|---|---|
| | +106 | +53 | +25 | +10 | +2 | Head |
| **Sulphides** | | | | | | |
| Fe-Sulphides | 0.16 | 0.26 | 0.65 | 0.72 | 0.78 | 0.42 |
| Pentlandite | 0.12 | 0.16 | 0.45 | 0.70 | 0.57 | 0.30 |
| Chalcopyrite | 0.15 | 0.18 | 0.20 | 0.26 | 0.23 | 0.19 |
| Other-Sulphides | 0.01 | 0.02 | 0.06 | 0.03 | 0.02 | 0.02 |
| **Silicates** | | | | | | |
| Feldspar | 55.62 | 45.61 | 42.02 | 44.19 | 44.54 | 47.74 |
| Orthopyroxene | 32.32 | 40.40 | 39.79 | 36.55 | 31.90 | 36.21 |
| Clinopyroxene | 6.14 | 6.97 | 8.28 | 8.54 | 10.18 | 7.57 |
| Olivine | 0.37 | 0.53 | 0.54 | 0.56 | 0.24 | 0.44 |
| Mica | 0.71 | 0.57 | 0.70 | 0.73 | 0.83 | 0.69 |
| Quartz | 1.13 | 1.18 | 1.79 | 1.06 | 2.64 | 1.50 |
| Other-Silicates | 1.04 | 0.95 | 0.99 | 1.21 | 1.64 | 1.11 |
| **Altered Silicates** | | | | | | |
| Talc | 0.16 | 0.17 | 0.15 | 0.19 | 0.16 | 0.16 |
| Serpentine | 0.08 | 0.07 | 0.05 | 0.07 | 0.06 | 0.07 |
| Chlorite | 0.70 | 0.53 | 0.56 | 0.77 | 0.90 | 0.66 |
| **Oxides** | | | | | | |
| Chromite | 1.12 | 2.11 | 3.16 | 3.66 | 4.01 | 2.41 |
| Oxides | 0.06 | 0.14 | 0.37 | 0.45 | 0.70 | 0.27 |
| **Others** | | | | | | |
| Carbonates | 0.12 | 0.14 | 0.24 | 0.31 | 0.60 | 0.24 |
| Others | 0.00 | 0.00 | 0.00 | 0.00 | 0.00 | 0.00 |
| **TOTAL** | **100** | **100** | **100** | **100** | **100** | **100** |

# APPENDIX B

# PRINCIPAL COMPONENTS

The results of the principal component analysis, conducted on the power spectral density data, are presented. The spectral data from the experiments were divided into the following groups:

1. Silica
   - Consisting of FILL, CAS, SLUR and MSS experiments
2. UG2
   - Consisting of all UBx data.
3. Merensky
   - Consisting of all MBx data.
4. Combination
   - Consisting of all SAM data.

Principal component analysis was applied separately to each group of data to obtain the feature vector of the specific ore system (e.g. silica, Merensky, UG2 and a combination of UG2 and Merensky ores).

The data presented in section 9.1:

a) illustrates the amount of the original data set which is described by each principal component and
b) shows how many principal components are required to describe most of the variance in the original spectral data set.

The eigen values ($E_n$) give the coefficient of the principal component (PCn) so that the variable (Y) is explained by

$$Y = E_1PC1 + E_2PC2 + ..... + E_nPCn. \qquad (B1)$$

## B.1 EIGENVALUES

The following tables summarize the eigenvalues and variance for the different principal components.

**Table B1.** Eigenvalues for the Merensky and UG2 experiments, with the amount of variance explained by each of the components from the original data set.

| | Eigenvalue | % total variance explained | Cum Eigenvalue | Cum% variance |
|---|---|---|---|---|
| **UG2 Training data set** | | | | |
| PC1 | 182.0 | 70.8 | 182.0 | 70.8 |
| PC2 | 18.4 | 7.2 | 200.4 | 78.0 |
| PC3 | 11.6 | 4.5 | 212.0 | 82.5 |
| PC4 | 5.6 | 2.2 | 217.6 | 84.7 |
| PC5 | 4.6 | 1.8 | 222.2 | 86.5 |
| **UG2 validation data set** | | | | |
| PC1 | 141.6 | 55.1 | 141.6 | 55.1 |
| PC2 | 15.3 | 5.9 | 156.9 | 61.0 |
| PC3 | 9.1 | 3.5 | 166.0 | 64.6 |
| PC4 | 7.1 | 2.8 | 173.1 | 67.3 |
| PC5 | 6.1 | 2.4 | 179.1 | 69.7 |
| **Merensky training data set** | | | | |
| PC1 | 177.4 | 69.0 | 177.4 | 69.0 |
| PC2 | 25.3 | 9.8 | 202.6 | 78.8 |
| PC3 | 12.2 | 4.8 | 214.8 | 83.6 |
| PC4 | 6.5 | 2.5 | 221.3 | 86.1 |
| PC5 | 5.6 | 2.2 | 227.0 | 88.3 |
| **Merensky validation data set** | | | | |
| PC1 | 140.3 | 54.6 | 140.3 | 54.6 |
| PC2 | 19.3 | 7.5 | 159.6 | 62.1 |
| PC3 | 12.7 | 4.9 | 172.3 | 67.0 |
| PC4 | 7.3 | 2.8 | 179.6 | 69.9 |
| PC5 | 5.6 | 2.2 | 185.2 | 72.1 |
| **Wet Merensky data set** | | | | |
| PC1 | 74.9 | 29.1 | 74.9 | 29.1 |
| PC2 | 32.9 | 12.8 | 107.8 | 41.9 |
| PC3 | 12.4 | 4.8 | 120.2 | 46.8 |
| PC4 | 11.0 | 4.3 | 131.2 | 51.0 |
| PC5 | 9.7 | 3.8 | 140.9 | 54.8 |

**Table B2**. Eigenvalues for the silica batch experiments, with the amount of variance explained by each of the components from the orginal data set.

| | Eigenvalue | % total variance explained | Cum Eigenvalue | Cum% variance |
|---|---|---|---|---|
| **Combination** | | | | |
| PC1 | 106.3 | 41.4 | 106.3 | 41.4 |
| PC2 | 40.1 | 15.6 | 146.4 | 57.0 |
| PC3 | 31.5 | 12.3 | 177.9 | 69.2 |
| PC4 | 30.1 | 11.7 | 208.1 | 81.0 |
| PC5 | 26.7 | 10.4 | 234.7 | 91.3 |
| **Fill** | | | | |
| PC1 | 149.0 | 58.0 | 149.0 | 58.0 |
| PC2 | 49.4 | 19.2 | 198.4 | 77.2 |
| PC3 | 26.0 | 10.1 | 224.4 | 87.3 |
| PC4 | 17.7 | 6.9 | 242.1 | 94.2 |
| PC5 | 14.9 | 5.8 | 257.0 | 100.0 |
| **Mill speed** | | | | |
| PC1 | 137.2 | 53.4 | 137.2 | 53.4 |
| PC2 | 26.5 | 10.3 | 163.8 | 63.7 |
| PC3 | 16.5 | 6.4 | 180.3 | 70.2 |
| PC4 | 13.2 | 5.1 | 193.5 | 75.3 |
| PC5 | 11.4 | 4.4 | 204.9 | 79.7 |
| **Slurry** | | | | |
| PC1 | 207.0 | 80.5 | 207.0 | 80.5 |
| PC2 | 22.2 | 8.6 | 229.2 | 89.2 |
| PC3 | 9.2 | 3.6 | 238.4 | 92.8 |
| PC4 | 6.7 | 2.6 | 245.1 | 95.4 |
| PC5 | 4.3 | 1.7 | 249.4 | 97.0 |
| **Charge addition** | | | | |
| PC1 | 137.1 | 53.4 | 137.1 | 53.4 |
| PC2 | 26.8 | 10.4 | 164.0 | 63.8 |
| PC3 | 23.9 | 9.3 | 187.9 | 73.1 |
| PC4 | 22.1 | 8.6 | 209.9 | 81.7 |
| PC5 | 18.8 | 7.3 | 228.8 | 89.0 |

## B.2 FACTOR LOADINGS

The factor loadings describe the specific components that contribute most to the respective principal components described in tables B1 and B2. For example, the first principal component (PC1) of the combination experiment in table B2, is sensitive to changes in the high frequency range with components 4032 Hz and 3827 Hz playing a 99.4% role in the make up of PC1, from table B3. Tables B3 to B6 show the individual spectral components which play a significant role in the composition of the feature vector described by the principal component. The data in the tables are arranged in descending order from frequencies with the most positive to frequencies with the most negative influence. The lighter columns next to the frequencies indicate the fraction of contribution that each frequency component makes to the respective principal component.

**Table B3.** Combination experiments (SAM) - Frequency component loading on principal components.

| *Hz* | *PC1* | *Hz* | *PC2* | *Hz* | *PC3* | *Hz* | *PC4* |
|---|---|---|---|---|---|---|---|
| 4032 | 0.994 | 1287 | 0.965 | 909 | 0.568 | 549 | 0.463 |
| 3827 | 0.994 | 1321 | 0.963 | 892 | 0.565 | 927 | 0.438 |
| 2848 | 0.992 | 1304 | 0.958 | 875 | 0.498 | 909 | 0.436 |
| 4135 | 0.992 | 1115 | 0.945 | 961 | 0.483 | 892 | 0.414 |
| 3380 | 0.991 | 412 | 0.944 | 1167 | 0.482 | 292 | 0.398 |
| 1939 | 0.991 | 1098 | 0.942 | 944 | 0.478 | 309 | 0.397 |
| 3844 | 0.991 | 395 | 0.938 | 1201 | 0.428 | 343 | 0.388 |
| 2780 | 0.991 | 1064 | 0.936 | 927 | 0.399 | 360 | 0.388 |
| 4015 | 0.991 | 257 | 0.933 | 1253 | 0.391 | 566 | 0.360 |
| 3449 | 0.991 | 1338 | 0.933 | 858 | 0.390 | 635 | 0.353 |
| 172 | -0.354 | 1596 | -0.246 | 686 | -0.311 | 172 | -0.258 |
| 154 | -0.363 | 3003 | -0.248 | 704 | -0.313 | 2471 | -0.263 |
| 17 | -0.390 | 1733 | -0.269 | 2471 | -0.318 | 1030 | -0.266 |
| 120 | -0.397 | 1613 | -0.289 | 2093 | -0.323 | 2522 | -0.274 |
| 103 | -0.404 | 1716 | -0.319 | 2162 | -0.325 | 995 | -0.289 |
| 34 | -0.406 | 1630 | -0.354 | 669 | -0.394 | 1836 | -0.297 |
| 137 | -0.410 | 1647 | -0.355 | 635 | -0.415 | 1785 | -0.301 |
| 69 | -0.413 | 1699 | -0.357 | 652 | -0.460 | 2505 | -0.304 |
| 86 | -0.417 | 1664 | -0.363 | 601 | -0.465 | 1012 | -0.339 |
| 51 | -0.422 | 1682 | -0.387 | 618 | -0.478 | 429 | -0.375 |

**Table B4**. Silica batch experiments (MSS, FILL, SLUR and CAS experiments) - Frequency component loading on principal components.

| Hz | PC1 | Hz | PC2 | Hz | PC3 | Hz | PC4 |
|---|---|---|---|---|---|---|---|
| 2986 | 0.995 | 2076 | 0.602 | 2076 | 0.364 | 1373 | 0.361 |
| 3157 | 0.993 | 120 | 0.565 | 3346 | 0.334 | 3415 | 0.359 |
| 3175 | 0.991 | 189 | 0.541 | 3329 | 0.301 | 1356 | 0.353 |
| 2231 | 0.989 | 240 | 0.528 | 120 | 0.255 | 3380 | 0.348 |
| 2368 | 0.988 | 2059 | 0.515 | 3312 | 0.253 | 3346 | 0.341 |
| 2351 | 0.988 | 172 | 0.514 | 2059 | 0.241 | 3329 | 0.340 |
| 2643 | 0.987 | 223 | 0.507 | 1304 | 0.213 | 3449 | 0.338 |
| 3260 | 0.987 | 137 | 0.501 | 137 | 0.204 | 3398 | 0.331 |
| 2214 | 0.986 | 3809 | 0.470 | 3363 | 0.200 | 3363 | 0.316 |
| 3003 | 0.985 | 154 | 0.453 | 3809 | 0.199 | 3312 | 0.305 |
| 343 | -0.766 | 1012 | -0.913 | 1390 | -0.416 | 669 | -0.187 |
| 395 | -0.774 | 1064 | -0.915 | 515 | -0.432 | 755 | -0.187 |
| 137 | -0.793 | 1081 | -0.915 | 1167 | -0.459 | 772 | -0.190 |
| 360 | -0.816 | 1338 | -0.918 | 498 | -0.525 | 789 | -0.190 |
| 326 | -0.823 | 1304 | -0.929 | 532 | -0.535 | 721 | -0.209 |
| 292 | -0.834 | 1030 | -0.935 | 618 | -0.573 | 292 | -0.211 |
| 378 | -0.847 | 1047 | -0.939 | 652 | -0.608 | 326 | -0.216 |
| 275 | -0.874 | 1098 | -0.944 | 1356 | -0.750 | 480 | -0.226 |
| 103 | -0.879 | 1115 | -0.948 | 1373 | -0.807 | 738 | -0.231 |
| 257 | -0.908 | 1321 | -0.953 | 635 | -0.813 | 309 | -0.285 |

**Table B5.** Merensky experiments (MBx) - Frequency component loading on principal components.

| Hz | PC1 | Hz | PC2 | Hz | PC3 | Hz | PC4 |
|---|---|---|---|---|---|---|---|
| 2540 | 0.971 | 480 | 0.919 | 189 | 0.682 | 103 | 0.463 |
| 2128 | 0.968 | 360 | 0.906 | 86 | 0.574 | 206 | 0.437 |
| 2522 | 0.966 | 498 | 0.893 | 978 | 0.537 | 240 | 0.435 |
| 2557 | 0.966 | 463 | 0.877 | 446 | 0.522 | 257 | 0.423 |
| 2402 | 0.963 | 378 | 0.872 | 172 | 0.497 | 275 | 0.362 |
| 2797 | 0.960 | 583 | 0.865 | 429 | 0.457 | 3140 | 0.356 |
| 2608 | 0.959 | 721 | 0.864 | 326 | 0.372 | 223 | 0.326 |
| 2093 | 0.959 | 738 | 0.857 | 120 | 0.364 | 3655 | 0.282 |
| 2231 | 0.957 | 395 | 0.854 | 292 | 0.357 | 995 | 0.274 |
| 2145 | 0.957 | 412 | 0.850 | 3569 | 0.351 | 3209 | 0.273 |
| 378 | -0.080 | 3329 | -0.213 | 1098 | -0.431 | 2848 | -0.269 |
| 463 | -0.092 | 2900 | -0.214 | 1167 | -0.433 | 1870 | -0.274 |
| 86 | -0.103 | 3346 | -0.217 | 1802 | -0.438 | 515 | -0.275 |
| 480 | -0.105 | 3106 | -0.218 | 1785 | -0.444 | 532 | -0.284 |
| 223 | -0.126 | 3363 | -0.219 | 1081 | -0.500 | 2763 | -0.299 |
| 137 | -0.170 | 2969 | -0.229 | 1064 | -0.501 | 669 | -0.360 |
| 189 | -0.195 | 3449 | -0.230 | 1287 | -0.503 | 446 | -0.487 |
| 395 | -0.226 | 2934 | -0.241 | 1047 | -0.504 | 429 | -0.601 |
| 172 | -0.349 | 3432 | -0.243 | 1321 | -0.506 | 635 | -0.610 |
| 154 | -0.369 | 2951 | -0.277 | 1304 | -0.523 | 652 | -0.704 |

**Table B6.** UG2 experiments (UBx) - Frequency component loading on principal components.

| Hz | PC1 | Hz | PC2 | Hz | PC3 | Hz | PC4 |
|---|---|---|---|---|---|---|---|
| 3329 | 0.962 | 515 | 0.839 | 137 | 0.550 | 206 | 0.672 |
| 3312 | 0.961 | 549 | 0.819 | 240 | 0.535 | 69 | 0.461 |
| 1630 | 0.959 | 566 | 0.811 | 875 | 0.421 | 463 | 0.452 |
| 2866 | 0.959 | 360 | 0.799 | 1956 | 0.411 | 738 | 0.433 |
| 2008 | 0.959 | 343 | 0.785 | 892 | 0.402 | 721 | 0.389 |
| 2951 | 0.958 | 498 | 0.771 | 1562 | 0.397 | 343 | 0.362 |
| 1819 | 0.958 | 532 | 0.758 | 1201 | 0.355 | 1579 | 0.338 |
| 1991 | 0.957 | 738 | 0.700 | 257 | 0.348 | 120 | 0.303 |
| 1613 | 0.952 | 154 | 0.687 | 1579 | 0.321 | 549 | 0.294 |
| 2488 | 0.952 | 806 | 0.660 | 1218 | 0.318 | 223 | 0.277 |
| 480 | -0.508 | 1407 | -0.370 | 309 | -0.454 | 2900 | -0.237 |
| 189 | -0.539 | 120 | -0.396 | 686 | -0.461 | 292 | -0.252 |
| 463 | -0.560 | 3380 | -0.405 | 326 | -0.517 | 412 | -0.280 |
| 69 | -0.561 | 2111 | -0.406 | 652 | -0.536 | 2917 | -0.306 |
| 154 | -0.576 | 1373 | -0.417 | 51 | -0.581 | 275 | -0.312 |
| 206 | -0.640 | 3398 | -0.419 | 103 | -0.629 | 103 | -0.353 |
| 137 | -0.713 | 3415 | -0.432 | 429 | -0.715 | 257 | -0.388 |
| 395 | -0.739 | 1424 | -0.441 | 412 | -0.716 | 240 | -0.482 |
| 172 | -0.818 | 3432 | -0.479 | 86 | -0.751 | 17 | -0.564 |
| 120 | -0.825 | 189 | -0.600 | 446 | -0.926 | 34 | -0.629 |

## B.3 FACTOR LOADINGS – GRAPHS

The factor loading data presented in tables B3 to B6 are shown here as scatterplots between the first and second and the third and fourth principal component of each respective data group. From these graphs it easy to identify frequency components from the spectral data set which have a major influence on the composition of the principal components. From these plots the general structure and relevant importance of the data can be obtained. The highly clustered region in fig B1 for example, shows that most of the 257 frequency parameters have a significant influence on the make-up of the first principal component which account for 73.5% of the total variance. Likewise the second principal component is mostly influenced by three groups of frequencies, namely P7-P14 (120-240Hz), P120-P122 (2059-2093Hz) and P58-P70(995-1201Hz).

The points in the graphs are marked according to the sample number for ease of illustration. To determine the actual frequency the following conversion is used:

$$f = \frac{Px}{257} \times 4410 \text{ Hz} \qquad \text{B1}$$

where f is the frequency component in Hz
and Px is the sample point.

**Figure B1**. Factor loadings for silica experiments. - PC1 & PC2.

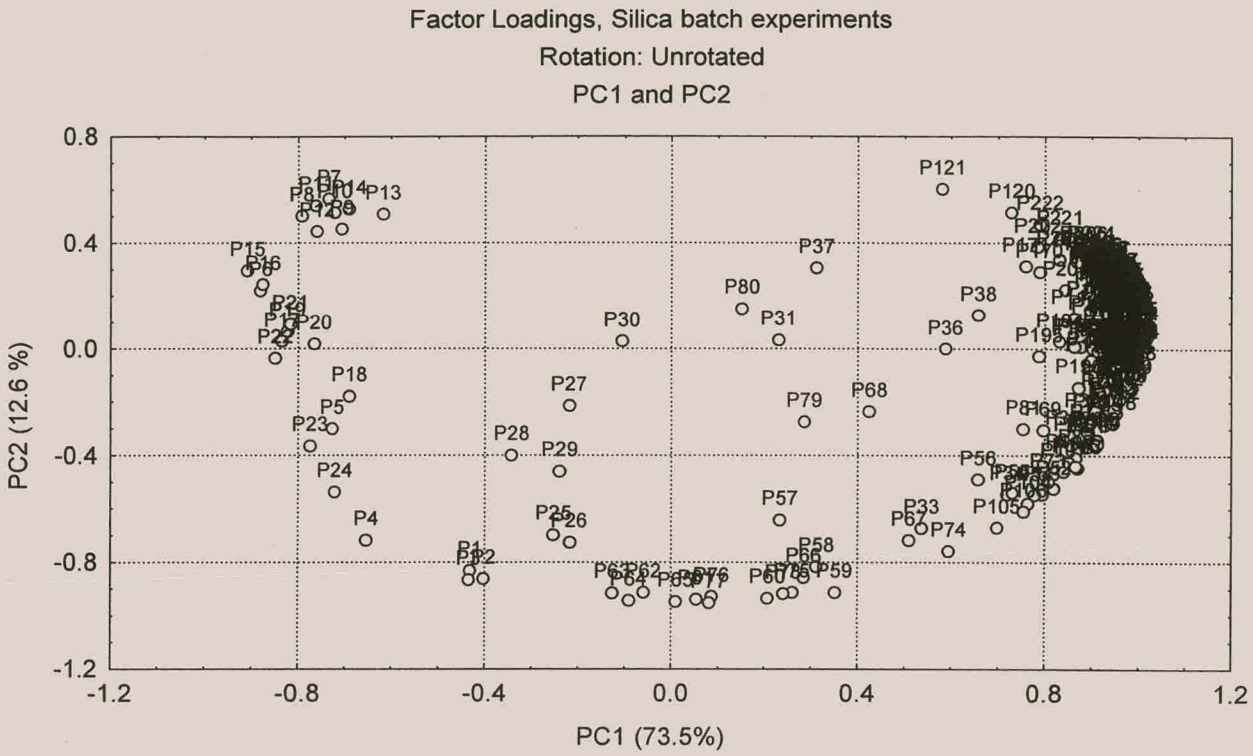

**Figure B2.** Factor loadings for UG2 and Merensky Combination experiments- PC1 & PC2.

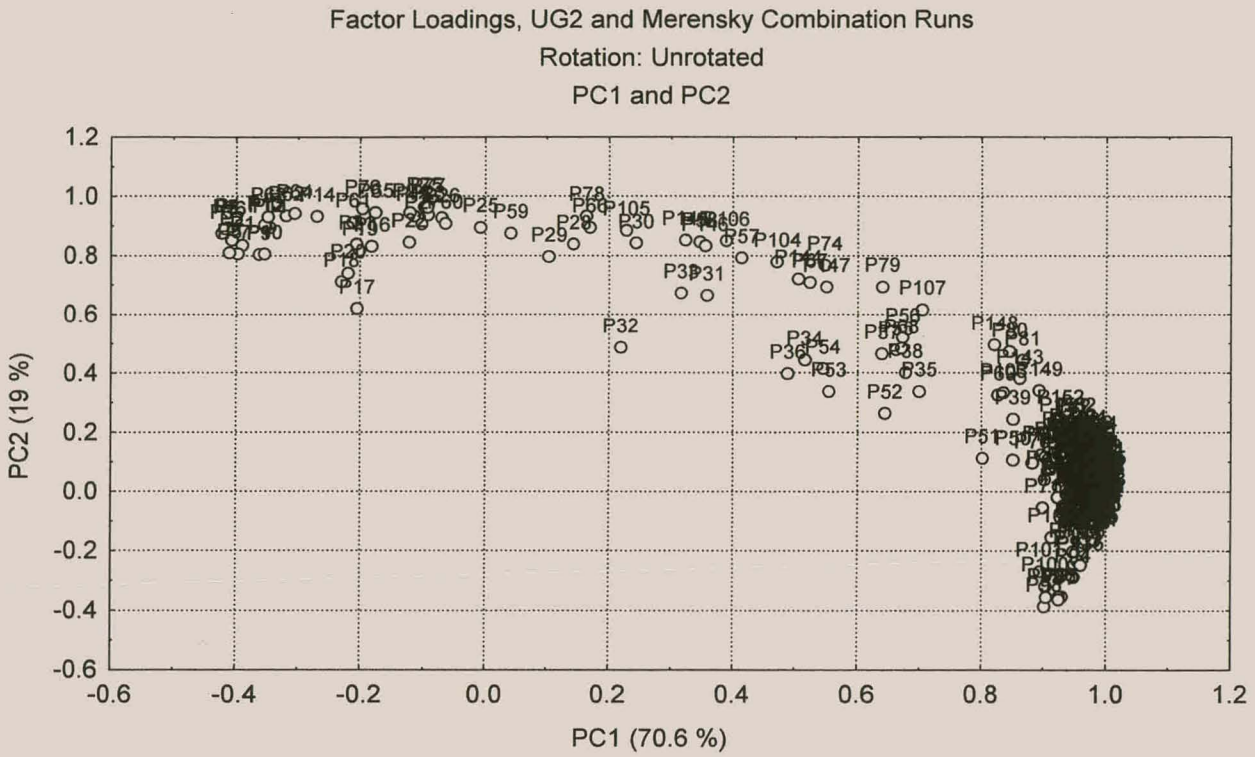


**Figure B3**. Factor loadings for UG2 and Merensky Combination experiments - PC3 & PC4.

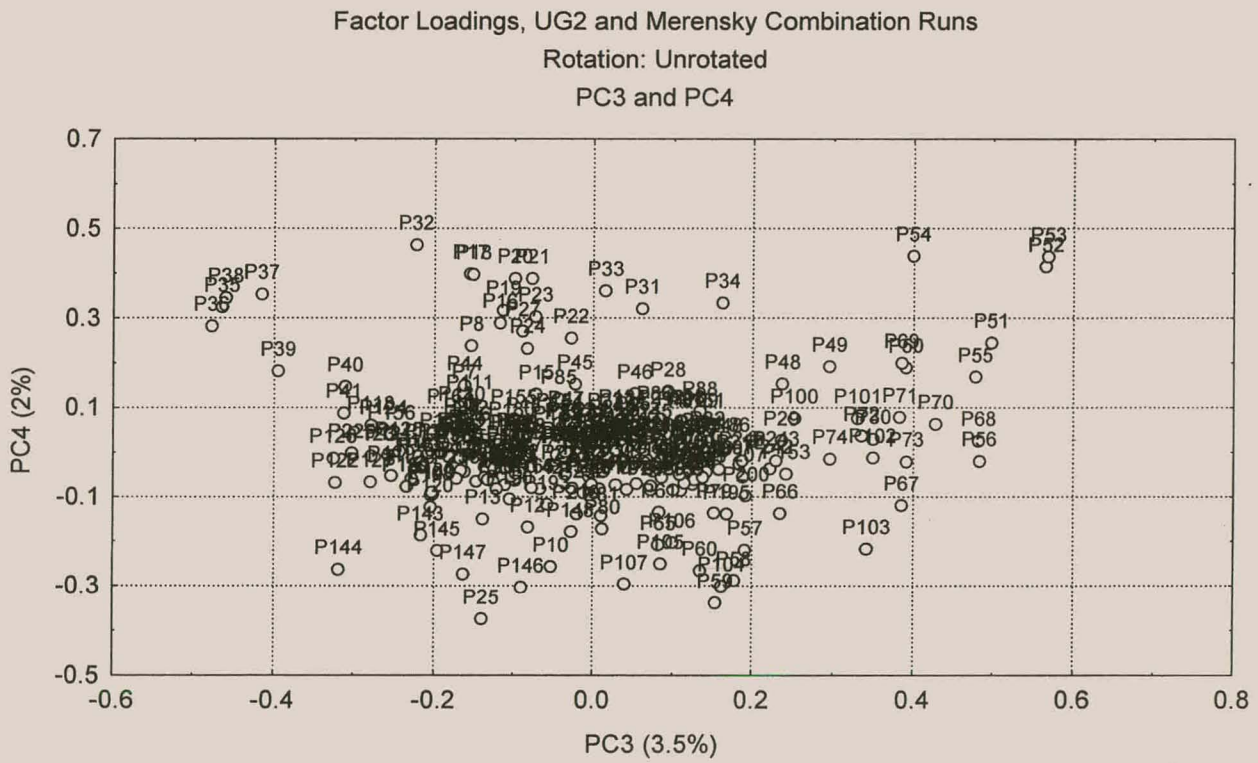

**Figure B4**. Factor loadings for Merensky training data set - PC1 & PC2.

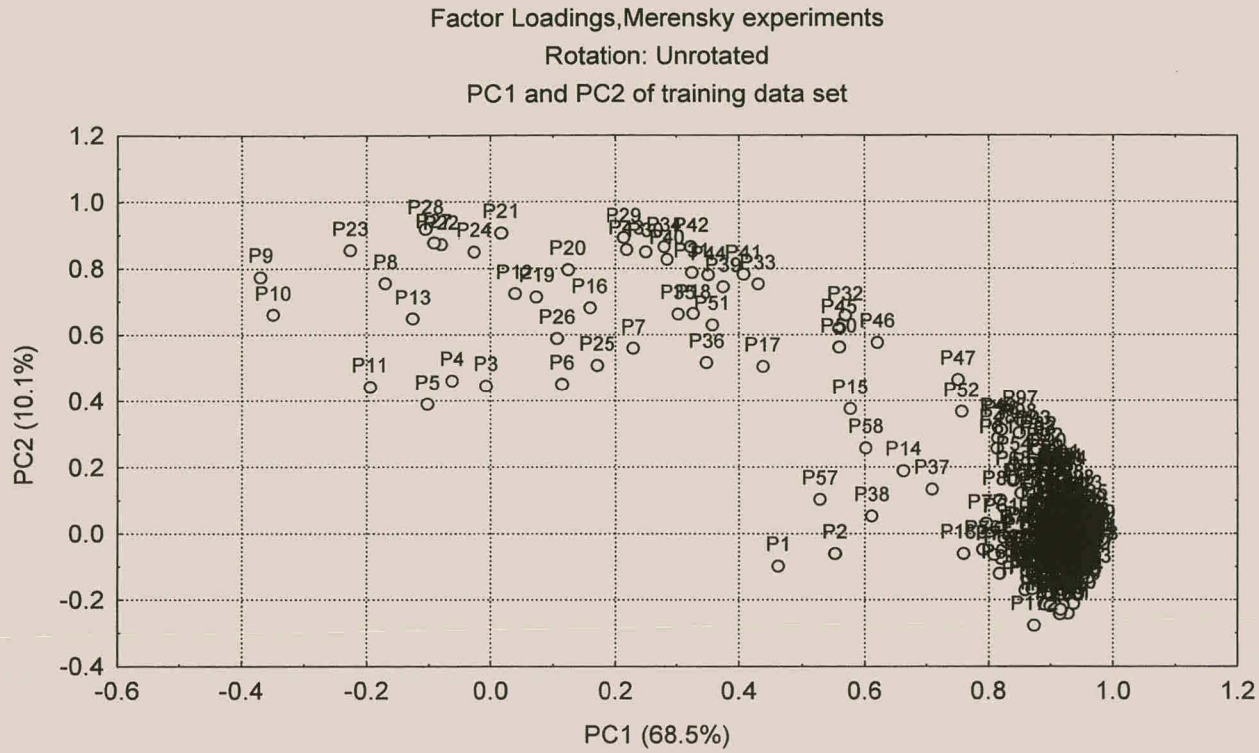


**Figure B5.** Factor loadings for Merensky training data set - PC3 & PC4.

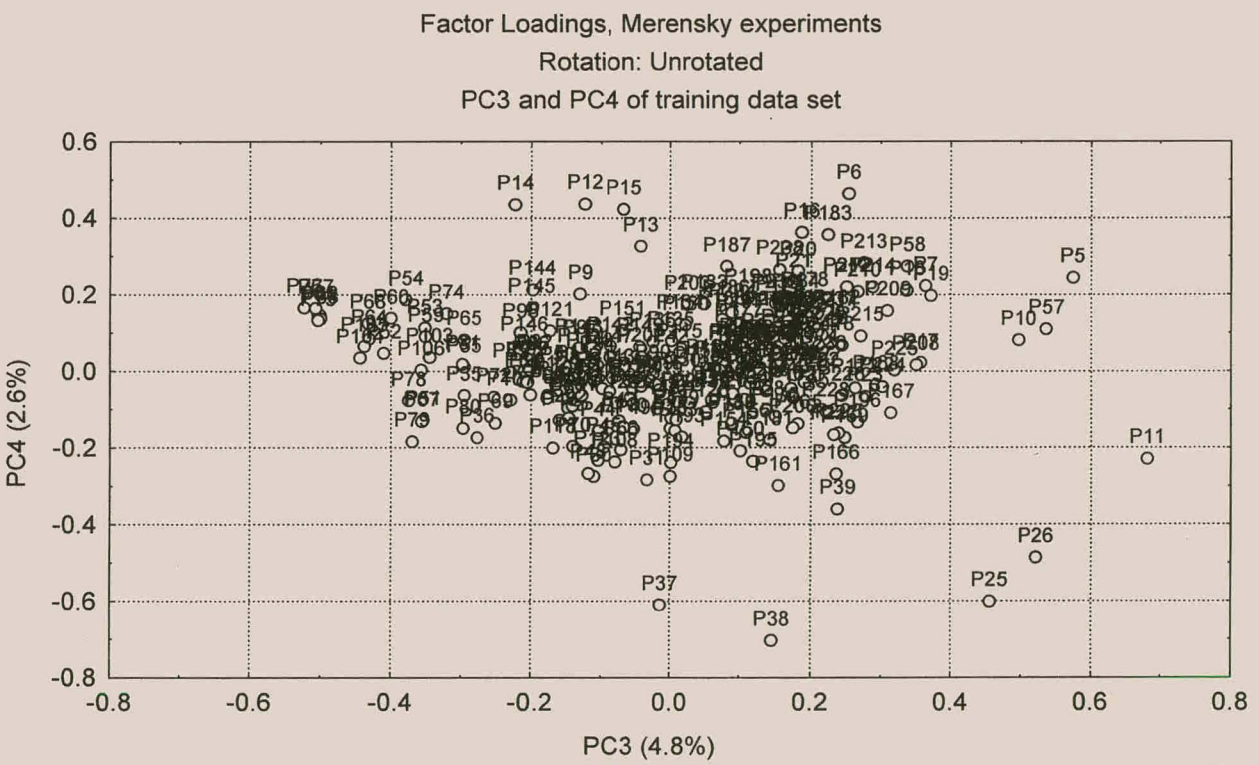

**Figure B6.** Factor Loadings of UG2 training data - PC1 & PC2.

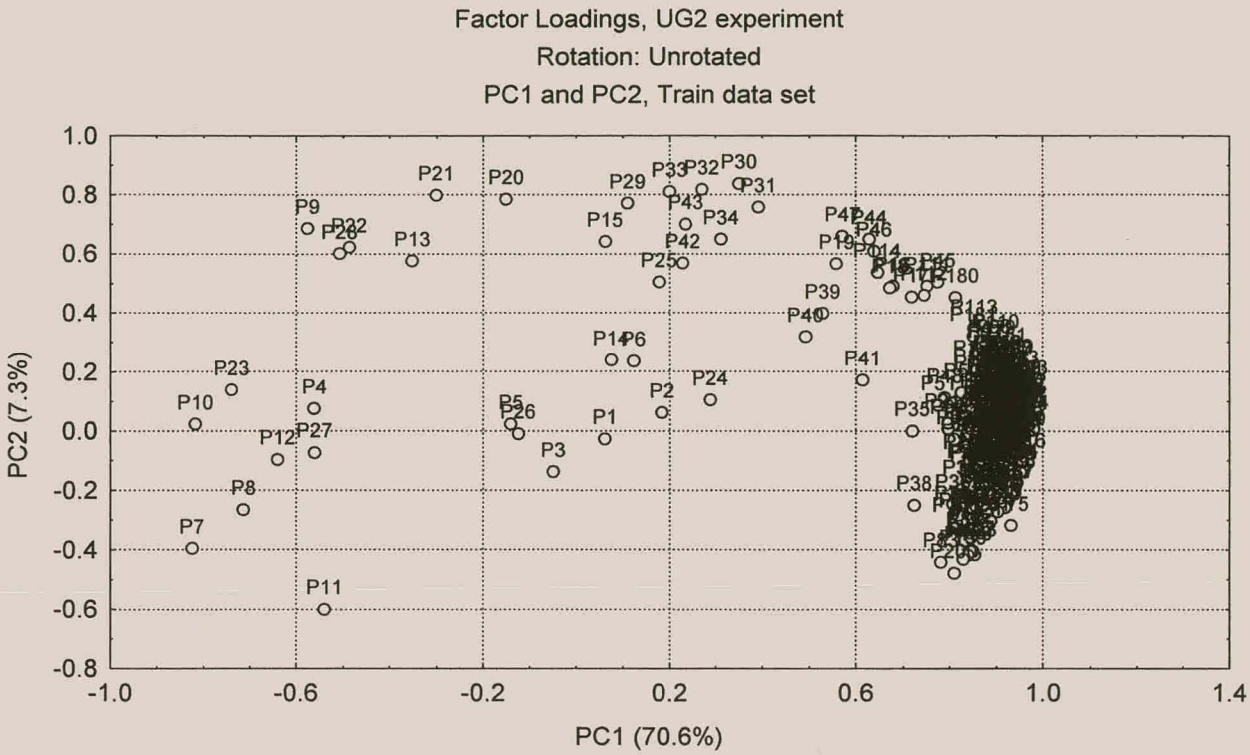


**Figure B7.** Factor Loadings of UG2 training data - PC3 & PC4 .

**-C-**

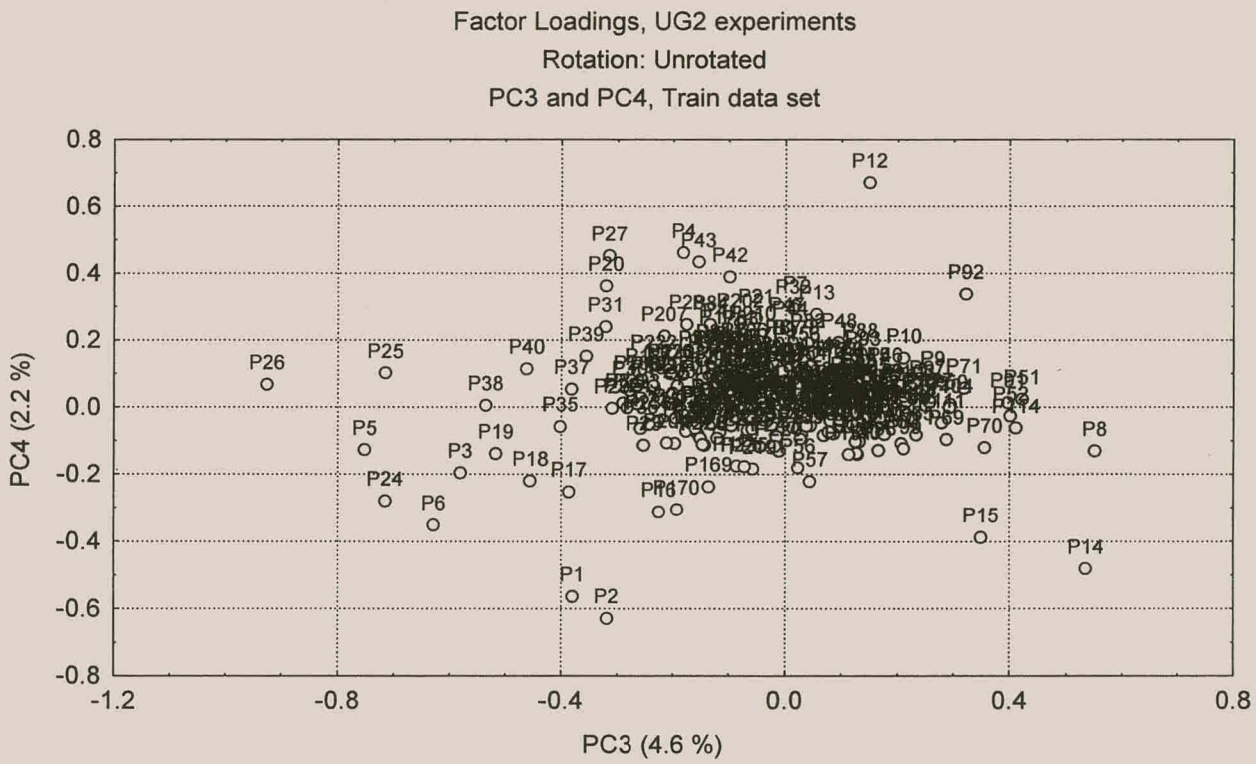

# APPENDIX C

# REGRESSION RESULTS

The modelling results obtained by linear regression of the experimental data are presented in Appendix C. The data will satisfy the equation of the form

$$Y = aPC1 + bPC2 + .... + ePC5$$

where **Y** is the variable being modelled, **PCn** the n'th principal component and **a** through **e** the coefficient obtained by linear regression.

## C.1 EXPERIMENTS

**% Fill experiment:** A perfect fit was obtained for the data from the FILL experiment using modelling by linear regression. The linear regression results for the other experiments are tabulated below.

**Table C1**. Water addition experiment.

| SUMMARY OUTPUT | | | | | | |
|---|---|---|---|---|---|---|
| **Regression Statistics** | | | | | | |
| Multiple R | 0.9934 | | | | | |
| R Square | 0.9869 | | | | | |
| Adjusted R Square | 0.9652 | | | | | |
| Standard Error | 0.3004 | | | | | |
| Observations | 9 | | | | | |
| **ANOVA** | | | | | | |
| | **df** | **SS** | **MS** | **F** | **Significance F** | |
| Regression | 5 | 20.445 | 4.089 | 45.319 | 0.005 | |
| Residual | 3 | 0.271 | 0.090 | | | |
| Total | 8 | 20.716 | | | | |
| | **Coefficients** | **Standard Error** | **t Stat** | **P-value** | **Lower 95%** | **Upper 95%** |
| Intercept | 2.322 | 0.100 | 23.193 | 0.000 | 2.004 | 2.641 |
| X Variable 1 | 0.898 | 0.106 | 8.457 | 0.003 | 0.560 | 1.236 |
| X Variable 2 | 1.301 | 0.106 | 12.250 | 0.001 | 0.963 | 1.639 |
| X Variable 3 | 0.056 | 0.106 | 0.525 | 0.636 | -0.282 | 0.394 |
| X Variable 4 | -0.001 | 0.106 | -0.013 | 0.990 | -0.339 | 0.337 |
| X Variable 5 | 0.231 | 0.106 | 2.178 | 0.118 | -0.107 | 0.569 |
| **RESIDUAL OUTPUT** | | | | | | |
| **Observation** | **Water content** | **Predicted water content** | **Residuals** | **Standard residuals** | | |
| 1 | 0.3 | 0.307 | -0.007 | -0.037 | | |
| 2 | 0.6 | 0.735 | -0.135 | -0.733 | | |
| 3 | 1 | 0.612 | 0.388 | 2.107 | | |
| 4 | 1.6 | 1.841 | -0.241 | -1.309 | | |
| 5 | 2.2 | 2.356 | -0.156 | -0.847 | | |
| 6 | 2.8 | 2.804 | -0.004 | -0.021 | | |
| 7 | 3.4 | 3.338 | 0.062 | 0.337 | | |
| 8 | 4 | 4.031 | -0.031 | -0.168 | | |
| 9 | 5 | 4.876 | 0.124 | 0.671 | | |

**Table C2**. Mill speed experiment.

| SUMMARY OUTPUT | | | | | | |
|---|---|---|---|---|---|---|
| **Regression Statistics** | | | | | | |
| Multiple R | 0.9798 | | | | | |
| R Square | 0.9599 | | | | | |
| Adjusted R Square | 0.9199 | | | | | |
| Standard Error | 7.2076 | | | | | |
| Observations | 13 | | | | | |
| **ANOVA** | | | | | | |
| | **df** | **SS** | **MS** | **F** | **Significance F** | |
| Regression | 6 | 7466.390 | 1244.398 | 23.954 | 0.001 | |
| Residual | 6 | 311.698 | 51.950 | | | |
| Total | 12 | 7778.088 | | | | |
| | **Coefficients** | **Standard Error** | **t Stat** | **P-value** | **Lower 95%** | **Upper 95%** |
| Intercept | 57.30 | 2.00 | 28.66 | 0.00 | 52.40 | 62.19 |
| X Variable 1 | 15.48 | 2.08 | 7.44 | 0.00 | 10.39 | 20.57 |
| X Variable 2 | 5.69 | 2.08 | 2.73 | 0.03 | 0.60 | 10.78 |
| X Variable 3 | 15.36 | 2.08 | 7.38 | 0.00 | 10.27 | 20.45 |
| X Variable 4 | -1.32 | 2.08 | -0.63 | 0.55 | -6.41 | 3.77 |
| X Variable 5 | -10.12 | 2.08 | -4.87 | 0.00 | -15.22 | -5.03 |
| X Variable 6 | 3.17 | 2.08 | 1.52 | 0.18 | -1.92 | 8.26 |
| | | | | | | |
| **RESIDUAL OUTPUT** | | | | | | |
| **Observation** | **Mill speed (rpm)** | **Predicted mill speed** | **Residuals** | **Standard residuals** | | |
| 1 | 16.72 | 16.67 | 0.05 | 0.01 | | |
| 2 | 24.91 | 23.83 | 1.08 | 0.21 | | |
| 3 | 33.10 | 44.58 | -11.48 | -2.25 | | |
| 4 | 41.29 | 33.32 | 7.97 | 1.56 | | |
| 5 | 41.29 | 40.93 | 0.36 | 0.07 | | |
| 6 | 49.48 | 54.31 | -4.83 | -0.95 | | |
| 7 | 57.67 | 61.39 | -3.72 | -0.73 | | |
| 8 | 65.86 | 62.75 | 3.12 | 0.61 | | |
| 9 | 69.14 | 61.75 | 7.39 | 1.45 | | |
| 10 | 74.06 | 74.78 | -0.73 | -0.14 | | |
| 11 | 82.25 | 84.07 | -1.83 | -0.36 | | |
| 12 | 90.44 | 90.91 | -0.47 | -0.09 | | |
| 13 | 98.63 | 95.55 | 3.08 | 0.60 | | |

**Table C3**. Charge addition experiment

| **SUMMARY OUTPUT** | | | | | | |
|---|---|---|---|---|---|---|
| **Regression Statistics** | | | | | | |
| Multiple R | 0.975 | | | | | |
| R Square | 0.951 | | | | | |
| Adjusted R Square | 0.870 | | | | | |
| Standard Error | 21.121 | | | | | |
| Observations | 9 | | | | | |
| **ANOVA** | | | | | | |
| | **df** | **SS** | **MS** | **F** | **Significance F** | |
| Regression | 5 | 26217.259 | 5243.452 | 11.754 | 0.035 | |
| Residual | 3 | 1338.297 | 446.099 | | | |
| Total | 8 | 27555.556 | | | | |
| | **Coefficients** | **Standard Error** | **t Stat** | **P-value** | **Lower 95%** | **Upper 95%** |
| Intercept | 82.22 | 7.04 | 11.68 | 0.00 | 59.82 | 104.63 |
| X Variable 1 | -30.82 | 7.47 | -4.13 | 0.03 | -54.59 | -7.06 |
| X Variable 2 | 42.59 | 7.47 | 5.70 | 0.01 | 18.83 | 66.36 |
| X Variable 3 | 21.82 | 7.47 | 2.92 | 0.06 | -1.95 | 45.58 |
| X Variable 4 | -1.08 | 7.47 | -0.14 | 0.89 | -24.84 | 22.69 |
| X Variable 5 | 5.99 | 7.47 | 0.80 | 0.48 | -17.77 | 29.76 |
| **RESIDUAL OUTPUT** | | | | | | |
| **Observation** | **# small balls** | **Predicted # small balls** | **Residuals** | **Standard residuals** | | |
| 1 | 0 | -3.120 | 3.120 | 0.241 | | |
| 2 | 20 | 11.035 | 8.965 | 0.693 | | |
| 3 | 40 | 60.413 | -20.413 | -1.578 | | |
| 4 | 60 | 53.673 | 6.327 | 0.489 | | |
| 5 | 80 | 89.652 | -9.652 | -0.746 | | |
| 6 | 100 | 106.942 | -6.942 | -0.537 | | |
| 7 | 120 | 106.942 | 13.058 | 1.010 | | |
| 8 | 140 | 152.468 | -12.468 | -0.964 | | |
| 9 | 180 | 161.996 | 18.004 | 1.392 | | |

**Table C4.** Combination Experiment – Prediction of Merensky ore mass fraction (X1).

| **SUMMARY OUTPUT** | | | | | | |
|---|---|---|---|---|---|---|
| **Regression Statistics** | | | | | | |
| Multiple R | 0.9143 | | | | | |
| R Square | 0.8359 | | | | | |
| Adjusted R Square | 0.0152 | | | | | |
| Standard Error | 198.4773 | | | | | |
| Observations | 7 | | | | | |
| **ANOVA** | | | | | | |
| | **df** | **SS** | **MS** | **F** | **Significance F** | |
| Regression | 5 | 200606.8 | 40121.35 | 1.018 | 0.633 | |
| Residual | 1 | 39393.25 | 39393.25 | | | |
| Total | 6 | 240000 | | | | |
| | **Coefficients** | **Standard Error** | **t Stat** | **P-value** | **Lower 95%** | **Upper 95%** |
| Intercept | 500.00 | 75.02 | 6.67 | 0.09 | -453.18 | 1453.18 |
| X Variable 1 | 36.29 | 81.03 | 0.45 | 0.73 | -993.27 | 1065.84 |
| X Variable 2 | 109.75 | 81.03 | 1.35 | 0.40 | -919.80 | 1139.31 |
| X Variable 3 | 86.61 | 81.03 | 1.07 | 0.48 | -942.94 | 1116.17 |
| X Variable 4 | -45.24 | 81.03 | -0.56 | 0.68 | -1074.79 | 984.32 |
| X Variable 5 | -102.59 | 81.03 | -1.27 | 0.43 | -1132.14 | 926.97 |
| **RESIDUAL OUTPUT** | | | | | | |
| **Observation** | **X1 mass** | **Predicted Y** | **Residuals** | **Standard residuals** | | |
| 1 | 700 | 678 | 21.77 | 0.27 | | |
| 2 | 700 | 310 | -9.95 | -0.12 | | |
| 3 | 700 | 562 | 138.19 | 1.71 | | |
| 4 | 500 | 353 | -52.72 | -0.65 | | |
| 5 | 300 | 698 | 2.11 | 0.03 | | |
| 6 | 300 | 272 | 27.77 | 0.34 | | |
| 7 | 300 | 627 | -127.16 | -1.57 | | |

**Table C5**. Combination Experiment – Prediction of UG2 ore mass fraction (X2).

| **SUMMARY OUTPUT** | | | | | | |
|---|---|---|---|---|---|---|
| **Regression Statistics** | | | | | | |
| Multiple R | 0.9143 | | | | | |
| R Square | 0.8359 | | | | | |
| Adjusted R Square | 0.0152 | | | | | |
| Standard Error | 198.4773 | | | | | |
| Observations | 7 | | | | | |
| **ANOVA** | | | | | | |
| | **df** | **SS** | **MS** | **F** | **Significance F** | |
| Regression | 5 | 200606.75 | 40121.35 | 1.02 | 0.63 | |
| Residual | 1 | 39393.25 | 39393.25 | | | |
| Total | 6 | 240000.00 | | | | |
| | **Coefficients** | **Standard Error** | **t Stat** | **P-value** | **Lower 95%** | **Upper 95%** |
| Intercept | 500.00 | 75.02 | 6.67 | 0.09 | -453.18 | 1453.18 |
| X Variable 1 | -36.29 | 81.03 | -0.45 | 0.73 | -1065.84 | 993.27 |
| X Variable 2 | -109.75 | 81.03 | -1.35 | 0.40 | -1139.31 | 919.80 |
| X Variable 3 | -86.61 | 81.03 | -1.07 | 0.48 | -1116.17 | 942.94 |
| X Variable 4 | 45.24 | 81.03 | 0.56 | 0.68 | -984.32 | 1074.79 |
| X Variable 5 | 102.59 | 81.03 | 1.27 | 0.43 | -926.97 | 1132.14 |
| **RESIDUAL OUTPUT** | | | | | | |
| **Observation** | **X2 mass** | **Predicted Y** | **Residuals** | **Standard residuals** | | |
| 1 | 300 | 322 | -21.77 | -0.27 | | |
| 2 | 300 | 690 | 9.95 | 0.12 | | |
| 3 | 300 | 438 | -138.19 | -1.71 | | |
| 4 | 500 | 647 | 52.72 | 0.65 | | |
| 5 | 700 | 302 | -2.11 | -0.03 | | |
| 6 | 700 | 728 | -27.77 | -0.34 | | |
| 7 | 700 | 373 | 127.16 | 1.57 | | |

**Table C6.** Combination Experiment – Prediction of Merensky ore size fraction (D1).

| **SUMMARY OUTPUT** | | | | | | |
|---|---|---|---|---|---|---|
| **Regression Statistics** | | | | | | |
| Multiple R | 0.988 | | | | | |
| R Square | 0.977 | | | | | |
| Adjusted R Square | 0.861 | | | | | |
| Standard Error | 239.314 | | | | | |
| Observations | 7 | | | | | |
| **ANOVA** | | | | | | |
| | **df** | **SS** | **MS** | **F** | **Significance F** | |
| Regression | 5 | 2411300 | 482260.1 | 8.4207 | 0.2556 | |
| Residual | 1 | 57271.06 | 57271.06 | | | |
| Total | 6 | 2468571 | | | | |
| | **Coefficients** | **Standard Error** | **t Stat** | **P-value** | **Lower 95%** | **Upper 95%** |
| Intercept | 3314.29 | 90.45 | 36.64 | 0.02 | 2164.99 | 4463.58 |
| X Variable 1 | -561.59 | 97.70 | -5.75 | 0.11 | -1802.98 | 679.79 |
| X Variable 2 | -14.72 | 97.70 | -0.15 | 0.90 | -1256.10 | 1226.67 |
| X Variable 3 | -71.62 | 97.70 | -0.73 | 0.60 | -1313.01 | 1169.76 |
| X Variable 4 | -134.08 | 97.70 | -1.37 | 0.40 | -1375.46 | 1107.31 |
| X Variable 5 | 251.34 | 97.70 | 2.57 | 0.24 | -990.04 | 1492.73 |
| **RESIDUAL OUTPUT** | | | | | | |
| **Observation** | **D1** | **Predicted Y** | **Residuals** | **Standard residuals** | | |
| 1 | 4000 | 3974 | 26.245 | 0.269 | | |
| 2 | 2800 | 4012 | -12.002 | -0.123 | | |
| 3 | 2800 | 2633 | 166.618 | 1.705 | | |
| 4 | 2800 | 2864 | -63.564 | -0.651 | | |
| 5 | 2800 | 2797 | 2.546 | 0.026 | | |
| 6 | 4000 | 3967 | 33.483 | 0.343 | | |
| 7 | 4000 | 2953 | -153.325 | -1.569 | | |

**Table C7**. Combination Experiment – Prediction of UG2 ore size fraction (D2).

| **SUMMARY OUTPUT** | | | | | | |
|---|---|---|---|---|---|---|
| **Regression Statistics** | | | | | | |
| Multiple R | 0.9986 | | | | | |
| R Square | 0.9971 | | | | | |
| Adjusted R Square | 0.9828 | | | | | |
| Standard Error | 84.1843 | | | | | |
| Observations | 7 | | | | | |
| **ANOVA** | | | | | | |
| | **df** | **SS** | **MS** | **F** | **Significance F** | |
| Regression | 5 | 2461484 | 492296.9 | 69.4648 | 0.0908 | |
| Residual | 1 | 7087 | 7087 | | | |
| Total | 6 | 2468571 | | | | |
| | **Coefficients** | **Standard Error** | **t Stat** | **P-value** | **Lower 95%** | **Upper 95%** |
| Intercept | 3314.29 | 31.82 | 104.16 | 0.01 | 2909.99 | 3718.58 |
| X Variable 1 | -452.00 | 34.37 | -13.15 | 0.05 | -888.69 | -15.32 |
| X Variable 2 | 106.27 | 34.37 | 3.09 | 0.20 | -330.42 | 542.95 |
| X Variable 3 | 389.53 | 34.37 | 11.33 | 0.06 | -47.16 | 826.21 |
| X Variable 4 | 147.72 | 34.37 | 4.30 | 0.15 | -288.96 | 584.41 |
| X Variable 5 | -145.23 | 34.37 | -4.23 | 0.15 | -581.92 | 291.45 |
| **RESIDUAL OUTPUT** | | | | | | |
| **Observation** | **D2** | **Predicted Y** | **Residuals** | **Standard residuals** | | |
| 1 | 4000 | 3991 | 9.232 | 0.269 | | |
| 2 | 2800 | 4004 | -4.222 | -0.123 | | |
| 3 | 4000 | 2741 | 58.612 | 1.705 | | |
| 4 | 2800 | 2822 | -22.360 | -0.651 | | |
| 5 | 2800 | 3999 | 0.895 | 0.026 | | |
| 6 | 2800 | 2788 | 11.778 | 0.343 | | |
| 7 | 4000 | 2854 | -53.936 | -1.569 | | |

**Table C8.** Merensky ore runs – Prediction of 80% passing size.

| **SUMMARY OUTPUT** | | | | | | |
|---|---|---|---|---|---|---|
| **Regression Statistics** | | | | | | |
| Multiple R | 0.6804 | | | | | |
| R Square | 0.4629 | | | | | |
| Adjusted R Square | 0.4166 | | | | | |
| Standard Error | 723.1699 | | | | | |
| Observations | 64 | | | | | |
| **ANOVA** | | | | | | |
| | **df** | **SS** | **MS** | **F** | **Significance F** | |
| Regression | 5 | 26141580 | 5228316.01 | 10.00 | 6.2E-07 | |
| Residual | 58 | 30332533 | 522974.72 | | | |
| Total | 63 | 56474113 | | | | |
| | **Coefficients** | **Standard Error** | **t Stat** | **P-value** | **Lower 95%** | **Upper 95%** |
| Intercept | 949.53 | 90.40 | 10.50 | 0.00 | 768.58 | 1130.48 |
| PC1 | 51.32 | 91.11 | 0.56 | 0.58 | -131.05 | 233.70 |
| PC2 | 316.26 | 91.11 | 3.47 | 0.00 | 133.88 | 498.63 |
| PC3 | -536.32 | 91.11 | -5.89 | 0.00 | -718.70 | -353.94 |
| PC4 | -102.59 | 91.11 | -1.13 | 0.26 | -284.97 | 79.78 |
| PC5 | 118.87 | 91.11 | 1.30 | 0.20 | -63.51 | 301.25 |
| **RESIDUAL OUTPUT** | | | | | | |
| **OMITTED** | | | | | | |

**Table C9.** Merensky ore runs – Prediction of 50% passing size.

| SUMMARY OUTPUT | | | | | | |
|---|---|---|---|---|---|---|
| **Regression Statistics** | | | | | | |
| Multiple R | 0.7860 | | | | | |
| R Square | 0.6178 | | | | | |
| Adjusted R Square | 0.5848 | | | | | |
| Standard Error | 185.0129 | | | | | |
| Observations | 64 | | | | | |
| **ANOVA** | | | | | | |
| | **df** | **SS** | **MS** | **F** | **Significance F** | |
| Regression | 5 | 3208954 | 641790.8 | 18.75 | 4.83E-11 | |
| Residual | 58 | 1985327 | 34229.78 | | | |
| Total | 63 | 5194281 | | | | |
| | **Coefficients** | **Standard Error** | **t Stat** | **P-value** | **Lower 95%** | **Upper 95%** |
| Intercept | 325.88 | 23.13 | 14.09 | 0.00 | 279.58 | 372.17 |
| PC1 | -1.74 | 23.31 | -0.07 | 0.94 | -48.40 | 44.92 |
| PC2 | 117.57 | 23.31 | 5.04 | 0.00 | 70.92 | 164.23 |
| PC3 | -186.94 | 23.31 | -8.02 | 0.00 | -233.60 | -140.29 |
| PC4 | -30.98 | 23.31 | -1.33 | 0.19 | -77.64 | 15.68 |
| PC5 | 34.65 | 23.31 | 1.49 | 0.14 | -12.01 | 81.31 |
| **RESIDUAL OUTPUT** | | | | | | |
| **OMITTED** | | | | | | |

**Table C10.** UG2 ore runs – Prediction of 80% passing size.

| **SUMMARY OUTPUT** | | | | | | |
|---|---|---|---|---|---|---|
| **Regression Statistics** | | | | | | |
| Multiple R | 0.5367 | | | | | |
| R Square | 0.2880 | | | | | |
| Adjusted R Square | 0.1767 | | | | | |
| Standard Error | 87.7651 | | | | | |
| Observations | 38 | | | | | |
| **ANOVA** | | | | | | |
| | **df** | **SS** | **MS** | **F** | **Significance F** | |
| Regression | 5 | 99701.89 | 19940.38 | 2.59 | 0.04 | |
| Residual | 32 | 246487.08 | 7702.72 | | | |
| Total | 37 | 346188.97 | | | | |
| | **Coefficients** | **Standard Error** | **t Stat** | **P-value** | **Lower 95%** | **Upper 95%** |
| Intercept | 136.026 | 14.237 | 9.554 | 0.000 | 107.026 | 165.027 |
| PC1 | 32.904 | 14.429 | 2.281 | 0.029 | 3.515 | 62.294 |
| PC2 | -7.930 | 14.429 | -0.550 | 0.586 | -37.320 | 21.459 |
| PC3 | -35.231 | 14.429 | -2.442 | 0.020 | -64.621 | -5.841 |
| PC4 | 10.056 | 14.429 | 0.697 | 0.491 | -19.333 | 39.446 |
| PC5 | 14.376 | 14.429 | 0.996 | 0.327 | -15.014 | 43.766 |
| **RESIDUAL OUTPUT** | | | | | | |
| **OMITTED** | | | | | | |

**Table C11**. UG2 ore runs – Prediction of 50% passing size.

| **SUMMARY OUTPUT** | | | | | | |
|---|---|---|---|---|---|---|
| **Regression Statistics** | | | | | | |
| Multiple R | 0.5062 | | | | | |
| R Square | 0.2562 | | | | | |
| Adjusted R Square | 0.1400 | | | | | |
| Standard Error | 464.8576 | | | | | |
| Observations | 38 | | | | | |
| **ANOVA** | | | | | | |
| | **df** | **SS** | **MS** | **F** | **Significance F** | |
| Regression | 5 | 2382335.23 | 476467.05 | 2.20 | 0.08 | |
| Residual | 32 | 6914963.61 | 216092.61 | | | |
| Total | 37 | 9297298.84 | | | | |
| | **Coefficients** | **Standard Error** | **t Stat** | **P-value** | **Lower 95%** | **Upper 95%** |
| Intercept | 434.37 | 75.41 | 5.76 | 0.00 | 280.76 | 587.97 |
| PC1 | 157.33 | 76.42 | 2.06 | 0.05 | 1.66 | 312.99 |
| PC2 | -41.22 | 76.42 | -0.54 | 0.59 | -196.88 | 114.45 |
| PC3 | -164.14 | 76.42 | -2.15 | 0.04 | -319.81 | -8.48 |
| PC4 | 72.70 | 76.42 | 0.95 | 0.35 | -82.97 | 228.36 |
| PC5 | 75.56 | 76.42 | 0.99 | 0.33 | -80.11 | 231.23 |
| **RESIDUAL OUTPUT OMITTED** | | | | | | |

# APPENDIX D

# TYPICAL NEURAL NETWORK RESULTS

The data given in the tables below represent the actual cumulative undersize distributions obtained for both Merensky and UG2 ore from the experiments for 0 minutes, 5 minutes and 10 minutes grinding. The training results represent the results of the neural network model after it was trained and simulated with the actual cumulative undersize distributions. The test data refers to the results of the model obtained by simulating the network with test data for a similar sample of the same ore type and milling time, and by using the trained network weights.

**Table D1.** Merensky ore prediction and validation results for 10 minutes milling time.

| Screen Size | 0 min | | | 5 min | | | 10 min | | |
|---|---|---|---|---|---|---|---|---|---|
| | *Cum % u/s* | *Train out* | *Test out* | *Cum % u/s* | *Train out* | *Test Out* | *Cum% u/s* | *Train Out* | *Test Out* |
| 2800 | 76.7 | 86.7 | 85.4 | 87.8 | 87.7 | 86.9 | 88.9 | 89.7 | 87.2 |
| 1400 | 57.8 | 75.8 | 73.7 | 81.8 | 79.5 | 76.9 | 83.7 | 83.3 | 78.4 |
| 600 | 42.2 | 52.8 | 62.1 | 71.8 | 66.8 | 64.8 | 76.9 | 73.3 | 68.3 |
| 425 | 32.8 | 25.3 | 49.3 | 55.2 | 51.8 | 49.3 | 66.6 | 62.7 | 56.4 |
| 300 | 23.5 | 10.2 | 38.3 | 40.5 | 40.8 | 38.9 | 52.0 | 48.5 | 41.3 |
| 212 | 10.5 | -22.4 | 22.7 | 26.0 | 28.8 | 27.8 | 31.9 | 33.5 | 26.0 |
| 150 | 4.6 | -19.4 | 11.3 | 11.6 | 14.5 | 13.9 | 18.0 | 19.2 | 14.1 |
| 106 | 1.2 | -26.4 | 4.8 | 6.0 | 8.0 | 7.3 | 10.4 | 12.9 | 8.4 |
| 75 | 0.5 | -23.7 | 2.5 | 2.9 | 4.5 | 4.2 | 6.0 | 8.6 | 5.4 |
| 0 | 0.1 | -18.8 | 1.6 | 1.3 | 1.9 | 1.8 | 4.1 | 6.7 | 4.3 |

**Table D2.** UG2 ore prediction and validation results for 10 minutes milling time.

| Screen | 0 | | | 5 | | | 10 | | |
|---|---|---|---|---|---|---|---|---|---|

| Size | min | | | min | | | min | | |
|---|---|---|---|---|---|---|---|---|---|
| | Cum% u/s | Train Out | Test Out | Cum % u/s | Train Out | Test Out | Cum % u/s | Train Out | Test Out |
| 2800 | 90.8 | 85.5 | 93.0 | 95.2 | 97.0 | 95.3 | 97.1 | 96.7 | 96.0 |
| 1400 | 77.4 | 73.7 | 78.9 | 86.4 | 92.9 | 87.7 | 90.5 | 93.0 | 90.3 |
| 600 | 65.6 | 70.8 | 65.8 | 79.8 | 90.3 | 76.6 | 84.9 | 90.9 | 83.9 |
| 425 | 53.8 | 47.4 | 56.4 | 74.3 | 88.7 | 75.5 | 80.9 | 89.1 | 83.3 |
| 300 | 45.3 | 45.9 | 49.9 | 70.0 | 88.5 | 78.2 | 79.0 | 89.2 | 81.6 |
| 212 | 34.8 | 20.0 | 39.2 | 61.6 | 86.1 | 66.7 | 73.7 | 87.1 | 76.2 |
| 150 | 25.8 | 18.1 | 26.3 | 47.6 | 77.1 | 49.6 | 58.0 | 78.6 | 66.1 |
| 106 | 14.9 | 19.1 | 15.3 | 32.9 | 60.2 | 34.4 | 39.3 | 61.6 | 51.8 |
| 75 | 9.9 | 21.1 | 7.4 | 20.8 | 43.7 | 22.2 | 27.6 | 44.9 | 37.1 |
| 0 | 6.7 | 10.7 | 6.3 | 14.5 | 32.7 | 15.6 | 19.0 | 33.9 | 27.8 |

# APPENDIX E

## E.1 MILL TYPES

The field of communition with regard to tumbling mills is characterised by the different types of mills encountered in the field, each with it's specific method of operation, product quality and important influential parameters.

The following chapter gives a brief background into the three main types of tumbling mills in use today. As the thesis as been based on operation in a laboratory ball mill, a section is devoted to the parameters that influence operation, and hence product, of industrial ball mills.

## E.2 ROD MILLS

Rod mills can be described as either fine crushers or coarse grinding machines, capable of reducing a 50 mm feed to 300 μm. The distinctive feature of these mills is that the length to diameter ratio is between 1.5 and 2.5.

The grinding mechanism of a rod mill relies on the spinning of the rods to act as a series of crushing rolls. The coarse feed tends to spread the rods at the feed end resulting in a wedge shaped array of the rods, with preferential grinding of the larger particles and reduction of the amount of ultra fine particles.

## E.3 AUTOGENOUS MILLS

Autogenous mills make use of the feed ore as the charge, instead of conventional steel rods or balls. The advantages over conventional methods include lower capital cost, ability to handle wet and sticky material, simpler flow sheets, the large size of available equipment, lower manpower requirements and minimal grinding media expense.

Primary autogenous mills can achieve size reductions from 25 cm to 100 μm in a single process unit. The particle size distribution of the product depends on the characteristics and structure of the particular ore being ground. The grinding action in these mills fracture the rock along the crystal or grain boundaries, leaving the product in the region of the grain or crystal size. This is desirable for most of the processes following the grinding process such as flotation. As the grinding media is the ore itself, and is variable, it is difficult to predict the product of the mill, whereas in conventional mills the size and amount of the rods or balls are known. This makes control of autogenous mills more difficult than normal types of tumbling mills.

## E.4 BALL MILLS:

As ball mills will be the equipment used in this study the following more elaborate discussion is taken from Mullen et al. (1996).

Ball mills are the most common form of tumbling mill. These mills are used for primary and secondary grinding as well as in some regrind operations. As these mills are usually the largest consumers of energy within a concentrator their optimisation has important performance and economic implications.

### E.4.1 Construction:

These mills consist of a cylindrical drum rotated around the longitudinal axis. The feed usually enters the mill in the form of a slurry at one end and leaves the mill from the other. Ball mills are classified according to the method of discharge. Two main types are found, the overflow mill where the product stream leaves the mill from the discharge trunnion which is larger than the inlet. This provides a hydraulic gradient driving the slurry through the mill.

Grate discharge mills have an internal grate and slurry lifters at the discharge end, providing a form of classification as the product leaves the mill. The slurry level is lower than in overflow mills.

In ball mills the key variables are: Mill size and power, ball (steel) loading and mill speed and the media ball size and shape.

### E.4.2 Mill Size and Power:

The most common mills have a length to diameter ratio of 1-1.5. Other ratios of 1:3 and 3:1 are also encountered. This is one of the few process units covering a scale of more than six orders of magnitude. Sizes range from small laboratory mills (200mm x 200mm) to huge industrial mills (6m x 9m).

### E.4.3 Ball Load and Mill Speed:

The ball load of an overflow discharge mill is typically in the range of 35 to 45%. Grate discharge mills tend to be filled with more material.

Mill speed is expressed as a fraction of the rotational speed, with the critical speed being where the load centrifuges.

The critical speed is calculated as follows:

$$C_s = \frac{42.3}{\sqrt{D-d}} \quad \text{rpm} \qquad \text{E1}$$

with D the mill diameter in metres.

Maximum grinding usually occurs at 80% of the critical speed.

### E.4.4 Media Size and Shape:

Harder ores and coarser feed require a higher impact energy and larger media, whereas fine grind sizes require large media surface area and small media. The choice of media therefore plays an important role in any specific application.

The media shape is an indication of the effectivity of the grinding process. The shape can be altered by wear patterns, ball quality or deliberate use of shapes with more surface area. Balls worn into a cubic shape with indented faces indicate a static region within the charge where no effective grinding occurs.

For fine grinding media shapes with more surface area per unit mass have proven to be more effective, which is true for smaller balls giving a finer grind.

### E.4.5 Mill Liners:

The purpose of the mill liners is to protect the mill shell from wear. Liners used in rod and ball mills are mostly arranged as a set of parallel waves, constructed from rubber or alloy steel.

The liner profile imparts energy to the outer layer of the charge, which leads to an imparting of energy to the layer on top of it.

Liner configuration is not as critical as it was expected previously, as most of the energy is transferred from ball to ball. Impact forces on the shell are small, as the charge motion comprises lifting and rolling of a bed of balls. This then leads to the safe use of rubber liners in most mills.

### E.4.6 Operation of Ball Mills:

The following operating conditions limit ball mill performance and will be discussed briefly (Mullen et al (1996):

- Feed too coarse
- Too high slurry density
- Too low slurry density
- Inappropriate slurry rheology
- Too small or large balls
- Poor liner design / condition
- Poor classifier operation

#### *E.4.6.1 Coarse Feed Size*

The feed size to the mill has a large influence on the mill operation. Product from semi- and fully autogenous mills (SAG/FAG) are rarely coarse enough to escape the

mill, while the coarse product from primary crushers plays an important role in the operation of mills further down in the circuit. The larger particles in the mill discharge also produce the most wear, thus playing a role in liner/lifter life. High circulating loads will further influence classifier life. It has been shown that the ball top size can be reduced and costs cut by reducing the feed top size to the mill.

### *E.4.6.2 Slurry Density*

Due to the mixing motion inside a mill the discharge slurry density will be similar to the density inside the mill. With the increase of water to the mill, the number of smaller particles that are available to interact with the balls, as well as the effective impacts, are reduced. When more water is added, the slurry becomes insufficiently viscous to coat the balls and grinding decreases rapidly.

An increase in slurry density will lead to an increase in grinding until a condition is reached where the viscosity increases rapidly. Slurry discharge will change from turbulent to almost laminar flow. The optimal density is just below the point of rapid viscosity increase.

### *E.4.6.3 Slurry Viscosity*

The effects of viscosity and density are distinct although they are strongly correlated. Viscosity is difficult to measure in industrial plants.

According to Mullen et al. (1996) viscosity has a non-linear dependence on the solids concentration of the slurry. Slurries exhibit many different rheological characteristics, depending on the prevailing solids concentration, particle size distribution, particle shape and physico-chemical conditions. Viscosity is the local ratio of shear stress to shear rate and varies with shear rate for all but Newtonian slurries.

Klimpel (1982,1983) observed the following trends for slurries in tumbling mills:

- In the normal low density, low viscosity region there is no variation in mill production with increase in viscosity.
- At a higher viscosity, induced by increasing slurry density and/or fines content, grinding improves.

- Excessive viscosity gives decreased production.

Increasing the solids concentration of the slurry induces pseudoplastic behaviour, with first order breakage, with higher rates of breakage than dilitant slurries. This represents the most efficient grinding practice. As the solids concentration increases further, the resulting stress leads to higher order breakage, and the consequent reduction in breakage rates.

### *E.4.6.4 Liner Selection*

Liner design is usually not critical for ball mill operation. However slip of the charge as a unit can cause problems. This effect is recognized by vertical stirations on the liners and rapid wear. It can sometimes be monitored as a series of sudden decreases in power draw. Lifters that are too high can generate a shear plane in the ball charge with low power draw and little grinding.

### *E.4.6.5 Ball Size Selection*

The smaller the feed size, the smaller the grinding ball size that is required. As small balls are more expensive, larger sizes are often used. This leads to a much higher production in fines with consequent higher cost implications.

### *E.4.6.6 Classifier Operation*

The most common cause of poor ball mill operation is poor classifier selection or performance. The effect of closed circuit operation is to produce fewer coarse particles without producing excessive fines. According to Bond (1961), the improvement in classification can amount to 20% more throughput at the same energy input and the same nominal product size.

### *E.4.6.7 Recirculating Loads*

A load that is too high will tend to carry coarse particles out of the mill with detrimental effects. It is important to realise that the circulating load is set by the magnitude of the difference in particle size distribution between the classifier product and feed. A primary mill/cyclone circuit will inherently tend to operate at higher circulating loads than a cyclone/mill circuit treating rod mill discharge. A lower circulating load will allow a longer mill residence time and a finer discharge. It also allows finished product to be broken further.

The optimum circulating load will provide a good compromise between overgrinding and minimisation of coarse particles in the mill discharge. This means matching the classifier cut-size to the mill product size with maximum water split to overflow which is best obtained by a well calibrated simulation model.

### *E.4.6.8 Mill Power*

The power drawn by a mill is usually used to monitor the ball or rod load. Mills are charged with new media to a target power on a regular schedule. This target should be increased as liners wear in and wear out (6-12 months).

Power prediction is easier for ball and rod mills than SAG/FAG because the shape of the charge media remains more or less constant. The charge motion can be considered as a distribution of impacts of known energy. The mill power is the sum of the energy in each of these events per unit time.

A ball and rod mill draw about the same energy whether filled with slurry or not. The challenge then is to use as many of these impacts as possible to break the ore.

### E.4.7 Parameters Affecting Mill Operation

Various parameters have been identified by Mullen et al (1996) to influence the power draw and hence the operation of the mill. The following section describes those parameters.

#### *E.4.7.1 Charge Shape:*

The resistance that the mill motor feels to its rotation is only caused by the part of the charge in contact with the mill shell. The part of the charge in free flight has no direct effect on the mill power draw. The part of the charge in the kidney zone in turn has little effect (5%) as it is situated very close to the mill centre of gravity. Only a crescent like shape remains which influences the mill power draw directly. This is true for most grate discharge mills. In overflow mills the slurry is only discharged once the slurry level reaches the discharge level trunnion. This leaves a pool of slurry consisting of a mixture of water and ore with the same density as the discharge slurry. The remainder of the charge is assumed to consist of the grinding media, taking up a shape similar to the grate discharge case.

#### *E.4.7.2 Charge Position:*

Charge position is defined by the position of the charge toe and shoulder. This is measured by means of photographic techniques when changing the mill speed and charge volume.

#### *E.4.7.3 Mill Speed:*

The position of the charge is raised by an increase in speed. This leads to an increase in shoulder angle. After leaving the shell at the shoulder the charge falls to the toe region and piles up, while waiting for the mill to accelerate it to the rotational speed. Liddell and Moys (1988) showed that the toe position does not vary over the speed range of normal mill fillings. As the speed is increased to the centrifuging speed the shoulder angle tends toward 90° until the whole load is centrifuged.

*E.4.7.4 Mill Filling:*

The percentage fill influences the position of the shoulder and toe of the charge. Large fillings tend to give high shoulder and low toe angles. Hence the speed at which the mill centrifuges is a strong function of the mill filling. The charge behaves as a collective body. Therefore, as pressure is exerted by the charge, the material lower down pushes the higher material further than would have been possible for single particles moving inside the mill. Higher fillings thus give rise to higher shoulder angles. This phenomenon is related to mill speed and the magnitude of the frictional forces inside the charge. These forces in turn are directly proportional to the charge weight.

*E.4.7.5 Charge Motion:*

By making use of photographic analysis of images from a laboratory glass mill a vector field description was generated. Fairly concentric paths were observed for the charge not in free flight - the active part. The velocity of particles in the mill can be expressed relative to the mill speed, while the radial position can be related to the mill radius. Pairs of data can be generated consisting of a normalised linear velocity and the associated radial position.

Vermeulen & Howat (1984) showed that an angular velocity gradient exists within the charge which is a function of the mill filling. This results due to slip occurring within the charge. Hence, as the mill filling is increased, the velocity gradient with respect to the mill radius will tend toward the no-slip condition.

# APPENDIX F

# SAMMON MAPPING TECHNIQUE

Sammon (1969) proposed a technique for the representation of *n*-dimensional data to a lower dimensionality of *d*, by point mapping the different vectors so that the inherent data structure is approximately preserved. Sammon's method maintains the approximate data structure by fitting N points in the lower dimensional space so as to preserve the corresponding distances in the higher n-dimensional space. The Sammon map is constructed from the *N* vectors in the *n*-space, $X_i$, with i=1, .....*N*. The corresponding *N* vectors in the lower dimension d (typically 2 or 3), are designated by $Y_i$, with i=1,....., *N*. The distance between the vectors $X_i$ and $X_j$ in the *n*-space is defined by

$$d_{ij}^{*} \equiv \text{dist}[X_i, X_j] \qquad \text{F1}$$

and the distance between the corresponding vectors $Y_i$ and $Y_j$ in the d-space by

$$d_{ij} \equiv \text{dist}[Y_i, Y_j] \qquad \text{F2}$$

A random d-space configuration is chosen for the Y vectors with the form:

$$\ldots\ldots\ Y_1 = \begin{bmatrix} y_{11} \\ \cdot\cdot \\ \cdot\cdot \\ y_{1d} \end{bmatrix} \quad \ldots \quad Y_2 = \begin{bmatrix} y_{21} \\ \cdot\cdot \\ \cdot\cdot \\ y_{2d} \end{bmatrix} \quad \ldots \quad Y_N = \begin{bmatrix} y_{N1} \\ \cdot\cdot \\ \cdot\cdot \\ y_{Nd} \end{bmatrix} \qquad \text{F3}$$

The interpoint distances $d_{ij}$ are calculated which are then used to determine the error E, which represents the extent to which the present configuration of N points in the d-

space fits the N points in the n-space. The procedure is repeated while the $y_{nm}$ values are adjusted until the smallest error is obtained

The error E, is calculated:

$$E = \frac{1}{\sum_{i<j} d_{ij}^{*}} \sum_{i<j}^{N} \frac{\left[d_{ij}^{*} - d_{ij}\right]^{*}}{d_{ij}^{*}} \qquad \text{F4}$$

and is also known as the Sammon stress. The Sammon stress is an indication of how well the interpattern distances are preserved when projected from the n-space to the d-space. Sammon originally proposed the use of a steepest descent algorithm to find the smallest error, for a large number of points the method soon becomes impractical. Mao and Jain (1995) described an algorithm for an unsupervised backpropagation learning algorithm for a feed forward neural network in order to perform the Sammon projection.

The following algorithm was proposed:

1. Initialize the weights randomly in the Sammon network
2. Select the patterns randomly, present them to the network and evaluate the network in a feed forward fashion.
3. Update the weights by backpropagation starting form the output layer.
4. Present the patterns, compute the Sammon stress and repeat if the error is too large.

A momentum constant can be added to speed up the convergence. In order to achieve the representation power of the Sammon algorithm a network with *Nd* free parameters is required. When the number of cases gets large the number of free weights required increase rapidly. The selection of data to the network should therefore be considered carefully in order to enhance the computational effort.

Mao and Jain (1995) investigated the pattern representation capability of various methods, including the Sammon map. They found that the Sammon projection attempts to preserve the interpattern distance as much as possible, which indicates that the variance is preserved by as much as possible as well. Further, the Sammon network offered the generalization capability of projecting new data, which was not true for the other networks tested.

# APPENDIX G

# MODELLING BY LINEAR REGRESSION

Linear regression is probably the most used modelling technique encountered. The least squares estimates of the vector parameter b in the model y=f(x,b) are obtained by $S(b)=\Sigma\,[y_i - f(x_i,b)]^2$ so that S(b') = min S(b), with b' the estimate of the true vector b. An iterative procedure is required when the relationship between y and b is non-linear.

For a model $y_i(x) = b_0 + b_1x_i$ with i = 1,2,3...N, the function $S(b) = \Sigma\,[y_i - b_0\text{-}b_1x_i]^2$ is minimized by differentiation yielding the two derivatives which are also known as the normal equations of the system:

$$\frac{\partial S}{\partial b_o} = -2\sum(y_i - b_0 - b_1x_i) = 0 \qquad \text{G1}$$

$$\frac{\partial S}{\partial b_1} = -2\sum(y_i - b_0 - b_1x_i)x_i = 0 \qquad \text{G2}$$

solution of equations 4.3 and 4.4 yield the least squares estimates of b,

$$b'_1 = \frac{\sum y_i(x_i - x_{avg})}{(\sum(x_i - x_{avg})^2)} \qquad \text{G3}$$

$$b'_0 = y_{avg} - b'_1 x_{avg} \qquad \text{G4}$$

where

$$x_{avg} = \sum\frac{x_i}{N} \text{ and } y_{avg} = \sum\frac{y_i}{N} \qquad \text{G5}$$

## G.1 MODEL COMPARISONS – R-SQUARE

The purpose of a model is to predict or forecast a parameter. The accuracy of the prediction is determined by how well the predicted value compares to the observed value. Probably the most common measure is the coefficient of determination or $r^2$. It is described as the proportion of the variation in the response variable Y that can be explained by the model, instead of viewing Y in isolation.

The $r^2$ is measured by use of the residual sums of the squares and is calculated from

$$r^2 = 1 - \frac{\sum (Y - Y^{est})^2}{\sum (Y - Y_{avg})^2} \qquad \text{G6}$$

Statistical Significance (p-value)

The statistical significance of a result is an estimated measure of the degree to which it is "true". The p-value represents a decreasing index of the reliability of a result. Thus the higher the p-level, the less valid the observed relation between the variables in the sample is a reliable indicator of the relation between the respective variables of the sample. Specifically, the p-level represents the probability of error that is involved in accepting our observed result as valid, that is, as "representative of the population."

# APPENDIX H

# PRINCIPAL COMPONENT ANALYSIS

Principal component analysis is a technique developed by Hotelling in 1933 to fit a set of axes through a data set in order to minimize the variance in the data. This gives a principal component which is the linear combination of the principal component coefficients and the original matrix of variables. The principal coefficients are the elements of the eigen vector corresponding to the largest eigen value of the sample covariance matrix of the original data matrix.

The method is well described by Aldrich (1998) for a data set consisting of p variables and n samples, from which the individual vector $\mathbf{x}^T = (x_1, x_2, \ldots x_p)$ is extracted. A (N x p) matrix can be constructed from these observations with elements $x_{ij}$. The p values observed on the i'th sample are denoted by $\mathbf{x}_i$, and the mean of the j'th variable calculated from:

$$x_{avg,j} = \frac{1}{n}\sum_{i=1}^{N} x_{ij} \qquad \text{H1}$$

The sample mean vector consists of the average of all the samples of x giving $\mathbf{x}_{avg}{}^T = (x_{avg,1}, x_{avg,2}, \ldots x_{avg,p})$. Further the variance of the j'th variable is described by

$$s_{ij} = \frac{1}{(n-1)}\sum_{i=1}^{N}(x_{ij} - x_{avg,j})^2 \qquad \text{H2}$$

while the covariance between the j'th and k'th variables is given by $S_{jk}$ which is explained in equation H3.

$$S_{jk} = \frac{1}{(n-1)}\sum_{i=1}^{N}(x_{ij} - x_{avg,j})(x_{ik} - x_{avg,k}) \qquad \text{H3}$$

These variances and covariances are represented by the sample covariance matrix **S**, which has $s_{jk}$ as the (j,k)'th element and is written as

$$S = \frac{1}{(n-1)}\sum_{i=1}^{N}(\bar{x}_i - \bar{x}_{avg})(\bar{x}_i - \bar{x}_{avg})^T \qquad \text{H4}$$

With principal component analysis a scalar variate $\mathbf{Y} = \mathbf{a}^T\mathbf{X}$ is formed, so that the value of **Y** corresponding to the i'th sample (of n) will be given by equation H5.

$$y_i = \bar{a}^T\bar{x}_i = a_1x_{i1} + a_2x_{i2} + ..... + a_px_{ip} \qquad \text{H5}$$

The mean of **Y** over the n samples will similarly be given by equation H6

$$y_{avg} = \bar{a}^T\bar{x}_{avg} = a_1x_{avg,1} + a_2x_{avg,2} + ..... + a_px_{avg,p} \qquad \text{H6}$$

The sample variance of Y is given by

$$S_y^{\,2} = \frac{1}{(n-1)}\sum_{i=1}^{N}(y_i - y_{avg})^2 \quad \text{and} \qquad \text{H7}$$

$$y_i - y_{avg} = \bar{a}^T\bar{x}_i - \bar{a}^T\bar{x}_{avg} = \bar{a}^T(\bar{x}_i - \bar{x}_{avg}) = (\bar{x}_i - \bar{x}_{avg})^T\bar{a} \qquad \text{H8}$$

As a consequence

$$(y_i - y_{avg})^2 = \bar{a}^T(\bar{x}_i - \bar{x}_{avg})(\bar{x}_i - \bar{x}_{avg})^T\bar{a} \quad \text{so that} \qquad \text{H9}$$

$$\sum_{i=1}^{N}(y_i - y_{avg})^2 = \sum_{i=1}^{N}\bar{a}^T(\bar{x}_i - \bar{x}_{avg})(\bar{x}_i - \bar{x}_{avg})^T\bar{a} \quad \text{or} \qquad \text{H10}$$

$$\sum_{i=1}^{N}(y_i - y_{avg})^2 = \bar{a}^T\left(\sum_{i=1}^{N}(\bar{x}_i - \bar{x}_{avg})(\bar{x}_i - \bar{x}_{avg})^T\right)\bar{a} \qquad \text{H11}$$

With **a** constant over i,

$$S_y^{\,2} = \frac{1}{(n-1)}\sum_{i=1}^{N}(y_i - y_{avg})^2$$

$$\therefore = \left[\bar{a}^T\frac{1}{(n-1)}\sum_{i=1}^{N}(\bar{x}_i - \bar{x}_{avg})(\bar{x}_i - \bar{x}_{avg})^T.\bar{a}\right]$$

$$\therefore = \bar{a}^T S\bar{a} \qquad \text{H12}$$

with **S** as defined above.

The derivation of principal components is based on the successive projection of lines through the p-dimensional space, so that the variance of the projections of the n points in the space onto these lines is a maximum. The first principal component can therefore be defined by the linear combination $\mathbf{Y}_1 = \mathbf{a}_1^T\mathbf{X}$ of the original variables that maximizes the value of $\mathbf{a}_1^T\mathbf{S}\mathbf{a}_1$, subject to the constraint that $\mathbf{a}_1^T\mathbf{a}_1 = 1$.

The first principal component is the linear combination $Y_1 = \mathbf{a}_1^T\mathbf{X}$ of the original variables and has the maximum variance among all such possible combinations. With large differences between the variables caused by scale of measurement, units, etc., different variables with large variances are obtained. This leads to principal components that correspond to the original variables $\mathbf{X}_i$ with the largest variance and little will be learnt from the data.

It is often necessary to ensure that the measured variables are at least comparable in their magnitude of variance and their units of measurements. If required, this can be achieved by standardizing the variables prior to principal component analysis (i.e. by extracting the principal components from the sample correlation matrix of the data, instead of the sample covariance matrix).

The number of principal components which are required are determined from the number of principal components which describe the required amount of variance. If a variance of 90% is deemed sufficient, the number of components would simply be determined by the number of components which describe at least 90% of the variance.

The loadings of the principal components describe the contribution of the original variables of dimension p to the respective principal components (e.g. variables 1 and 3 contributing most to factor 1, etc.). The principal component scores denote the value of the principal component for each specific sample point.

# APPENDIX I

# ARTIFICIAL NEURAL NETWORKS

It is not the aim of this work to give a detailed discussion of the field of neural networking. The following discussion is based on the works of Swingler (1996) and LiMin (1994) and briefly introduces the reader to neural networks and the feed forward network that was used in this study.

### I.1.1 Background

Neural networks are statistical models which are built by tuning a set of parameters or weights, which forms a mapping of a set of inputs, to an associated set of inputs. Training is carried out by adjusting the weights for a set of input-output pairs in order to minimize the error between the network answer and the output. With the weights set the model can produce answers for inputs which were not included in the training data. Care should however be taken that the new data do not contain larger absolute values than the original training data set.

### I.1.2 Feedforward Networks

A neural network builds a mathematical model consisting of a set of simple functions lumped together by weights. The weights describe the effect that each simple function has on the overall model. The feed forward network used in this study consisted of different layers of units or nodes. The input layer is the entry point for external data to the network. A number of hidden layers which contain the processing nodes extract the useful features from the input data and use them to predict the output data. The structure of a typical feed forward network is shown is figure 16.1.

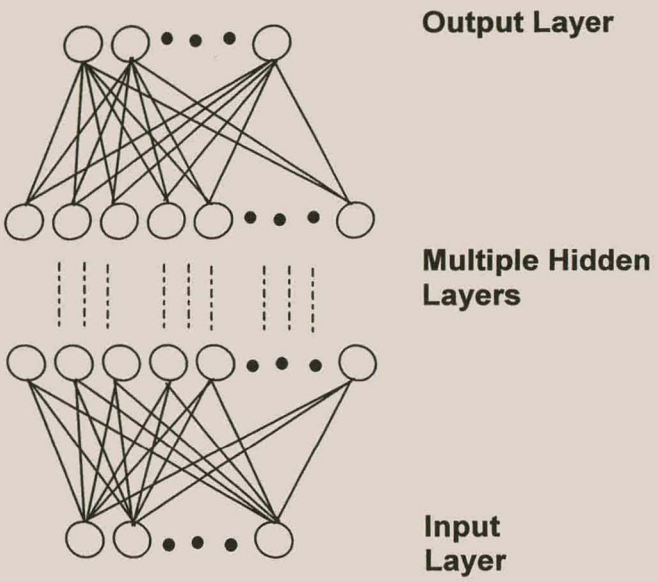


**Figure I1**. Typical neural network configuration

### I.1.3 Transfer Functions

The function used to predict values from one node to another in the next layer is called a transfer function. A few common transfer functions are given below:

- The sigmoidal function, also known as the log-sigmoidal function, is the most common for these types of networks and gives a continuous range of values between 0 and 1 for F(x).

$$F(x) = \frac{1}{1+e^{-x}} \qquad I1$$

- The hard limit function limits the output of a node to either zero or 1 and is typically encountered in classification networks.
- A linear transfer function enables the output of a node to take on a linear approximation of the input data, thereby allowing outputs of any value.
- The tan-sigmoid transfer function is similar to the log-sigmoidal function with the difference that outputs are limited between –1 and 1.

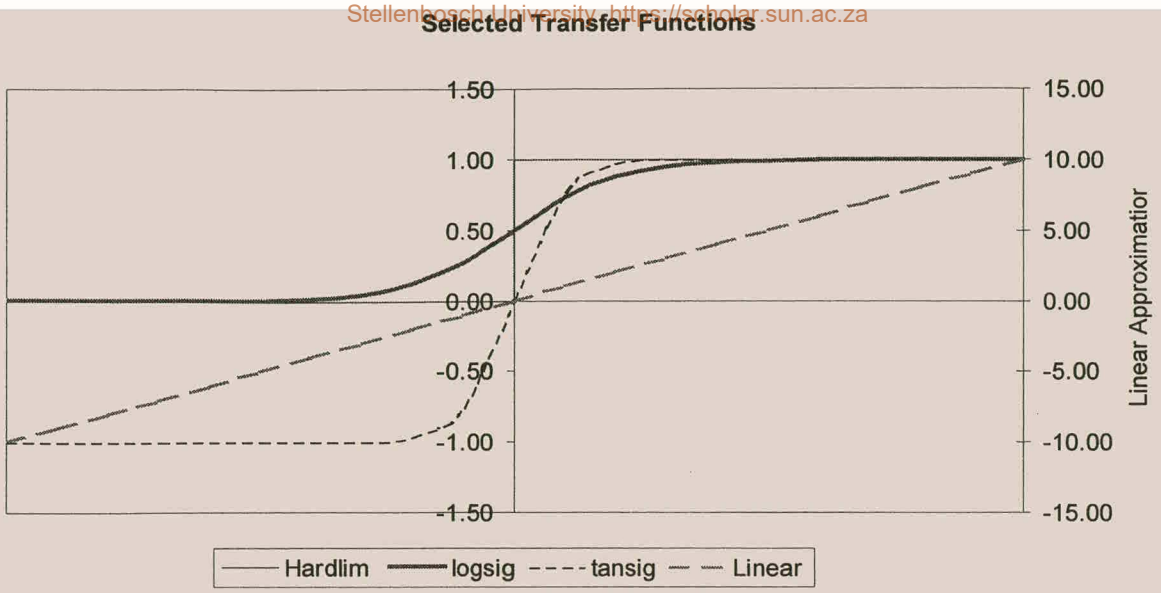


**Figure I2**. Selected transfer functions used in neural networks

### I.1.4 Backpropagation

Weights for a feed forward network are typically trained by backpropagation. This method learns a mapping from a set of inputs to a set of outputs. The nodes in the hidden layer learn to respond to features of the input patterns. The extracted features correspond to the correlation of activity among the different input units. With training the network can generalize over similar features found in different patterns.

The standard backpropagation algorithm (Swingler (1996)) is:

1. Initialize weights to small random numbers.
2. Choose a training pair at random.
3. Copy the network so that the activation from the inputs generates activation in the hidden and output layers.
4. Calculate the error derivative between the output and the target values.
5. Back propagate the summed product of the weights and errors to calculate the error in the hidden nodes.
6. Update the weights.
7. Train until the network stabilizes or a minimum error is reached.

With the weights in the network trained, the network is ready for modelling in a feed forward fashion.